University of California
Santa Barbara

Combining Biochemical Signaling and Mechanics to Understand Yeast Mating Morphogenesis

A dissertation submitted in partial satisfaction
of the requirements for the degree

Doctor of Philosophy
in
Mechanical Engineering

by

Michael D. Trogdon

Committee in charge:

Professor Linda Petzold, Chair
Professor Otger Campàs
Professor Megan Valentine
Professor Robert McMeeking

September 2018

The Dissertation of Michael D. Trogdon is approved.

Professor Otger Campàs

Professor Megan Valentine

Professor Robert McMeeking

Professor Linda Petzold, Committee Chair

May 2018

Combining Biochemical Signaling and Mechanics to Understand Yeast Mating Morphogenesis

by

Michael D. Trogdon

For my mom, who made all of this possible.
And my childhood best friend Julius, gone too soon.

Acknowledgements

I would first and foremost like to thank my PhD advisor, Linda Petzold, for her guidance, mentorship and support. I would also like to thank the rest of my committee: Otger Campàs, Megan Valentine and Robert McMeeking for their time and insight.

I would like to thank all of my close scientific collaborators. In particular, thanks to Tau-Mu Yi for his guidance and for providing new ideas at every juncture. I would like to thank Otger Campàs for being a wealth of knowledge in physics and biology. Also thanks to Samhita Banavar for all of the discussions, mutual encouragement and support. Lastly, I would like to thank Carlos Gomez for always being a good source of experimental knowledge and data.

For much of my growth over the last several years, I am grateful for the everyone in the Petzold lab, both past and present. In particular, thanks to Brian Drawert for his mentorship and our many collaborations together. Also thanks to Stefan and Andreas Hellander for their technical expertise and advice. I am perhaps most thankful for the friendships that I have formed with Tie Bo Wu, Ben Bales and Arya Pourzanjani at various installments of movie night, happy hour and holidays.

I also gratefully acknowledge my various funding sources over the years including the National Science Foundation and the National Institutes of Health.

Finally, I would like to thank all of my friends and family for their unwavering support and understanding over the years. While there are too many to list, I would just like to thank my mom and Toby for making all of this possible. Thanks to Casey and Chris for being my creative wellspring. Also thanks to all the friends made in Santa Barbara, particularly the Pasado house and the dog house affiliates. Lastly, thanks to my loving girlfriend, Surabhi, for being my closest friend and support through everything.

Curriculum Vitæ

Michael D. Trogdon

Education

May 2018 (Expected)
Ph.D., Mechanical Engineering
with an emphasis in Computational Science and Engineering
University of California - Santa Barbara, Santa Barbara, CA
GPA: 3.910
Advisor: Linda Petzold

May 2012
B.S., Mathematics, *with high distinction*
B.S., Mechanical Engineering
University of Nebraska - Lincoln, Lincoln, NE
GPA: 3.844
Advisor: George Avalos
Thesis: "Numerical Approximations for the Null Controllability of Nonlinear Parabolic-Like Thermoelastic Dynamics."

June 2015
q-bio Summer School on Stochastic Gene Regulation
Colorado State University, Fort Collins, CO

Publications

Michael Trogdon, Samhita P. Banavar, Brian Drawert, Tau-Mu Yi, Other Campàs, Linda Petzold. "Combining polarization and mechanics to understand yeast mating morphogenesis" in preparation.

Michael Trogdon, Brian Drawert, Carlos Gomez, Samhita P. Banavar, Tau-Mu Yi, Other Campàs, Linda Petzold. "The effect of cell geometry on polarization in budding yeast" *PLOS Computational Biology* 14 (06) 1-22, June 2018

Samhita P. Banavar, Carlos Gomez, Michael Trogdon, Linda Petzold, Tau-Mu Yi, Other Campàs. "Mechanical feedback coordinates cell wall expansion and assembly in yeast mating morphogenesis" *PLOS Computational Biology* 14 (01) 1-19, January 2018.

Brian Drawert*, Stefan Hellander*, Michael Trogdon*, Tau-Mu Yi, Linda Petzold. "A Framework for Discrete Stochastic Simulation on 3D Moving Boundary Domains" *Journal of Chemical Physics* 145, 184113, doi: 10.1063/1.4967338, November 2016. * contributed equally to this work

Brian Drawert, Michael Trogdon, Salman Toor, Linda Petzold, Andreas Hellander. "MOLNs: A cloud platform for interactive, reproducible and scalabe spatial stochastic computational experiments in systems biology using PyURDME" *SIAM Journal on Scientific Computing*, 38(3), C179-C202, June 2016.

Yi Hua, Linixia Gu, Michael Trogdon. "Three-dimensional modeling of carbon/epoxy to titanium single-lap joints with variable adhesive recess length" *International Journal of Adhesion and Adhesives*, Vol. 38, p. 25-30, October 2012.

Selected Oral Presentations

August 2017	"Effect of Geometry on Models of Polarization in Yeast" Graduate Student Simulation Seminar, University of California - Santa Barbara, Santa Barbara, CA.
July 2015	"Coupling Spatial Stochastic Biochemical Models with Mechanics to Simulate Mating in Yeast *Saccharomyces cerevisiae*" q-bio Summer School on Stochastic Gene Regulation, Colorado State University, Fort Collins, CO.
November 2011	"Numerical Approximations for the Null Controllability of Parabolic-Like Differential Equations" Conference on Undergraduate Research in Mathematics, Penn State University, State College, PA.

Selected Poster Presentations

February 2018	"The Effect of Cell Geometry on Polarization in Budding Yeast" Winter q-bio, Maui, HI.
September 2017	"High Performance Algorithms for Discrete Stochastic Simulation" DOE Office of Advanced Scientific Computing Research Applied Mathematics PI Conference, Rockville, MD.
January 2017	"Spatial Stochastic Simulation on Moving Domains of Shmoo Formation During Mating in *S. cerevisiae*" Gordon Research Conference for Stochastic Physics in Biology, Ventura, CA.
July 2016	"Spatial Stochastic Simulation on Moving Domains of Shmoo Formation During Mating in *S. cerevisiae*" The Tenth q-bio Conference, Vanderbilt, Nashville, TN.
August 2015	"Simulating Yeast Polarization in the Cloud" The Ninth q-bio Conference, Virginia Tech, Blacksburg, VA.
January 2015	"Simulating Yeast Polarization in the Cloud" Southern California Systems Biology Conference, University of California - Irvine, Irvine, CA.

June 2013	"Virtual Blood Vessels" IGERT Video and Poster Competition Award Ceremony, NSF Headquarters, Arlington, VA.
October 2011	"Numerical Approximations for the Null Controllability of Parabolic-Like Differential Equations" AMS Sectional Meeting, University of Nebraska - Lincoln, Lincoln, NE.
April 2011	"Numerical Approximations for the Null Controllability of Parabolic-Like Differential Equations" UNL Undergraduate Research Conference, University of Nebraska - Lincoln, Lincoln, NE.
October 2010	"Numerical Approximations for the Null Controllability of Parabolic-Like Differential Equations" Nebraska Research and Innovation Conference, Lincoln, NE.

Abstract

Combining Biochemical Signaling and Mechanics to Understand Yeast Mating Morphogenesis

by

Michael D. Trogdon

How biological systems are able to form and maintain such a wide variety of patterns and structures is one of the central questions in science. In this dissertation we focus on one example of pattern formation and morphogenesis found in yeast cells. Specifically, we present our work related to understanding how yeast cells are able to change their physical structure and form projections during mating. This is an interesting example of a problem that deals with both intracellular protein signaling and cell mechanics. One issue that has become increasingly important to understanding the dynamics of proteins inside of single cells is the inherent randomness or stochasticity of biochemical reactions. As mathematical modeling and computational techniques have become essential tools in systems biology over the last half century, we first mention our software framework for the efficient simulation of spatial stochastic reaction-diffusion problems which can leverage high-performance computing and cloud infrastructure. This work serves as the basis for our investigation into yeast mating morphogenesis.

The first step of yeast mating projection growth is the localization (or polarization) of proteins on the cell membrane. This is a well-studied, yet not fully understood, example of pattern formation in biology. In this dissertation we discuss several mathematical models of polarization and their various properties. When a yeast cell forms a mating projection the cell shape naturally changes in time. To deal with this from a mathematical modeling standpoint, we have developed a novel algorithm for the simulation of spatial stochastic

dynamics on moving domains. These technical advances have led to new insight into the biology of yeast mating morphogenesis. In particular, we have elucidated the effects that complex geometries can have on current models of polarization.

While polarization is certainly necessary for yeast mating morphogenesis, it is not the whole story. Yeast cells have a cell wall that is responsible for defining cell shape and providing mechanical integrity. To further explore mating projection growth, we have developed methods to couple models of polarization with physically based models for the mechanics of the cell wall. This coupling of biochemical signaling and mechanics allows for a more systems level understanding of yeast mating morphogenesis. We conclude by summarizing our findings about the coupling of polarization and mechanics, and discussing which biological links between the two are important from a mathematical modeling perspective.

Contents

Chapter 1

Introduction

How biological systems are able to form such a variety of shapes and patterns is one of the central questions in science. While most life starts as a nearly homogenous single cell, development inevitably leads to a wide array of heterogeneous and beautiful structures. Understanding the physical mechanisms behind these "pattern forming" systems is a rich field of research in both physics and biology. As is often the case in science, focusing on a simple model system, such as how a yeast cell changes shape, can yield insight into broader questions of pattern formation and morphogenesis in biology.

Mathematical modeling and computational methods have become a critical tool in systems biology research in the last half century. The localization (or polarization) of proteins on the membrane during the mating of *Saccharomyces cerevisiae* is a well-studied, yet not fully understood, example of pattern formation in biology where much work has been done in both mathematical modeling and experimental investigation to understand the physical mechanisms at play. One key feature that has only recently been addressed is the effects that stochasticity due to intrinsic noise can have on polarization, with some studies having shown that it can be critical for certain models of polarization [1, 2, 3].

Stochastic dynamics at the intracellular signaling level has become a standard modeling paradigm in many areas of biology. There are numerous cases where deterministic or mean-field techniques do not capture the relevant dynamics of biological systems [4, 5, 6]. Stochasticity is critical particularly when the copy number of a key chemical species is very small, as is often the case within single cells. Many methods exist to numerically simulate stochastic biochemical networks, the most common of which is the Stochastic Simulation Algorithm (SSA) or Gillespie algorithm [7, 8]. One assumption of the SSA is that the system is well-mixed, meaning that the reactants are assumed to be equally likely to be anywhere in the spatial domain. This assumption clearly does not apply in many systems, including our system of interest: polarization in yeast mating. The spatial nature of our system necessitates the use of spatial stochastic methods, of which there are many. One common approach relies on the Reaction-Diffusion Master Equation (RDME) formalism [9, 10, 11, 12]. Using RDME techniques, we have studied the protein signaling network involved in polarization in previous works [13, 14]. In particular, we are interested in understanding how these protein signaling networks interact with cell mechanics to yield morphogenetic change, such as the growth of the mating projection.

When the coupling of mechanics and biochemistry in this system is considered, the physical domain of the numerical simulations necessarily becomes time-dependent as the cell changes shape over time. To address this, we have developed an algorithm to simulate spatial stochastic reactions on time-dependent domains using the RDME formalism [14]. Many existing models [15, 16, 3, 2] treat polarization as a Partial Differential Equation (PDE) in simple 1 or 2 dimensional geometries (such as a line or circle). A key feature that is lost in these simulations is the effect that a more realistic geometry can have on these reaction networks. Our work has shown that there is a significant and biologically relevant impact of cell geometry during mating projection growth on current models of polarization [17]. Specifically, there seems to be a clear bias away from the tip of projec-

tion shaped geometries for a number of models tested. This is important when considered in the context of mating projection growth in yeast. When growing a mating projection, the cell establishes a spatial localization of proteins on the membrane, ultimately leading to actin cable formation and vesicle transport. The vesicles carry, among other proteins, cell wall modifying enzymes that change the material properties of the cell wall, leading to projection growth. During the growth of the projection *in vivo*, it is critical that the polarization cap remains at the tip of the projection to direct growth. However, our simulations suggest that current models of polarization could fail to capture this behavior due to a previously under-appreciated or unacknowledged effect of geometry on the dynamics of these polarization models. As a first attempt to address this issue, we present a model that contains a direct mechanical feedback on the dynamics of polarization. This model is shown to increase the stability of polarization in the case of growing projections and is based on a plausible biological mechanism.

In this dissertation, we present work that is guided by the overarching goal of understanding how biochemical signaling and cell mechanics interact to yield stable morphogenesis during mating projection growth in yeast. En route to this larger goal, we first mention our work on new software for efficient spatial stochastic simulation. We also present a novel algorithm for simulating spatial stochastic reaction-diffusion dynamics on moving domains. These technical contributions in turn led to new biological insight to our problem of interest. Specifically, we present work that addresses a previously under-appreciated effect of geometry on the dynamics of polarization. Lastly, we propose a new model for the maintenance of polarization during mating projection growth, via a direct mechanical feedback. This model is then used to fully couple a detailed model of polarization with a physically based model of mechanics, to provide a complete simulation of stable projection growth.

1.1 Outline

The remainder of this dissertation is organized as follows: in Chapter 2 we give a background of current models of polarization in both budding and mating. We also give details on the current methods for spatial stochastic simulation that will be referenced throughout the dissertation. Next, we mention our work on the development of new software for efficient spatial stochastic simulation (published in [13]). Lastly, we discuss theoretical work that shows that mechanical feedback can coordinate cell wall expansion and assembly during mating projection growth (published in [18]) and give more background on the role of the cell wall in yeast morphogenesis. In Chapter 3 we present our work on a novel algorithm to simulate spatial stochastic dynamics on moving domains (published in [14]). In Chapter 4 we present our work that provided insight into the biologically relevant effect that cell geometry can have on the dynamics of polarization (under review in [17]). Lastly, in Chapter 5 we present work on a new model for the maintenance of polarization during mating projection growth via a direct mechanical feedback, and couple detailed models of polarization with a physically based model of mechanics to simulate mating projection growth (in preparation in [19]). We conclude by summarizing our results and discussing future directions.

Chapter 2

Background

2.1 Models of Polarization in Yeast Budding and Mating

2.1.1 Pattern formation in reaction-diffusion systems

The ability of biological systems to form heterogeneous structures with near homogeneous initial conditions is one of the hallmarks of life and development. This "symmetry breaking" can be seen everywhere in nature, from the stripes on a tiger to the structure of a leaf. But exactly how these patterns are formed and what are the physical mechanisms behind them, has remained elusive. One model system where progress has been made is that of reaction-diffusion dynamics.

Reaction-diffusion systems are a classic instance of pattern formation in physics and biology. Turing was the first to mathematically formalize the idea of instabilities in reaction-diffusion systems in his groundbreaking 1952 paper [20]. What has now become known as Turing stability analysis refers to treating the reaction and diffusion of different chemical species as a partial differential equation (PDE) and performing linear stability

analysis on the homogeneous steady state. This analysis has shown that it is possible to create a variety of patterns, such as spots and stripes, by considering the interaction of two diffusing and reacting "morphogens", or chemical species. Since Turing's seminal work, much effort has been put towards trying to understand the pattern forming ability of reaction-diffusion systems and which, if any, biological systems utilize these types of mechanisms for development.

One extension to the work of Turing came from Gierer and Meinhardt in 1972 [21]. This work showed that simple molecular mechanisms could lead to pattern formation in reaction-diffusion systems. In particular, it was shown that short range activation and long range inhibition are sufficient for stable pattern formation. The long range inhibition can also be replaced by a substrate depletion mechanism. In the case of substrate depletion, a particular chemical species that is critical for activation can become depleted throughout the domain, leading to the possibility of pattern formation.

Throughout this dissertation, we will see that simple mechanisms for pattern formation such as those discussed here will be relevant to more complex models of polarization in yeast. Another mechanism that has not been studied extensively in the literature, but is nonetheless relevant to our work later on in this dissertation, is that of the interaction between the inherent stochasticity in biochemical reactions and pattern formation. An intriguing result presented in [22] showed that pattern formation can extend well beyond the parameter region predicted by Turing type analysis when stochastic effects are considered for a specific model problem (the Brusselator model). These patterns were referred to as stochastic Turing patterns. To come to this conclusion, the authors used the van Kampen perturbative development for the probability distribution of the fluctuations [23], which led to predictions for the power spectra of the fluctuations and predicted spatial order in regions of parameter space for which there is no order in the Turing paradigm. Another interesting result from this study was that the domains

yielding stochastic Turing patterns were different for each of the species in the model, which is something not seen in the mean-field theory. In fact, there were regions observed with spatial order for one species and a homogeneous distribution for the other. In another study [24] it was shown there can be noise-induced temporal dynamics in Turing systems. Specifically, one spatiotemporal behavior that was observed in stochastic reaction-diffusion systems, even when the deterministic analogue has a stable steady state, was polarity switching. Essentially, this means that when a pattern has formed, peaks can switch to troughs and the pattern remains as time progresses. This notion of polarity switching, which is observed only in stochastic systems, was distinct from the phenomena of oscillating patterns which can be predicted deterministically. The study looked in detail at only Schnakenberg kinetics [25] in one dimension but predicted similar results in other systems.

Another body of work has examined the robustness of patterns in a stochastic environment and suggested domain growth as a possible mechanism for the stability of pattern formation [26]. Most of the studies mentioned here use a combination of analytic results and stochastic simulation. Stochastic simulation of reaction-diffusion systems can be done in many ways. The most typical is the mesoscopic approach of the Reaction Diffusion Master Equation (RDME), which involves partitioning the space into discrete voxels and treating diffusion as an event between voxels (this will be discussed in detail in Section 2.2). Some of the issues that can arise when studying pattern formation using compartment based methods such as the RDME are described in [27].

Lastly, there have been several interesting studies looking at pattern formation in real biological systems. The system that has arguably been studied in the most quantitative depth is that of the oscillation of Min proteins in E. coli [28]. One study in particular claimed that the full range of phenotypic behavior could not be captured unless a stochastic model was used [9]. Another fascinating study experimentally showed that the

Min proteins themselves formed surface waves in vitro, and quantitatively characterized the reactions responsible [29]. In the next section, we will discuss the current state of understanding with regard to our particular system of interest: polarization in yeast.

2.1.2 Standard models of polarization in yeast

The polarization of proteins during the mating of *Saccharomyces cerevisiae* is a well-studied, yet not fully understood, example of pattern formation in biology. During the mating process, haploid yeast cells respond to a gradient of mating pheromone via a cascade of intracellular protein reactions, culminating in a localization of key proteins on the membrane that facilitate actin cable formation and vesicle transport [30]. Many quantitative models exist, at varying levels of mathematical complexity, for the different levels of polarization in both budding and mating. Broadly, the majority of models have been developed to study the dynamics of the main polarity regulator, the Rho GTPase Cdc42 [15, 2, 16], the formation of actin cables and the polarisome [3, 31, 32], or the interaction between the two [33, 31, 34]. Reviews of polarization models can be found in [35, 36, 37, 38]. The literature for models of polarization in yeast is vast and often contains conflicting results regarding the role of different mechanisms.

There are several existing models of the polarization of the main polarity regulator Cdc42. A common type of model for the reaction-diffusion dynamics of Cdc42 involves what is known as a guanosine nucleotide dissociation inhibitor (GDI) [15, 16]. These relatively detailed mechanistic models of polarization are formalized as PDEs and rely on a mechanism in which GDI is thought to preferentially lead to the detachment of the inactive, GDP-bound form of Cdc42 from the membrane to the cytoplasm [15, 16] (see Chapter 4 for more details). The difference in diffusion rates between the cytoplasm and the membrane (diffusion in the cytoplasm is typically much faster), and thus between

the active and inactive forms of Cdc42, is what leads to a Turing type mechanism for polarization. Even within this class of models there are differences in the dynamics of polarization and disagreement about which mechanisms are more biologically relevant. For example, the model presented in [16] was developed to form one, and only one, broad polarization cap that eventually narrows as time progresses. This is in contrast to the model presented in [15] in which multiple polarization sites initially form and ultimately compete to form one distinct polarization site. Another important consideration is the experimental work presented in [39] which calls into question the necessity of the GDI mechanism for polarization. Specifically, the authors in [39] suggest that a difference in diffusion rates on the membrane may be sufficient to provide polarization, as opposed to the GDI mechanism which relies on the transfer of species from the membrane to the cytoplasm (although there haven't been any serious modeling efforts to understand how this might work from a mathematical perspective).

In addition to the more detailed, mechanistic models of Cdc42 polarization, there are several simplified, phenomenological models that can provide very useful insight. The most well known of the simple motif models is presented in [1]. This model has only a membrane bound and cytoplasmic version of Cdc42 along with three reactions: attachment and detachment from the membrane and recruitment of cytoplasmic species by the membrane bound species (see Chapter 4 for more details). Interestingly, this model has been shown to exhibit clustering behavior only when modeled stochastically, as opposed to deterministically (at least for the parameters considered). Another simplified model of polarization is the so called "wave-pinning" model of polarization presented in [40]. Intriguingly, recent work has shown that the displacement of local equilibria by lateral mass redistribution is in fact the key mechanism of pattern formation in mass-conserved systems, and unites models that were previously thought distinct (such as the Turing type and the wave-pinning mechanism for example) under one mechanism [41].

While this work is certainly a step towards more fully understanding the mechanisms underlying biological pattern formation in reaction-diffusion systems, there is still a lot that is not well understood. Some very recent work has stated that stochastic dynamics can expand the regions of parameter space that yields polarization, and can result in faster polarization than deterministic models, for certain detailed models of Cd42 polarization [42].

As mentioned above, in addition to models describing the dynamics of Cdc42, there is a substantial literature dealing with the formation of actin cables and vesicle traffic. One model, presented in [3], dealt with the dynamics of actin and two key proteins related to actin cable formation (Spa2 and Bni1) as a reaction-diffusion system. This study showed that stochastic dynamics can more robustly reproduce two fundamental characteristics of polarization observed in wild-type cells: a highly polarized phenotype via a mechanism that the authors referred to as spatial stochastic amplification, and the ability of the polarisome to track a moving pheromone input. One key physical aspect of actin cable formation that is often left out of current models is the extended nature of the cables. The fact that actin cables are actually one dimensional structures embedded in three dimensional space makes the resultant dynamics very difficult to simulate with standard modeling approaches. While there are techniques for doing this in a rigorous fashion (see [43]) it is not common. We will discuss some of these issues in more detail in Chapter 4.

The conclusions about the interaction of the two parallel pathways of reaction-diffusion Cdc42 polarization and actin-mediated vesicle transport are also disputed. For example, one major question is whether vesicle delivery provides positive [33] or negative [31] regulation of polarization. Work presented in [32] provides evidence for a mechanism of polarization dependent on the dynamics of endocytosis and exocytosis which leads to a corralling of key polarization proteins throughout the cell cycle. A central difficulty in understanding polarization is the role of each pathway in the establishment and main-

tenance of the polarization site. It is likely that the diversity of opinion about the role of actin cables arises because of the vastly different ways in which vesicle transport is modeled mathematically. Throughout this dissertation we will consider various models of polarization from the literature, as well as present some novel models of certain aspects of polarization.

2.2 Stochastic Simulation of Biochemical Reactions

Recent advances in biology have shown that proteins and genes often interact probabilistically. The resulting effects that arise from these stochastic dynamics differ significantly from traditional deterministic formulations, and have biologically significant ramifications. This has led to the development of discrete stochastic computational models of the biochemical pathways found in living organisms. These include spatial stochastic models, where the physical extent of the domain plays an important role. For mesoscopic models, similar to popular solution frameworks for partial differential equations (PDEs), the computational domain is discretized with a computational mesh, but unlike PDEs, the reaction-diffusion dynamics are modeled by a Markov process where diffusion and reactions are discrete stochastic events. The dynamics of a spatially inhomogeneous stochastic system modeled by such a Markov process formalism are governed by the Reaction-Diffusion Master Equation (RDME) [44].

The RDME extends the classical well-mixed Markov process model [45] to the spatial case by introducing a discretization of the domain into K non-overlapping voxels. Molecules are point particles and the state of the system is the discrete number of molecules of each of the species in each of the voxels on Cartesian grids or unstructured triangular and tetrahedral meshes. The RDME is the forward Kolmogorov equation governing the time evolution of the probability density of the system. For brevity of no-

tation, we define $p(\mathbf{x}, t) = p(\mathbf{x}, t|\mathbf{x}_0, t_0)$ as the probability that the system can be found in state $\mathbf{x}$ at time t, conditioned on the initial condition $\mathbf{x}_0$ at time t_0. For a general reaction-diffusion system, the RDME can be written as

$$\begin{aligned}
\frac{\partial p(\mathbf{x}, t)}{\partial t} = &\quad \mathcal{R}p(\mathbf{x}, t) + \mathcal{D}p(\mathbf{x}, t) \\
\mathcal{R}p(\mathbf{x}, t) = &\quad \sum_{i=1}^{K}\sum_{r=1}^{M} a_{ir}(\mathbf{x} - \nu_{ir})p(\mathbf{x} - \nu_{ir}, t) \\
&\quad -a_{ir}(\mathbf{x})p(\mathbf{x}, t) \\
\mathcal{D}p(\mathbf{x}, t) = &\quad \sum_{s=1}^{N}\sum_{i=1}^{K}\sum_{j=1}^{K} d_{sij}(\mathbf{x} - \mu_{sij})p(\mathbf{x} - \mu_{sij}, t) \\
&\quad -d_{sij}(\mathbf{x})p(\mathbf{x}, t)
\end{aligned}$$

where $\mathbf{x}_{i\cdot}$ denotes the i-th row and $\mathbf{x}_{\cdot j}$ denotes the j-th column of the $K \times S$ state matrix $\mathbf{x}$, and S is the number of chemical species. The functions $a_{ir}(\mathbf{x}_i)$ define the propensity functions of the M chemical reactions, and ν_{ir} are stoichiometry vectors associated with the reactions. The propensity functions are defined such that $a_{ir}(\mathbf{x})\Delta t$ gives the probability that reaction r occurs in a small time interval of length Δt. The stoichiometry vector ν_{ir} defines the rules for how the state changes when reaction r is executed. $d_{ijk}(\mathbf{x}_i)$ are propensities for the diffusion jump events, and μ_{ijk} are stoichiometry vectors for diffusion events. μ_{ijk} has only two non-zero entries, corresponding to the removal of one molecule of species X_k in voxel i and the addition of a molecule in voxel j. The propensity functions for the diffusion jumps, d_{ijk}, are selected to provide a consistent and local discretization of the diffusion equation, or equivalently the Fokker-Planck equation for Brownian motion. It is important to note, as will be discussed in depth in Chapter 3, that this formalism is defined for a physical domain that is static in time. We will relax this assumption with our method to accommodate time-dependent domains.

In most cases, the RDME is too high-dimensional to solve directly. Thus, algorithms

have been developed that generate exact realizations of the Markov process described by the RDME, in a Monte Carlo fashion. One particularly efficient algorithm that we focus on for our implementation is the Next Subvolume Method (NSM) [11]. In this algorithm, the time to the next event in each voxel (either a chemical reaction or diffusion event) calculated by the Direct Method formulation of the SSA [7]. To identify in which voxel the event occurs, the algorithm uses the Next Reaction Method formulation of the SSA [46]. If it was a chemical reaction event that occurred, then only the voxel in which the event occurred needs to be updated, while if a diffusion event occurs, both the voxel where the molecule started and the voxel where the molecule ended up need to be updated. The key to the efficiency of the NSM is the use of an event priority queue which gives a scaling of $\mathcal{O}(\log_2(K))$ where K is the number of voxels in the mesh [11].

The use of unstructured meshes allows for complicated geometries in 3D to be more easily accommodated, such as the curved surfaces of cell membranes. For the theoretical details of how to obtain mesoscopic diffusion constants on unstructured meshes, see [47]. Using the finite element package DOLFIN [48] we obtain the diffusion matrix for the system, from which we get the jump coefficients for individual voxels.The flexibility of simulating on unstructured meshes allows our method to handle complex time-dependent domains in 3D.

Despite the large computational cost, mesoscopic simulation with the RDME, when applicable, is typically orders of magnitude faster than alternatives such as reactive Brownian dynamics. Individual realizations can be feasibly sampled for fairly complex models in complicated geometries on commodity computational resources such as laptops and workstations. However, since the models are stochastic, single realizations are not sufficient. Rather, large ensembles of independent samples of the process need to be generated to form a basis for statistical analysis. Furthermore, key parameters of the biological process may be known only to an order of magnitude or two, thus necessitat-

ing an exploration of parameter space and/or parameter estimation. The need for an infrastructure to manage the computation and data has motivated the development of specialized software platforms for efficient stochastic simulation.

The ability to easily, efficiently and reproducibly simulate spatial stochastic models with appropriate software is crucial. To address this issue, we have developed a software framework, PyURDME, meant for the design, implementation and simulation of spatial stochastic models in Python. We have also developed MOLNs, a cloud computing appliance that allows for spatial stochastic simulation on different cloud and high-performance computing architectures. This work was done in close collaboration with Brian Drawert and Andreas Hellander and was originally published in [13]. All of the spatial stochastic simulations presented in the remainder of this dissertation were performed using PyURDME and MOLNs.

2.3 Role of the Cell Wall in Morphogenesis

Up to this point we have discussed the importance of understanding how yeast cells can localize key proteins during the mating process. This is an interesting problem from both the mathematical and biological perspective. We have mentioned several existing mathematical models of polarization and methods for simulating reaction-diffusion dynamics when taking into account the inherent stochasticity present in biochemical reactions. While the physical mechanisms responsible for polarization are an important piece of morphogenesis during yeast mating, they are certainly not the whole story. In particular, yeast cells, along with plant and bacterial cells, have a rigid cell wall that defines their shape. This is in contrast to animal cells in which the cytoskeleton is the main structural component of the cell. An understanding of how polarization and the mechanics of the cell wall interact to yield stable projection growth is our main goal in

this dissertation. In this section we will give a brief overview of the cell wall itself and how it relates to morphogenesis.

The yeast cell wall is a polymer network constructed mostly of β 1,3-glucan chains to which β 1,6-glucan, chitin and a number of mannoproteins are attached [49, 50, 51]. Maintaining the structural integrity of the cell wall throughout the cell cycle is critical. The cell wall has four main functions among others: maintain stable internal osmotic conditions, protect against physical stress, maintain cell shape and act as a scaffold for proteins [49]. These factors allow walled cells to maintain a large, isotropic internal turgor pressure. In budding yeast, the Cell Wall Integrity (CWI) pathway is known to help the cell prevent loss of cell wall mechanical integrity [51]. Five transmembrane proteins, namely Wsc1, Wsc2, Wsc3, Mid2, and Mtl1, are thought to act as stress sensors and relay information about the mechanical state of the cell wall to multiple intracellular processes via the activation of Rho1 GTPases [52, 53]. Growth of a cell is then a delicate balance between expansion and cell wall assembly. If the cell wall expands too much without proper assembly of new material, the cell will lose structural integrity and lyse. In the case of mating projection growth we are interested particularly in highly localized changes of cell shape. There are several theoretical descriptions in the literature that have attempted to model different parts of these processes in walled cells.

Many studies have focused either on cell wall assembly [54, 55] or cell wall mechanics [56, 57] separately. More recent work has dealt with both cell wall assembly and mechanics but assumed these two processes to be independent [58, 59, 60, 61]. In work presented in [18] (conceived of by and done in collaboration with Otger Campàs, Samhita P. Banavar, Tau-Mu Yi and Carlos Lopez), we showed by directly solving the dynamics of cell wall assembly and expansion that treating these two processes as independent always leads to unstable cell wall expansion and lysis. This work then went on to show that a mechanical feedback coordinating cell wall assembly and expansion is essential

to sustain mating projection growth in yeast. The model presented in [18] will be our basis for combining polarization and mechanics to simulate mating projection growth in Chapter 5 of this dissertation.

In [18] the cell wall is treated as a thin viscous shell building on previous work in tip-growing cells [61] and the expansion of thin viscous shells [62]. The expansion of the cell wall is driven by the high internal turgor pressure of the cell. Once the yeast cell has become polarized and established actin cables, vesicles are delivered to the cite of polarization that contain, among other proteins, cell wall degrading enzymes (glucanases) [63]. Thus the cell wall of the growing mating projection is assumed to behave as an inhomogeneous viscous fluid with a spatially varying viscosity which is minimal at the apex and increasing away from it. To sustain this localized, pressure-driven expansion the cell wall requires constant assembly of new cell wall in the expanding region. Cell wall assembly occurs through synthesis of the primary component of the wall, β 1,3-glucan [49], by transmembrane β 1,3-glucan synthases Fks1/2, which localize at the apical, growing region of the mating projection [64, 65]. While only inactive Fks1/2 molecules, unable to synthesize glucans, are incorporated into the plasma membrane through exocytosis, Fks1/2 can be activated by Rho1 once at the plasma membrane [66]. The activated form of Fks1/2 synthases extrudes β 1,3-glucan chains into the extracellular space, thereby assembling new cell wall onto the preexisting wall [67]. The dynamics of active and inactive Fks1/2 are then characterized by rates on and off the membrane dictated by exo- and endocytosis. The activation of inactive Fks1/2 is mediated by the GTPase Rho1 through the CWI pathway, providing a direct coupling between the local mechanical state of the wall and the local cell wall synthesis machinery via the Fks1/2 activation rate [68, 53, 69]. This coupling between the activation of Fks1/2 (responsible for the assembly of new cell wall) and the mechanical state of the cell (relayed by stress sensors such as Mid2 and Wsc1 via Rho1) provides a direct mechanical feedback of cell

wall mechanics on cell wall assembly and leads to stable projection growth.

The theoretical model described above from [18] was then used to generate predictions about the characteristics of mating projection growth. Specifically, the model is formalized as a partial differential equation (PDE) in the axisymmetric, curved geometry of the cell. To numerically simulate this model we discretized the spatial domain and used the method of lines (MOL) technique to generate a system of differential algebraic equations (DAE) describing the expansion and assembly of the wall. This system of DAEs was numerically approximated with custom Python code that made use of the SUNDIALS library of nonlinear and differential solvers [70]. In the absence of mechanical feedback, numerical integration revealed that mating projection growth was unstable for all parameter values. Unstable growth was either an unbounded thinning or thickening of the cell wall, depending on the parameters. In the presence of mechanical feedback, numerical integration revealed stable projection growth for a wide range of model parameter values. A key prediction of the model was that the shape of the mating projection was largely insensitive to variations in the mechanical feedback strength, while the radius of the mating projection increased linearly with the size of the exocytosis region. These predictions were then explored experimentally through various genetic mutants. For example, the prediction that mating projection shape was independent of feedback strength and dependent on the size of the exocytosis region was confirmed by various deletions of the key stress sensors in the cell (Mid2 and Wsc1) which lowered the feedback strength and deletion of Spa2 which increases the size of the exocytosis region.

The work described in this section was key in showing that coordination between cell wall expansion and assembly via a direct mechanical feedback on the activation of Fks1/2 is critical for stable mating projection growth. In Chapter 5 of this dissertation we will combine models of polarization described in Section 2.1 and the mechanics described here to explore further the interactions of biochemical signaling and mechanics during

projection growth. Specifically, we will propose a new mechanism whereby a direct mechanical feedback on the dynamics of polarization can stabilize the polarization cap during projection growth.

Chapter 3

Spatial Stochastic Simulation on Moving Domains

As mentioned above, the main goal of this dissertation is to understand how the interplay between biochemical signaling and mechanics leads to morphogenesis in yeast mating projection growth. We have also noted that spatial stochastic dynamics are often critical to faithfully capturing the biologically relevant features of polarization. In this chapter, we present a novel algorithm for simulating spatial stochastic dynamics on moving domains. This work was done in close collaboration with Brian Drawert and Stefan Hellander and was originally published in [14].

3.1 Introduction

Stochastic simulation of biochemical reactions has become an essential part of systems biology. Many examples exist where mean-field or deterministic analysis is insufficient to capture the relevant dynamics of real biological systems [4, 5, 6]. In particular, systems in which the copy number of any relevant species is small will often be more accurately

modeled with stochastic simulation. There exist several methods to model biochemical reactions stochastically, the most popular of which is the Stochastic Simulation Algorithm (SSA), also known as the Gillespie algorithm [8]. This algorithm assumes that the system is spatially homogeneous, or well-mixed, which is not the case in many interesting biological problems.

Polarization in yeast [30] and neutrophils [71], Min oscillations during cell division of *E. coli* [9, 72], and development [21] are a few examples where the well-mixed assumption does not apply. There are several different methods for modeling spatial stochastic biochemical reactions, which can be broadly grouped into two categories. First are the particle-tracking, or free-space based on the Brownian dynamics formalism [73], methods that resolve the system on a microscopic scale [74, 75, 76]. These methods are more accurate but can be quite difficult to simulate in an efficient manner. The other group of methods works on the mesoscopic scale and is based on the reaction-diffusion master equation (RDME) formalism [10, 11, 9, 12]. These methods discretize the domain into spatially homogeneous subvolumes (or voxels). Reactions within a voxel are modeled with the SSA algorithm, while diffusion between voxels is modeled as events occurring at intensities chosen to be consistent with the diffusion equation. The RDME is significantly faster to simulate than microscopic methods, with some sacrifice in accuracy. A more detailed background on these methods was given in Section 2.2. An assumption that underlies all of these methods is that the physical domain is static in time. This is often not the case in biology.

Shmoo growth during the mating of yeast [77], tip growth in fungal hyphae [78], chemotaxis in neutrophils [71], cell migration [79] and cell division [9, 72] are some examples where the physical domain of the cell is changing in time. There has also been recent work dealing with the critical role that geometry can play in fundamental biological processes, such as polarization [80]. In this chapter, we present a method to

efficiently model stochastic reaction-diffusion systems in complicated, three dimensional (3D), time-dependent geometries using the RDME framework. Previous work to model stochastic reaction-diffusion systems in time-dependent domains has focused on particle-based approaches [81]. While these methods are viable in some settings, it is generally accepted that particle-tracking methods become prohibitively expensive as the system size grows large. An efficient implementation of the RDME on time-dependent domains can effectively handle complex geometries as well as large reaction networks, while still being practical in terms of simulation time. Previous work has dealt with particle migration on 1D growing domains using the RDME formalism, where results have been compared to those of partial differential equation (PDE) models [82, 83, 84]. Additionally, we note that the particle-based software Smoldyn [74] has capabilities to change the size of domain during simulation.

A key problem that our method addresses arises in systems where the biochemical reaction network is fully coupled to cell mechanics. We seek to model the growth of the mating projection in yeast. In this system, enzymes modify the material properties of the cell wall, softening it, and as a result the force of the internal turgor pressure deforms the cell. At the same time, cell wall construction proteins strengthen the cell wall and slow the movement. A diagram of this process is illustrated in Figure 3.1. Our method does not propose to solve arbitrary mechanics of the model system under consideration. Instead, we integrate an external function or software that models and solves the equations governing the mechanics of the system, which will take as input the state of our biochemical system, and provide as output the instantaneous velocity of the boundary of the domain. It is important to note however, that this is simply one possible problem that can be handled by our proposed algorithm. In general, the function that moves the boundary does not need to be defined by mechanics (e.g. a constantly expanding sphere). The only requirement is that there is a velocity field provided to

move the boundary, which can be empirically or theoretically derived.

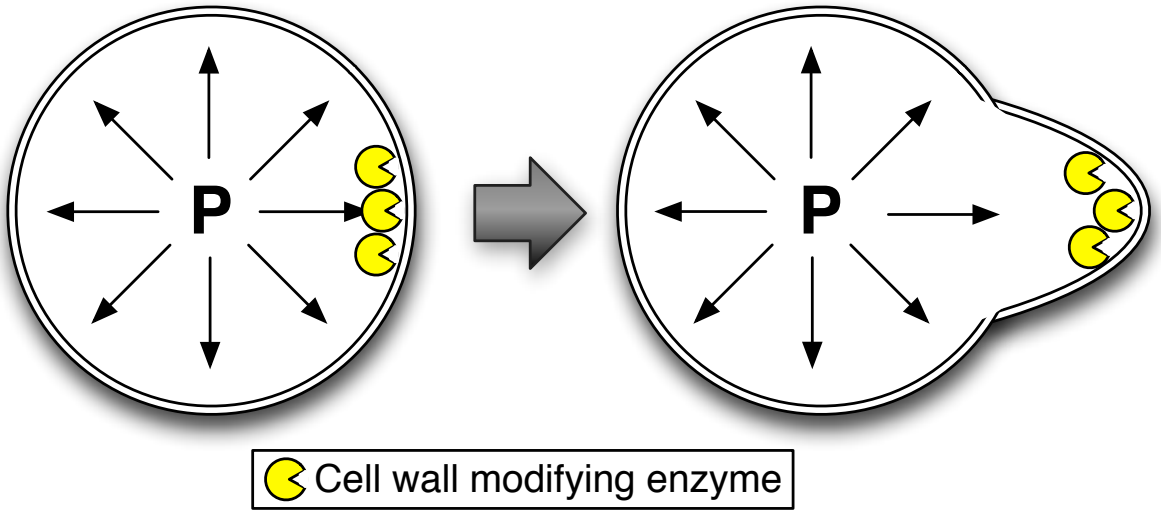

Figure 3.1: Illustration of how the yeast mating projection grows. Cell wall modifying enzymes (yellow) are localized to the polarized region of the cell membrane. These enzymes soften the cell wall. The internal turgor pressure pushes on the cell wall, deforming it and creating the mating projection.

It is important to note that in our method it is necessary to have a separation of timescales between the diffusion of the biochemical species and the movement of the boundary. It is critical that diffusion is faster than the boundary velocity to accurately simulate the system. In Sections 3.3.1 and 3.3.2 we characterize the error our method incurs and how it relates to the difference in timescales of diffusion and the velocity of the boundary. Essentially, it is possible to find a time step small enough to satisfy a user specified error tolerance if there is in fact a separation of timescales.

In this chapter we present a method to efficiently simulate stochastic reaction-diffusion models coupled to time-dependent domains using the RDME formalism. An outline for the rest of this chapter is as follows: in Section 3.2, we present our method and discuss implementation and theoretical considerations. Next, in Section 3.3, we present three examples that demonstrate the convergence properties and accuracy of the method

along with its applicability to biologically relevant problems. Specifically, in Section 3.3.1, we compare the results of our method to a microscale implementation of a single species diffusing within an expanding 1D line that can react with the boundary. This example serves to demonstrate the accuracy and convergence (in the spatial distribution of molecules) of our method compared with a microscale implementation over a range of expansion velocities and time steps. To accurately compare these different scales of simulation, we also derived the relationship between mesoscale and microscale reaction rates (see [14] for details). Next, in Section 3.3.2, we present a more biologically relevant, yet still theoretically tractable, model of polarization in yeast, introduced in [35]. This model contains a density dependent switch for polarization which we explore through an expanding and contracting sphere and compare to theoretical steady state results from [35]. Lastly, in Section 3.3.3 we present a model in which the state of the biochemical system dictates the movement of the boundary. In particular, we present a new model for the polarization of Cdc42 in mating yeast and qualitatively compare to experimental data. Finally, we end the chapter in Section 3.4 with a discussion of the method and our results.

3.2 Computational Method for Spatial Stochastic Simulation with a Moving Boundary

In this section we develop a computational method for simulation of spatial stochastic systems defined by the RDME formalism on domains with moving boundaries. Our method utilizes the timescale separation between the diffusion of the biochemical species in the RDME system and the movement of the boundary of the domain. The method is formulated for systems where diffusion is faster than boundary movement. In this

context we use operator splitting to decouple the reaction-diffusion operator from the domain movement operator, solving each operator sequentially over the same time step.

In the formulation of the RDME, the spatial domain is discretized into volume units known as voxels. For example, in our PyURDME software package [13] the 3D domain is discretized using tetrahedral elements. Since the RDME is formulated to be solved on a static domain, we cannot directly adapt it to a moving domain. Instead, we employ an operator splitting style simulation, by first solving the RDME for a small time τ (the splitting time step) on a static mesh. Then we use the state of the biochemistry to find the velocity of the boundary of the domain through a function specified by the user, and evolve the the mesh over the same time step τ. Finally, the state of the biochemical system is transformed to the newly evolved mesh. A sequence of these steps are taken until the simulation reaches the final time.

The algorithm for moving the mesh has four components. Figure 3.2 illustrates these components and the process flow between them. The first component is the simulation of the biochemical system for a time τ on a specific mesh (denoted as Ω_a) starting from an initial state $\mathbf{x}_a(t)$ to a final state $\mathbf{x}_a(t+\tau)$:

$$\mathbf{x}_a(t+\tau) = \text{RDME}(\mathbf{x}_a(t), \Omega_a, \tau).$$

The second component is the computation of the velocity field v at the boundary of the domain, as a function the state of the biochemical system. In our motivating example of the growth of the yeast mating projection, the internal turgor pressure pushes uniformly on the cell wall, but the wall expands preferentially where it has been softened by the enzymes. Thus, the instantaneous velocity field of the growing mating projection is a function of the spatial distribution of the cell wall modifying enzymes within cell. See Section 3.3.3 for more details, and Figure 3.7 for an illustration.

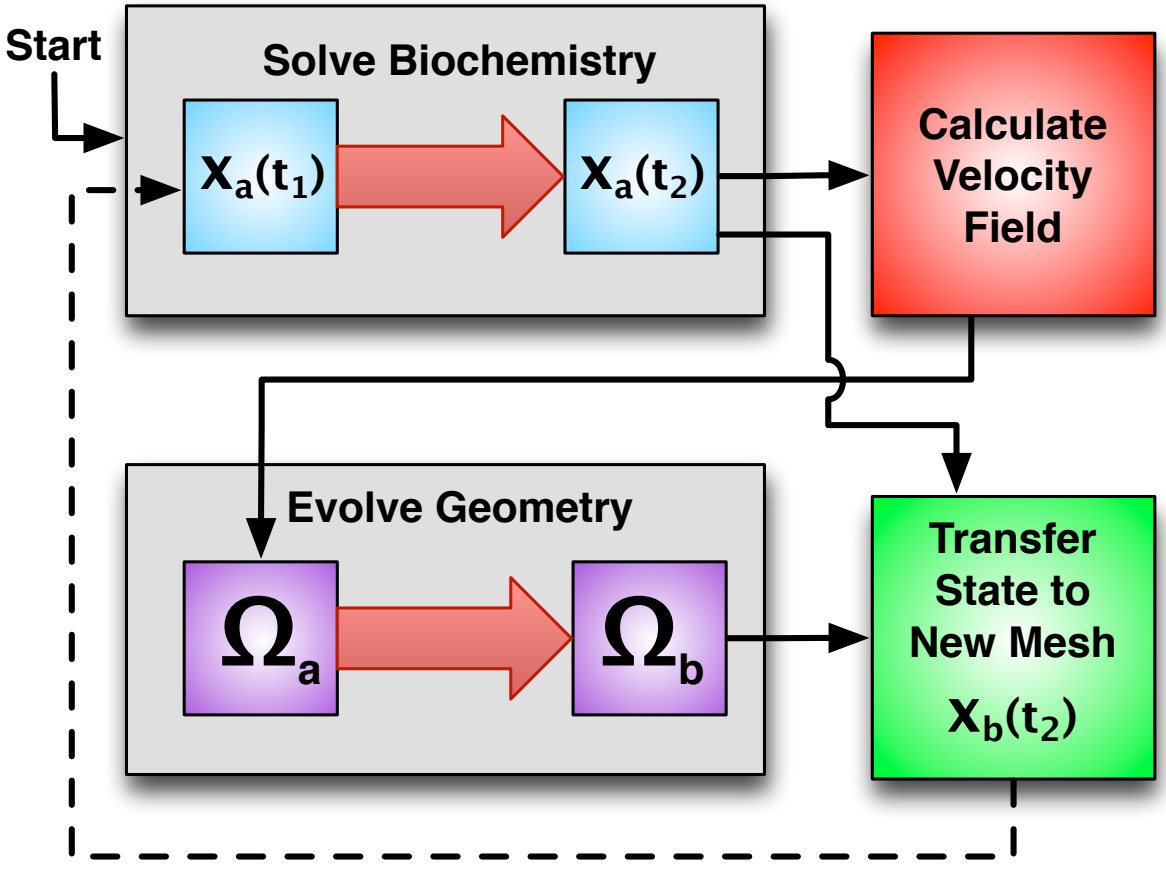

Figure 3.2: Diagram illustrating the process flow of the moving mesh algorithm.

This is the component that couples the biochemical simulation with the moving domain. This function is part of the model being simulated, and is thus provided by the user as input to the method. The function can be of only the final state of the biochemical system, $\mathbf{x}_a(t+\tau)$, or of some aggregate of all previous states, $\mathbf{x}_a(0:t+\tau)$:

$$v = \left.\frac{d\Omega}{dt}\right|_{t+\tau} = f_{\Delta\Omega}(\mathbf{x}_a(0:t+\tau)).$$

The third component is the evolution of the mesh over the simulation time step τ. Using the domain boundary velocity calculated previously, a new mesh is created by evolving the mesh linearly over the time step. This is done by moving each mesh point according to the velocity field at that point, via the forward Euler method. In our software implementation, this is done via the FEniCS/Dolfin package [48].

$$\Omega_b = \Omega_a + \tau\, v$$

The final component of the algorithm is the method for transferring the state of the biochemical system from the current mesh, Ω_a to the newly created mesh, Ω_b. On each step of the moving mesh simulation the x, y, z position of each particle is sampled on Ω_a. An assumption of the RDME is that particles are uniformly distributed within each voxel. Consequently, the position of the particle is sampled uniformly from its containing voxel's volume. Since the boundaries of a voxel are often difficult to compute on an unstructured mesh, we make an approximation and sample the position from a sphere with a volume equivalent to that of the containing voxel. It is important to note that this assumption induces a spatial error that is proportional to the mesh resolution and the quality of the mesh. That is, the more elongated the tetrahedrons are, the more error is induced in the sampled particle's spatial position. Implementations of this algorithm must ensure that

the mesh is of sufficient quality throughout the simulation. Next, the particle is assigned to the closest voxel new mesh, Ω_b (minimizing Euclidian distance) to the sampled x, y, z position. Often in systems biology models, biochemical species are required to remain in specific subdomains of the system. For example, membrane bound proteins must remain on the membrane, which is modeled as the voxels on the boundary of the mesh. If the species of a particle is restricted to a subdomain in this way, then it is moved to the closest voxel that is within that subdomain. If the sampled position of a particle falls outside the domain Ω_b, then it is placed at the closest voxel (that is of an appropriate subdomain) within Ω_b. See Figure 3.3 for an illustration. This procedure is repeated for each particle within the system, thus the biochemical state of the system is transferred from Ω_a to Ω_b, which we denote as

$$\mathbf{x}_b(t) = \text{ParticleRedistribution}(\mathbf{x}_a(t), \Omega_a, \Omega_b).$$

The iterative algorithm is described in Algorithm 1.

Algorithm 1 Spatial Stochastic Simulation for a Domain with a Moving Boundary

Require: Ω_0, $f_{\Delta\Omega}$, τ_{split}, $\mathbf{x}_0(0)$, t_{final}, and the Biochemical Reaction Network

Ensure: $[\Omega_0 \cdots \Omega_n]$, $[\mathbf{x}_0 \cdots \mathbf{x}_n]$

1: $i = 0, \quad t = 0, \quad \tau = \tau_{split}$

2: **while** t $< t_{final}$ **do**

3: $\quad \mathbf{x}_i(t : t + \tau) = \text{RDME}(\mathbf{x}_i(t), \Omega_i, \tau)$

4: $\quad v = f_{\Delta\Omega}(\mathbf{x}_i(t : t + \tau))$

5: $\quad \Omega_{i+1} = v\,\tau\, + \Omega_i$

6: $\quad \mathbf{x}_{i+1}(t + \tau) = \text{ParticleRedistribution}(\mathbf{x}_i(t + \tau), \Omega_i, \Omega_{i+1})$

7: $\quad i = i + 1, \quad t = t + \tau$

8: **end while**

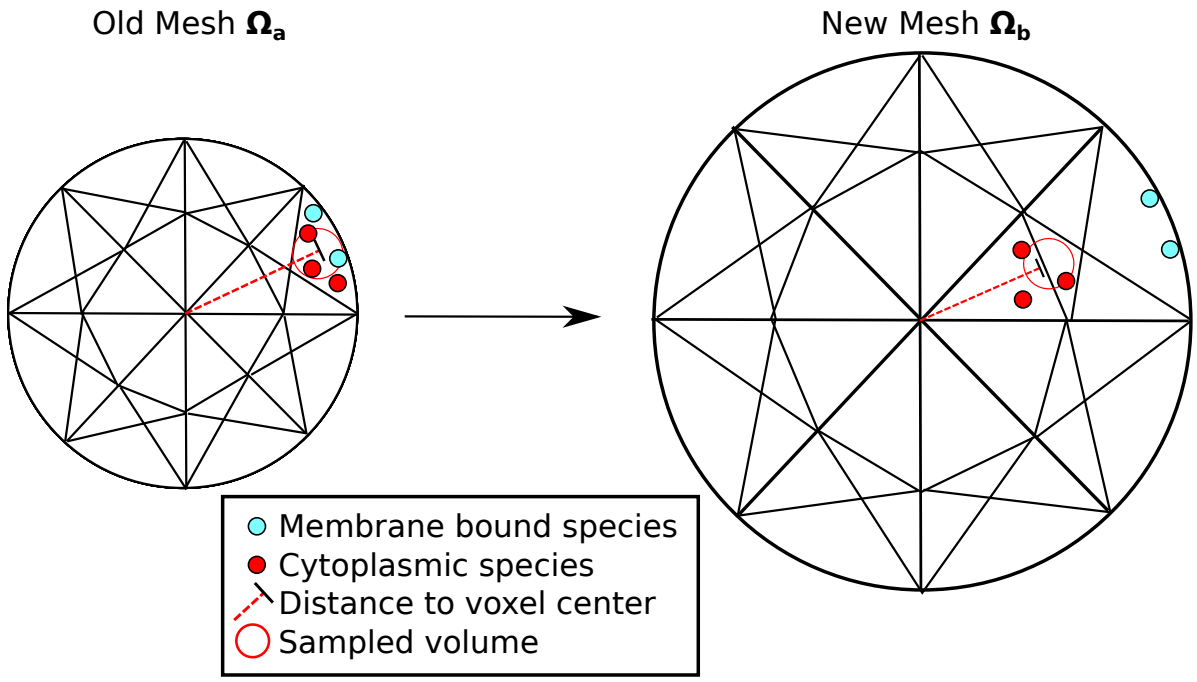

Figure 3.3: Diagram illustrating the particle redistribution process. On each step of the moving mesh simulation the state of the biochemical system is transferred from the old mesh (left) to the new mesh (right). The x, y, z position of each particle is sampled on the old mesh (uniformly from within the volume of the containing voxel), the particle is assigned to the voxel in the new mesh that is closest to that sampled position . If the species of a particle is restricted to a subdomain (e.g. membrane-bound proteins), then it is moved to the closest voxel in that subdomain.

3.2.1 Rejection-based step size selection

We extend the method presented in Algorithm 1 to include an adaptive method for error control. We will see in Example 2 that the error our method incurs will depend on the velocity of the domain and the operator splitting time step. To implement our adaptive error control time stepping scheme, we define a new input d_{max} as the maximum distance any given point on the boundary is allowed to move in any single time step. In each step, if the magnitude of any component of the velocity multiplied by the time step τ is greater than d_{max}, then that step is rejected, the time step is set to half its previous value, and the state is recomputed over the new time step. The accepted time step will then be used for the next step of the algorithm. Finally, if the step is accepted on the first pass (no rejection) and the time step had been previously reduced (τ is less than τ_{split}), then the time step for the subsequent step, τ_{next}, is increased to double the current time step size. See Algorithm 2 for details. Note that, as the simulation of the RDME by the NSM algorithm is a continuous operator, we are able to sample at any specified time within the interval $[t, t+\tau]$. This allows us to avoid recomputing the biochemical state when a step is rejected, leading to a more efficient implementation. In our simulations, for each invocation of the NSM operator we sample the state of the RDME at $[t+\frac{\tau}{8}$, $t+\frac{\tau}{4}$, $t+\frac{\tau}{2}$, $t+\tau]$. This allow us to halve the timestep three times without recomputation of the biochemical system. It should be noted that to avoid biased simulations, the state of the random number generator must be preserved when the step is rejected and the step restarted with the same state.

Algorithm 2 Adaptive Spatial Stochastic Simulation for a Moving Boundary Domain

Require: Ω_0, $f_{\Delta\Omega}$, d_{max}, τ_{split}, $\mathbf{x}_0(0)$, t_{final}, and the Biochemical Reaction Network

Ensure: $[\Omega_0 \cdots \Omega_n]$, $[\mathbf{x}_0 \cdots \mathbf{x}_n]$

$i = 0, \quad t = 0, \quad \tau = \tau_{split}$
while t $< t_{final}$ **do**
  $\mathbf{x}_i(t : t + \tau) = \mathrm{RDME}(\mathbf{x}_i(t), \Omega_i, \tau)$
  $v = f_{\Delta\Omega}(\mathbf{x}_i(t : t + \tau))$
  $d = ||v||_\infty \tau$
  if $d > d_{max}$ **then**
    repeat
      $\tau = \tau/2$
      $v = f_{\Delta\Omega}(\mathbf{x}_i(t : t + \tau))$
      $d = ||v||_\infty \tau$
      $\tau_{next} = \tau$
    until $d \leq d_{max}$
  else if $\tau < \tau_{split}$ **then**
    $\tau_{next} = 2\tau$
  end if
  $\Omega_{i+1} = v\,\tau\, + \Omega_i$
  $\mathbf{x}_{i+1}(t + \tau) = \mathrm{ParticleRedistribution}(\mathbf{x}_i(t + \tau), \Omega_i, \Omega_{i+1})$
  $i = i + 1, \quad t = t + \tau, \quad \tau = \tau_{next}$
end while

3.3 Results

Here we present three examples to verify and to demonstrate the utility of our method.

3.3.1 Example 1

In our first example, we demonstrate numerically that our method converges in distribution as the time step decreases. In a general problem the error depends on multiple factors, such as the time step, the mesh resolution, and the quality of the mesh. To isolate the error induced by the time step selection, we consider a 1D domain Ω of width $R - L$, where R is the right endpoint and L the left endpoint. A single species S diffuses (with $D = 1$), associates with and dissociates from the left boundary. We let Ω expand to the left; thus L is a function of time t. Specifically we let

$$L(t) = -vt,$$

where v is the constant speed of the expansion.

The domain is discretized into N_{vox} voxels, each of width h. We denote the microscopic association rate by k_r and the microscopic dissociation rate by k_d. The mesoscopic rates, k_a^{meso} and k_d^{meso}, are then given by $k_a^{\text{meso}} = k_a/h$ and $k_d^{\text{meso}} = k_d$, as shown in [14]. We set $L = 0$ and $R = 1$ initially.

To show that our method is accurate, we simulate the system until the final time $T = 1$, and compare the spatial distribution of particles to the spatial distribution obtained with a more detailed Brownian dynamics method [73]. The error will be a function of the speed of expansion v, the time step Δt_{split}, the number of voxels N_{vox}, and the reaction rates k_r and k_d. We expect the error to be larger for a large v, as the boundary moves more during each time step. For small enough N_{vox} the spatial resolution will be insufficient, and the error will consequently be large. To demonstrate these effects we ran simulations with Δt_{split} varying from 0.01 to 0.2 with $N_{\text{vox}} \in \{5, 20, 50\}$.

We simulated 10^6 molecules and computed the Kolmogorov-Smirnov distance between the spatial distributions of unbound particles at the final time point T (with the domain

expanding at constant velocity, convergence at the final time point implies convergence throughout). In Figure 3.4 we show that, as expected, the error decreases with decreasing time step Δt_{split}.

3.3.2 Example 2: Density Dependent Switch for Polarization in an Expanding and Contracting Sphere

In our second example, we verify the accuracy of our method by comparing against the analytical solution of a biochemical model found in the literature. To demonstrate the applicability of our method to biologically relevant problems, we have implemented a simple model of polarization in yeast on a moving domain. In particular, we focus on a model of polarization presented in [35] that relies on a minimal positive feedback circuit. This model is particularly interesting, as it has been shown to polarize only when modeled stochastically, opposed to deterministically. The yeast cell is modeled as a sphere with a membrane on the surface of the sphere. The model has three reactions between two species: cytosolic Cdc42 spontaneously attaches to the membrane with rate k_{on} (Eq. 3.1), membrane-bound Cdc42 likewise spontaneously detaches with rate k_{off} (Eq. 3.2), and finally membrane-bound Cdc42 recruits cytosolic Cdc42 to the membrane at rate k_{fb}, to close the positive feedback loop (Eq. 3.3).

$$Cdc42_c \xrightarrow{k_{on}} Cdc42_m \tag{3.1}$$

$$Cdc42_m \xrightarrow{k_{off}} Cdc42_c \tag{3.2}$$

$$Cdc42_c + Cdc42_m \xrightarrow{k_{fb}} 2Cdc42_m \tag{3.3}$$

The cytosolic and membrane-bound species can diffuse at rates D_{cyt} and D_{mem} respectively (the diffusion of the membrane-bound Cdc42 being restricted to the membrane).

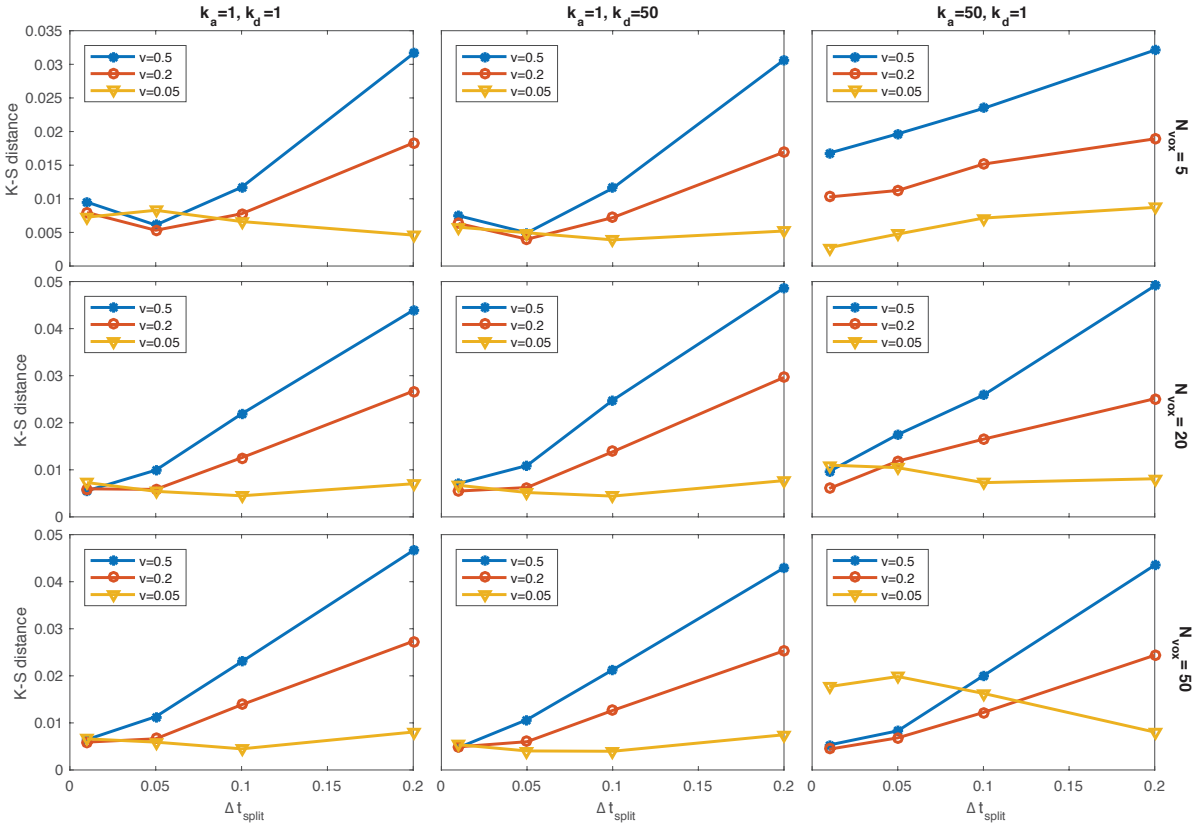

Figure 3.4: Error in distribution as a function of the size of the time step for a 1D moving domain with an absorbing/desorbing boundary for three different reactive rates (columns), and three different spatial discretizations (rows). Our mesoscopic method was compared a Brownian dynamics microscopic simulation of 10^6 molecules. We define the error as the Kolmogorov-Smirnov distance between the spatial distributions of unbound particles at the end time (1s). As we can see by comparing the middle three panels to the bottom three panels, the error is similar with $N_{vox} = 20$ and $N_{vox} = 50$, meaning that the problem is spatially well-resolved already with $N_{vox} = 20$, while for $N_{vox} = 5$ we can see that the system is not fully resolved for the case of $k_a = 50$ and $k_d = 1.0$. As expected, the larger the speed v of the expansion, the larger the error, but as the splitting time step Δt_{split} decreases, so does the error. For $v = 0.05$, the domain is expanding so slowly that the stochastic error dominates, and no difference is seen as Δt_{split} varies between 0.01 and 0.2.

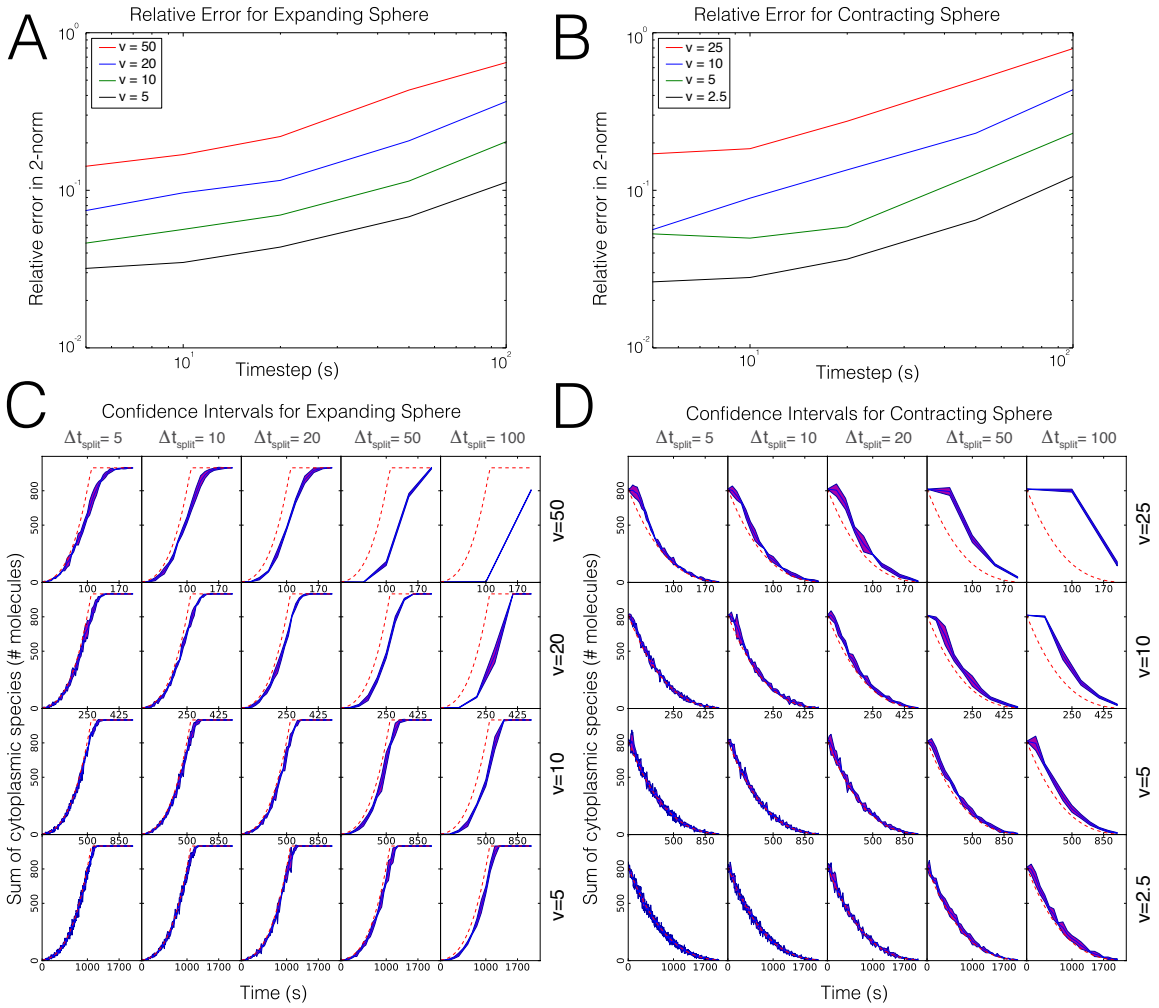

Figure 3.5: Comparison of our method to theoretical results from the literature. As expected, the error for our method decreases with the velocity of the boundary and the time step. A: Relative error in 2-norm for a variety of expansion velocities (v) and operator-split timesteps for an expanding sphere. B: Relative error in 2-norm for a variety of contraction velocities (v) and operator-split timesteps for a contracting sphere. C: 95% confidence intervals for three trajectories at a variety of expansion velocities (v) and operator-split timesteps (Δt_{split}) for an expanding sphere, along with the theoretical value (dashed red). D: 95% confidence intervals for three trajectories at a variety of contraction velocities (v) and operator-split timesteps (Δt_{split}) for a contracting sphere, along with the theoretical value (dashed red).

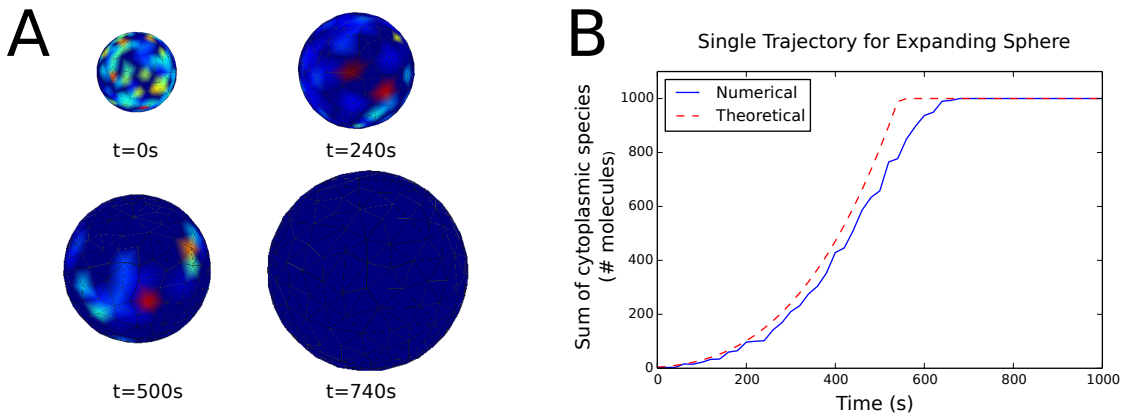

Figure 3.6: A: Time series of heatmaps showing the number of membrane-bound molecules on the surface of an expanding sphere (note that the radii are not to scale and by 740 seconds there are no molecules on the membrane). B: An example of a single trajectory showing the number of cytoplasmic molecules versus time for an expanding sphere along with the theoretical value as calculated from [35]. Note that for each parameter value, multiple realizations were run and averaged before being compared to the theoretical value.

This model was shown in [35] to have a density dependent switch. That is, there is a critical range for polarization of molecules on the membrane. This range is from a lower critical density necessary to facilitate polarization to an upper density above which molecules become essentially homogeneous on the membrane (i.e. not polarized). From [35] it is also possible to calculate theoretically the steady state ratio of molecules in the cytoplasm for any given density, which we will use as a comparison for our simulations.

To test our moving boundary algorithm, we implemented the model described above in an expanding and contracting sphere for a fixed number of total molecules. For the expanding sphere case, the initial radius was set below the theoretical switch value calculated from [35]. Specifically, the critical radius can be calculated as follows

$$\frac{4}{3}\pi r_{crit}^3 = N\frac{k_{fb}}{k_{off}} \tag{3.4}$$

where N is the total number of molecules (cytosolic and membrane-bound) and r_{crit} is the critical radius. Here we set $N = 1000$ and $\frac{k_{fb}}{k_{off}} = 0.9$, thus from Eq. 3.4 we have $r_{crit} = 6.425\mu m$. From the initial radius (below the critical radius), the radius of the sphere expands at a constant velocity to a final value which is greater than the critical radius. The error incurred by our operator split method is dependent on both the speed at which the sphere expands and the operator split time step that is chosen. Again, the error here is defined as the relative error between the number of cytosolic molecules in the simulation and the theoretical steady state value calculated from [35]. We calculated this error over a range of expansion velocities and operator split time steps to investigate the convergence behavior for our method. A similar test was performed for a contracting sphere which starts at a radius just below the critical value and decreases at a constant velocity to some final radius. The results of these convergence studies are shown in Fig. 3.5. As expected, the larger the velocity of radial expansion, the more error the method will generate for both the expanding (Fig. 3.5A) and contracting (Fig. 3.5B) sphere cases. The same trend can be seen for large time steps (Fig. 3.5A,B). Note that for each parameter value multiple realizations were run and averaged before being compared to the theoretical value. The 95% confidence interval for three realizations of the number of cytosolic molecules at each parameter value is shown for the expanding sphere in Fig. 3.5C and for the contracting sphere in Fig. 3.5D. An example time series of heatmaps showing the number of membrane bound molecules on the surface of an expanding sphere can be seen in Fig. 3.6A, with red being a higher number of molecules and blue a lower value. Also, a sample trajectory of the expanding sphere simulation can be seen in comparison to the theoretical steady state solution in Fig. 3.6B (here with parameter values of $\frac{dr}{dt} = 10nm/s$ and $t_{split} = 20s$). Again, the purpose of this example problem is to characterize the error incurred by our method as compared to theoretical results in the literature and specifically, to elucidate how this error depends

on the velocity of the boundary and the time step. This example also demonstrates the utility of our method for studying problems of biological relevance.

3.3.3 Example 3: Formation of the Yeast Mating Projection

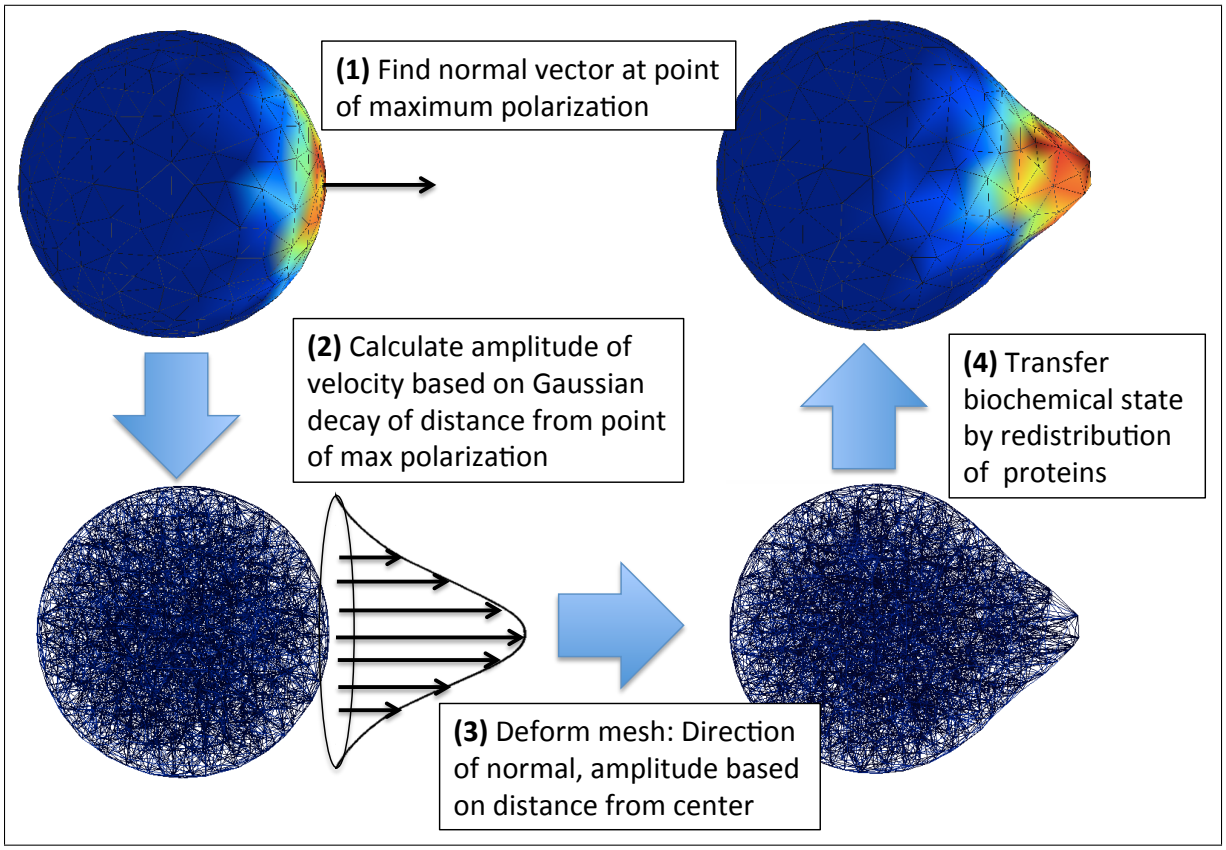

Figure 3.7: Diagram describing the process where polarization of the yeast model (spatial profile of protein concentration) is used to calculate the deformation of the domain. At each time step of the algorithm the following process is repeated. First the biochemical system is simulated using the spatial stochastic solvers in PyURDME for a length of Δt. Next the point of maximum polarization is found and the normal vector calculated at that point. Then, the velocity of the surface is calculated using the normal vector as the direction, with the amplitude calculated from a Gaussian function centered at the maximum polarization point (empirically parameterized). The mesh is then deformed by the application of the velocity field. Finally, the biochemical state of the system is transferred to the new mesh.

In our third example, we show the use of our method on a biologically relevant

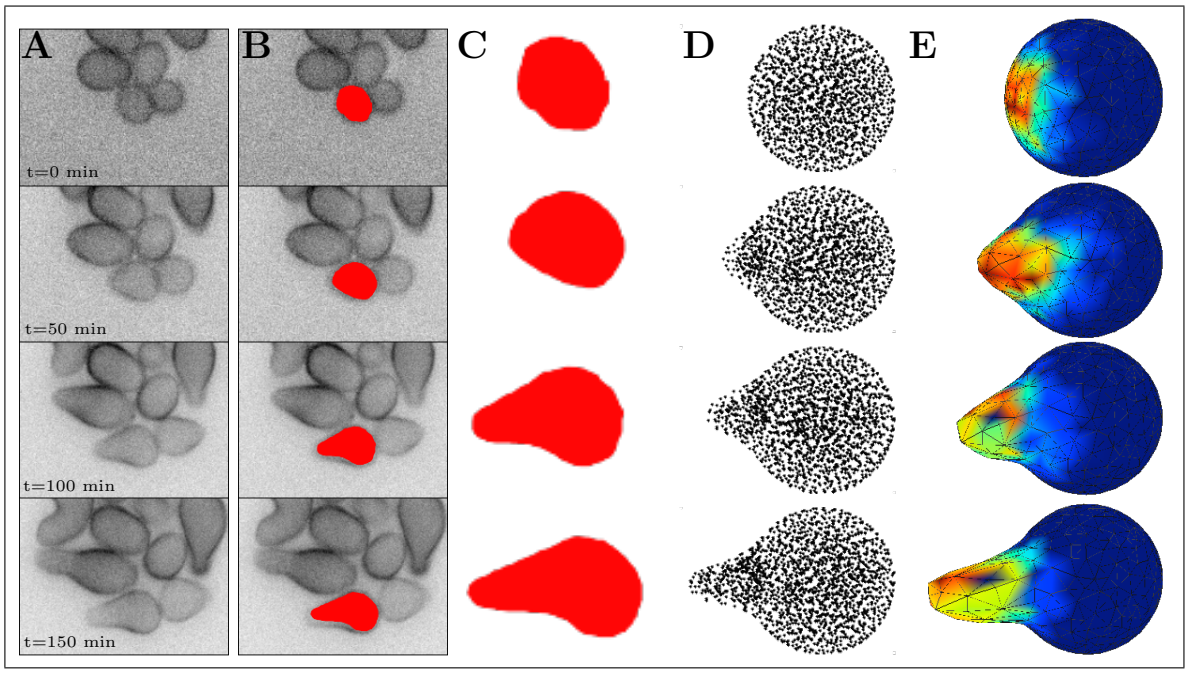

Figure 3.8: Comparison between microscopy images of yeast cells during polarized growth and simulations of the growing yeast mating projection. A: Fluorescent microscopy time-lapse images of yeast cells during exposure to mating pheromone (α-factor). Cells are tagged with Mid2-GFP (see Section 3.5 for experimental details). B: Manual cell shape extraction overlaid on microscopy images for a single cell. C: Enlarged cell shape without microscopy image. D: Scatter plot of the voxel centers of our simulation results projected onto a plane containing the origin and the point of greatest polarization. E: 3D visualization of the simulated growing yeast cell, where the color map shows the concentration of active Cdc42 on the membrane (red corresponds to the highest concentration, and blue to the least).

system that couples the biochemical reactions with the moving boundary. Our motivating problem is the polarization of proteins during mating of *Saccharomyces cerevisiae*, and the resulting growth of the mating projection.

Yeast cells sense mating pheromone in their extra-cellular environment, and determine the direction of their mating partner by sensing the chemical gradient. The chemical gradient of pheromone induces polarization of the yeast cell, localizing proteins and actin cables to the region of the yeast cell that is closest to a nearby mating partner. The mating projection starts to form when the polarisome organelle is formed at the site of polarization. The polarisome acts to coordinate the formation of the mating projection via the transport of cell wall cutting enzymes as well as cell wall material and synthase proteins. As these processes work together, the yeast cell changes shape from a spheroid to grow a projection.

To simulate this process we present a new spatial stochastic biochemical model of yeast polarization, centered around the polarization of the protein Cdc42. This model is a novel combination of reactions published in [16] and [85]. As these models were originally presented deterministically, for use with this method we have converted the reactions to a mechanistic and stochastic formulation. The key component from [16] is what is known as a GDI reaction which preferentially moves the inactive form of $Cdc42$ from the membrane to the cytosol. Diffusion is much faster in the cytosol than on the membrane and this difference in diffusion is what leads to a Turing-type mechanism for pattern formation, as originally discussed in [15]. The essential components from [85] are a negative feedback mechanism through the protein $Cla4$ and recruitment of $Cdc24$ to the membrane by *Gbg* (the $\beta\gamma$ subunit of the heterotrimeric G-protein which is activated in response to pheremone during yeast mating). Both [16] and [85] originally modeled their respective reactions using deterministic PDE models. Here we take certain key reactions from both models and model them mechanistically using the RDME formalism.

To present a simplified model of polarization, we omit the dynamics of the receptor-ligand binding (presented elsewhere [86, 87]) and take as input to the model a time-constant spatially varying concentration of the activated G-protein (beta-gamma subunit). A detailed description of this model can be seen in Figure 4.1 and the S1 Model in Section 4.5. The biochemistry determines the moving boundary by expanding the sphere at the point of greatest polarization, in the direction of the normal at that location. The other points on the boundary of the domain are moved in a parallel direction, with the magnitude attenuated by a Gaussian of the distance to the point of maximum polarization. This is illustrated in Figure 3.7.

Figure 3.8 shows a comparison between our yeast polarization simulation results (columns D and E) and microscopy images of a polarizing yeast cell (columns A-C). Column B shows the outline of the yeast cells overlaid on the microscopy images, and column C shows just the outline of these cells. Column D shows a scatter plot of the voxel centers of our simulation results, projected onto a plane containing the origin and the point of greatest polarization. Column E shows the 3D visualization of the simulated growing yeast cell, where the color map shows the concentration of active Cdc42 on the membrane (red corresponds to the highest concentration, and blue to the least). The frames (rows) in column A-C are separated by 50 minute intervals. In this simulation, the state of the biochemical system and the movement of the boundary are fully coupled. This figure shows a qualitative match between a real cell phenotype and our biochemical model simulated via our method.

3.4 Conclusions

We have developed a method for simulating stochastic biochemical reactions on time-dependent domains using the RDME formalism. This method involves the following

steps: simulating the RDME on a fixed geometry for a given time step, using the state of the biochemical system as input to a function that moves the boundary in a user-specified manner, over that same time step, redistributing the molecules in the system to the new geometry and then repeating until a specified end time. Our method simulates the RDME on unstructured meshes, which enables it to easily handle the complex geometries that often show up in biological applications. We have shown, through various example problems, that the error our method will incur depends on a few key factors, including the specified time step, the speed of the moving domain, the diffusion constants of the species and the reaction rates of the system. We have also demonstrated the potential usefulness of such a method by simulating the biologically relevant problem of shmoo formation during the mating of yeast, a problem where spatial stochastic effects are important and the geometry is changing in time as a result of the state of the biochemical system.

We have implemented this method in our spatial stochastic modeling and simulation software package PyURDME [13]: the Python package for simulation of Unstructured mesh Reaction-Diffusion Master Equation models. The reaction-diffusion biochemical model system has been extended to allow the inclusion of a movement of the mesh, as well as inspection of the resulting mesh quality and adaptive mesh refinement are accomplished via integration of the open source finite element package FEniCS/Dolfin [48]. The software package, along with instructive examples, are available from our code repositories on Github.

This method is generally applicable to problems arising in systems biology where spatial and stochastic effects are critical and the physical geometry is changing in time. In particular, this method is applicable to the common case in systems biology where the movement of the boundary of a cell is directly determined by the state of certain biochemical species. The error will be more manageable for systems where there is some separation of timescales between the movement of the boundary and the diffusion rate

of the biochemical system. In the future, we hope to extend our analysis of biologically relevant problems with coupled biochemistry and domain movement, such as in shmoo formation in yeast mating. Other specific systems where this method could be useful include: tip growth in fungal hyphae [78], chemotaxis in neutrophils [71], cell migration [79] and cell division [9, 72]. Another future direction is to develop a method that more closely couples the dynamics of the moving boundary and the biochemistry thus avoiding the error involved in splitting the two, but this is a considerably more involved problem.

3.5 Experimental Details

Time-lapse imaging was performed on Mid2-GFP cells adhered to glass slides using concanavalin A in standard yeast-peptone-dextrose (YPD) media with the stage heated to 30°C. Both fluorescent and bright-field images were taken at 10 minute intervals over a three hour period using a Nikon TE-2000 inverted microscope with an ORCA-2 CCD camera controlled by MetaMorph software. The yeast strain was constructed by fusing GFP onto the C-terminal end of *MID2* using genomic integration of a W303-1A strain that is *bar1*Δ (RJD863).

Chapter 4

The Effect of Cell Geometry on Polarization in Budding Yeast

In the previous chapter, we presented a method for simulating spatial stochastic dynamics on moving domains. Ultimately we will use this method for simulating both polarization and mechanics to yield mating projection growth. One issue that has previously not been considered in depth in the polarization literature is what the effect of non-spherical geometries (such as those produced during projection growth) on the dynamics of polarization can be. In this chapter, we present work that more thoroughly investigates the effect that complex, tip-shaped geometries can have on the dynamics of polarization. This work was done in close collaboration with Brian Drawert, Carlos Gomez, Samhita P. Banavar, Tau-Mu Yi and Otger Campàs and was originally published in [17].

4.1 Introduction

The polarization of proteins during the mating of *Saccharomyces cerevisiae* is a well-studied, yet not fully understood, example of pattern formation in biology. During the

mating process, haploid yeast cells respond to a gradient of mating pheromone via a cascade of intracellular protein reactions, culminating in a localization of key proteins on the membrane that facilitate actin cable formation and vesicle transport [30]. Many quantitative models exist, at varying levels of mathematical complexity, for the different levels of polarization in both budding and mating. Broadly, the majority of models have been developed to study the dynamics of the main polarity regulator, the Rho GTPase Cdc42 [15, 2, 16], the formation of actin cables and the polarisome [3, 31, 32], or the interaction between the two [33, 31, 34]. Reviews of polarization models can be found in [35, 36, 37, 38]. The literature for models of polarization in yeast is vast and often contains conflicting results regarding the role of different mechanisms. One key feature that has only recently been addressed is the effect of stochasticity, with some studies having shown that it can be critical for certain models [3, 2]. In particular, stochastic dynamics can more robustly reproduce a highly polarized phenotype and track a moving pheromone input [3].

Stochastic dynamics at the intracellular signaling level has become a standard modeling paradigm in many areas of biology. There are numerous cases where deterministic or mean-field techniques do not capture the relevant dynamics of biological systems [4, 5, 6]. Stochasticity is critical particularly when the copy number of a key chemical species is very small, as is often the case within single cells. Many methods exist to numerically simulate stochastic biochemical networks, the most common of which is the Stochastic Simulation Algorithm (SSA) or Gillespie algorithm [7, 8]. One assumption of the SSA is that the system is well-mixed, meaning that the reactants are assumed to be equally likely to be anywhere in the spatial domain. This assumption clearly does not apply in many systems, including our system of interest, polarization in yeast mating. The spatial nature of our system necessitates the use of spatial stochastic methods, of which there are many. One common approach relies on the Reaction-Diffusion Master Equation

(RDME) formalism [9, 10, 11, 12]. Using RDME techniques, we have studied the protein signaling network involved in polarization in previous works [3, 13, 14]. In particular, we are interested in understanding how these protein signaling networks interact with cell mechanics to yield morphogenetic change, such as the growth of the mating projection.

When the coupling of mechanics and biochemistry in this system is considered, the physical domain of the numerical simulations necessarily becomes time-dependent as the cell changes shape over time. We have previously developed an algorithm to simulate spatial stochastic reactions on time-dependent domains using the RDME formalism [14]. Many existing models [15, 16, 3, 2] treat polarization as a Partial Differential Equation (PDE) in simple 1 or 2 dimensional geometries (such as a line or circle). One key feature that is lost in these simulations is the effect that a more realistic geometry can have on these reaction networks. Although recent work has noted a qualitative effect of geometry on simplified models of polarization in yeast mating [88], a thorough characterization of these effects on more complex reaction networks and geometries has yet to be performed. In this chapter, we investigate the effect of cell geometry during mating projection growth on recently developed models of polarization in yeast mating. In particular, we simulate 3D spatial stochastic models of polarization in tip-shaped geometries obtained from simulations of the mechanics of the yeast cell wall. We show that this effect is meaningful and needs to be studied further to more deeply understand how biochemistry and mechanics interact to create morphogenetic change, such as the growth of a mating projection.

The effect of geometry on biochemical reaction networks, and in particular on the spatial localization of such models, has been studied in other contexts. Notably, a model of protein localization and cell division in *E. coli* showed that the geometry of the cell can induce pattern formation even in networks with no dynamic instability [80]. The effect of complex geometries on models of polarization for different systems has also been studied and shown to be important [89, 90, 91, 92, 93, 94, 95]. For example, cell shape

and elongation were shown to be critical for polarization in cell chemotaxis and the speed of response to chemical gradients [89, 90, 95]. Another study revealed that an interaction between cell shape and biochemical regulatory loops with negative regulators can help explain information flow in neurons [94]. Most models of polarization in cells contain both membrane bound and cytoplasmic species, with reactions taking place on the membrane. A critical feature mentioned in the above studies is the surface area to volume ratio of different shapes. This will no doubt have an effect on models of this type, but exactly what the effect will be for a given nonlinear network of reactions is not known.

To address these issues in the context of yeast mating, it is our goal to study the effect of realistic, 3D tip-shaped geometries on current spatial stochastic models of polarization in yeast. To this end, we use computational studies to generate predictions of the effects of geometry on polarization during yeast mating, and compare to experimental results. These simulations have been performed in our software PyURDME [13] which can simulate spatial stochastic dynamics on complex, 3D and time-dependent geometries. Our results certainly do not encompass all current models of polarization or even attempt to quantify all of the possible effects different geometries can have on these models, but rather demonstrate that realistic geometries can have major effects on a general class of polarization models and thus needs to be considered more thoroughly in modeling moving forward. We also raise the question of what mechanisms the cell uses to overcome the apparent destabilizing effect of cell geometry on the location of the polarization cap *in vivo*, and provide some plausible answers.

4.2 Results

4.2.1 Effect of geometry on models of Cdc42 polarization

To study the effect of realistic geometries on the dynamics of models of Cdc42 polarization, we first needed to create computational meshes of such realistic geometries. To do this, we extracted shapes from a model that combines cell wall mechanics and assembly to determine the shape of the cell during projection growth [18]. This model was critical in showing that a feedback between growth and mechanics is needed to stabilize mating projection growth in such systems. Since the timescales of cell wall expansion and growth (cell shape changes) are much longer than the timescales of the molecular reactions involved in cell polarization, we simulate molecular polarization models in a fixed geometry. Our first test was to run a relatively detailed, mechanistic model of Cdc42 polarization adapted from the budding literature [16] (see Figure 4.1A and the S1 Model in Section 4.5 for details) with polarized initial conditions in a typical tip-shaped geometry. A detailed description of the models and parameters used in this chapter can be found in Section 4.5, along with a more detailed description of the computational methods in the Materials and Methods section. As seen in Figure 4.1B, the polarization of active Cdc42 can be seen "drifting" out of the tip over the course of 700 seconds. The top panel of Figure 4.1B shows a time series of a histogram of active Cdc42 density on the surface versus arc-length away from the tip, while the bottom panel shows the same time series with a plot of the full 3D surface concentration of active Cdc42. The polarization cap can be seen to start in the tip of the projection and then drift out (while staying as an intact cap) as time goes on. This model of polarization is known to be stable in time for spherical geometries (see results below and [16]) so this drifting behavior would seem to indicate that there is some clear destabilizing effect on the location of the cap by the geometry itself. This is a crucial result because during mating projection growth,

polarization of key proteins must stay in the tip of the projection for proper growth. It is important to note that Figure 4.1B represents results from only one stochastic realization. To further characterize and understand this result we have run multiple realizations of similar simulations for different geometries, which we discuss further below.

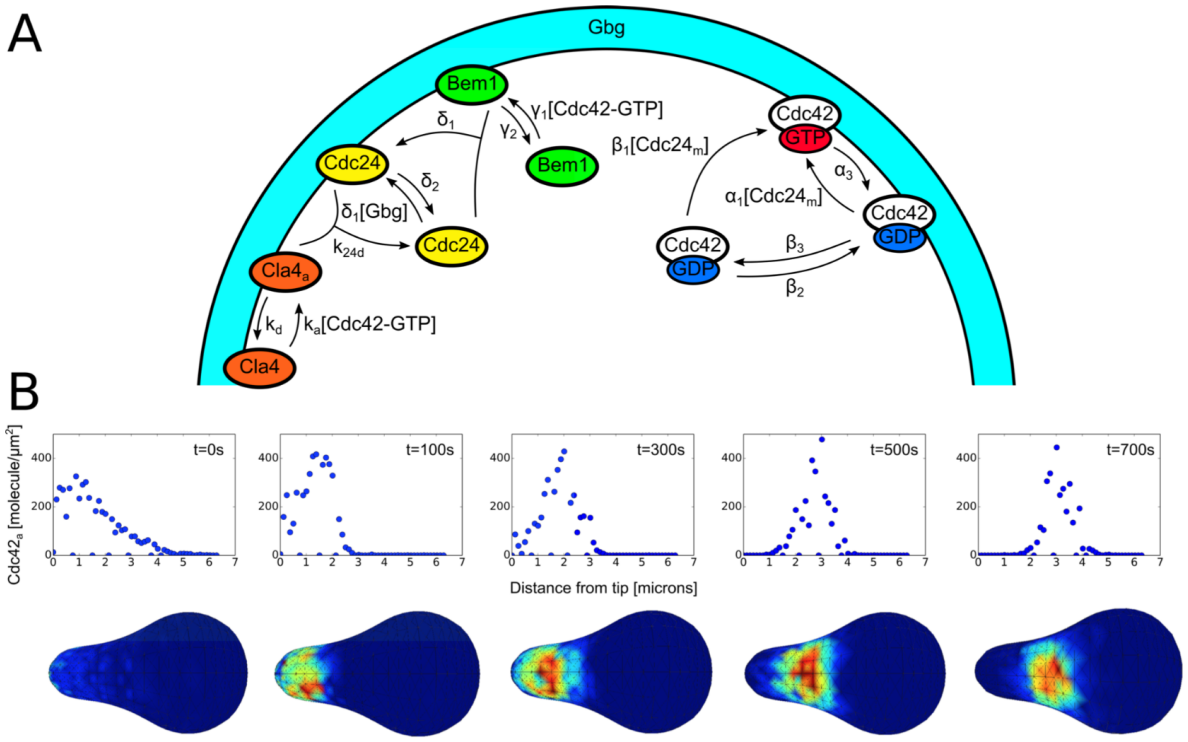

Figure 4.1: **Schematic of Cdc42 model and drifting of Cdc42 cap for one realization.** A: Schematic of the detailed, mechanistic model of Cdc42 polarization. Adapted from [16]. Here a uniform input of Gbg is used to model the effect of mating pheromone. B: Visualization of the active Cdc42 polarization cap drifting away from the tip during one realization. The top panel is a plot of the surface density of active Cdc42 versus the distance away from the tip along the perimeter of the shape for various time points (to get a 1D plot, the 3D profile was averaged along the surface of the shape). The bottom panel shows the corresponding 3D visualization of the active Cdc42 distribution. The drifting shown here took place in a matter of 700 seconds.

To more fully characterize the effect of geometry on the dynamics of this model of Cdc42 polarization, we have run similar simulations to that presented in Figure 4.1B on a variety of shapes. Specifically, we look at four shapes chosen to roughly approximate

the different shapes a yeast cell can take during the formation of a mating projection. The computational meshes (again obtained from a simulation of the mechanics of the cell wall [18]) can be seen in Figure 4.2B. The first set of experiments is equivalent to that of Figure 4.1B. Namely, we start the simulation with the species polarized in the "tip" of the geometry (for the sphere there is obviously no tip but the polarization is simply started in the same place for each realization) and run multiple realizations for each geometry in Figure 4.2B. To quantify the end result of each realization, we record the center of the polarization cap (see Figure 4.2A for visualization) in spherical coordinates after 1000 seconds of simulation. The results of these simulations can be seen in Figure 4.3 where the spherical coordinates for the center of polarization of active Cdc42 after 1000 seconds are plotted for 800 realizations. The tip of the shape is set to be at $\theta = 90°$ and $\phi = 180°$ and the dashed red lines in Figure 4.3 represent $\pm 10°$ from the tip. For the spherical geometry, the active Cdc42 polarization cap is very stable for the duration of the simulation, while for the other tip-shaped geometries the cap can be seen to drift to a manifold away from the tip (as visualized for one realization in Figure 4.1B). Moreover, the polarization cap ends on a different manifold for each of the tip-shaped geometries (each realization ends in a ring that is much larger for the "Slight Deform" geometry than for the "Projection" geometries, for example). These results add evidence to the observation that the dynamics of the polarization cap are being significantly impacted by the geometries. Moreover, the polarization cap appears to be stable in a region bounded away from the tip for these projection geometries.

One key feature of the models of polarization that we are using is that they can spontaneously polarize from random initial conditions. To further test the effect of tip-shaped geometries on the dynamics of polarization, we have run a similar set of experiments as those presented in Figures 4.1B and 4.3, but start with random initial conditions rather than polarized. Again, the center of the polarization cap was recorded

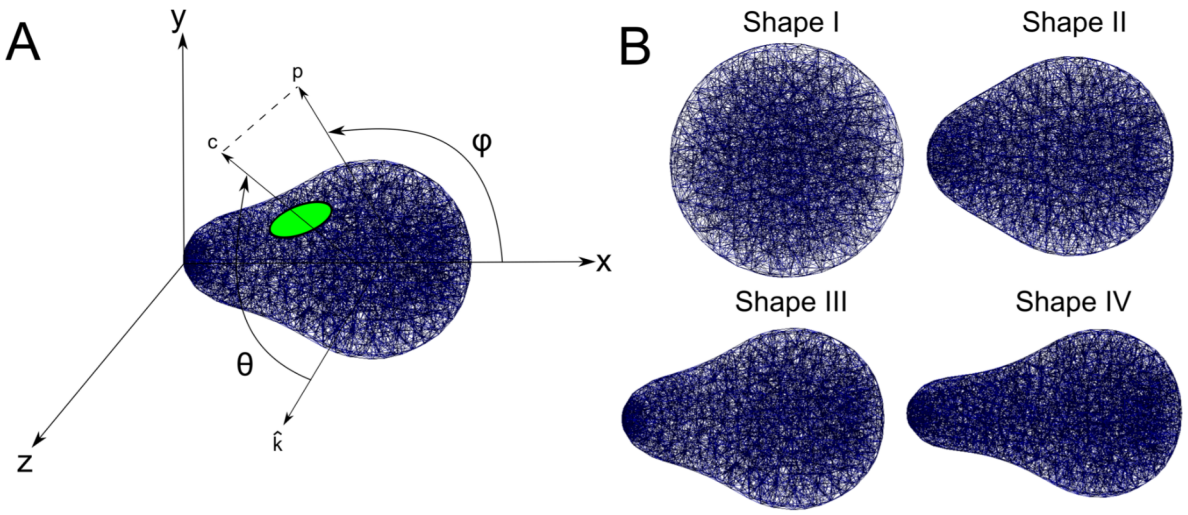

Figure 4.2: **Diagram of angles and geometries used in subsequent simulations.** Visualization of the geometries and computational meshes used throughout this study. A: Shown here is an example of the relevant geometry and angle definitions that will be used in later analysis. The green ellipse is meant to symbolize the active Cdc42 polarization cap. The vector c is drawn from an origin on the x-axis through the center of the polarization cap and the vector p is the projection of c onto the xy-plane. The angle θ is defined in the usual way in spherical coordinates and is the angle from the z-axis to the vector c and is between 0 and 180 degrees. The angle ϕ is defined as between the x-axis and p and is between 0 and 360 degrees. In this way we can quantify the position of the polarization cap. B: The four computational meshes that will be used throughout this study. They are meant to represent yeast mating projections at different stages of formation. To solve for these shapes, a mechanics solver from [18] was used.

after 1000 seconds and the results of several realizations can be seen in Figure S1. In the spherical geometry, the polarization cap is distributed randomly over the sphere for several realizations (as expected, as the model has no preference or external bias and polarizes spontaneously) while, again, for the tip-shaped geometries the polarization caps cluster in a manifold away from the tip. Moreover, these polarization sites are the same as those seen in Figure 4.3, meaning that the polarization cap is stabilizing in the same place for both polarized and random initial conditions. This result adds evidence to the claim that these locations in the tip-shaped geometries are globally stable for

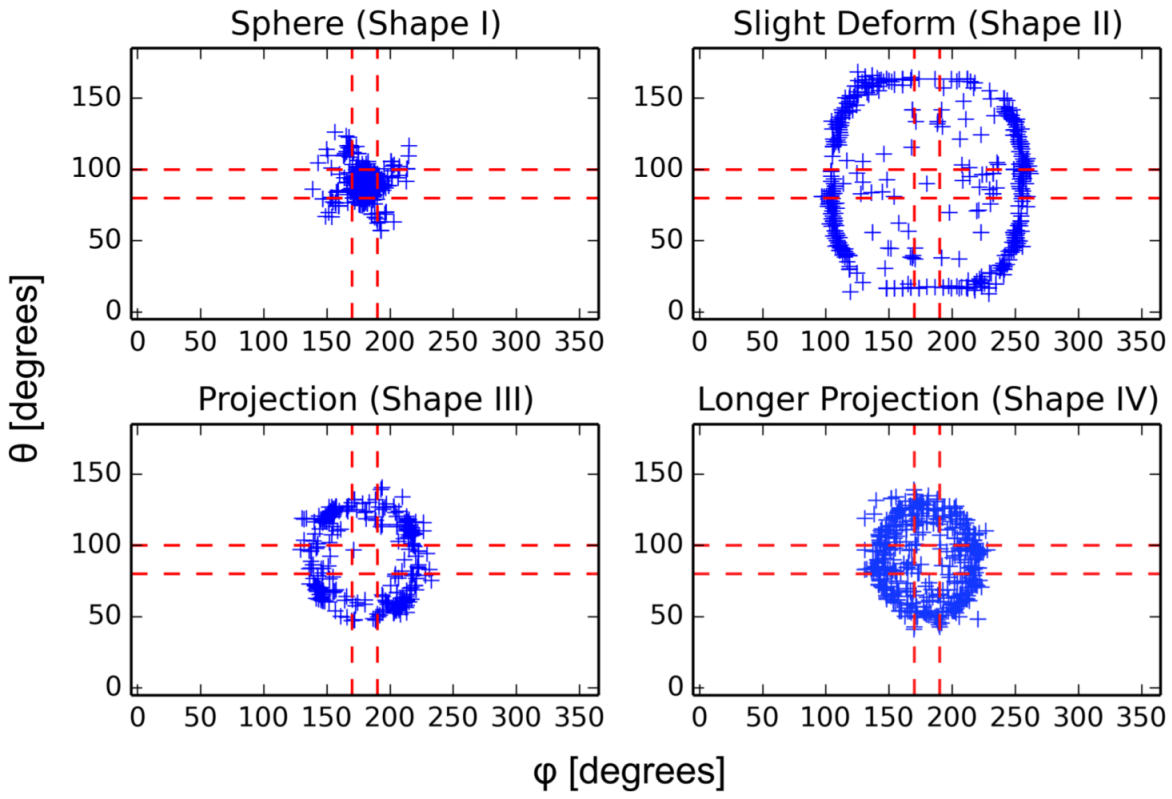

Figure 4.3: **Spherical coordinates of the center of active Cdc42 polarization for multiple realizations with polarized initial conditions.** Here the center of the polarization cap is tracked for four different shapes with 800 realizations each. Plotted is the θ and ϕ coordinates (explained in Figure 4.2A) of the center of the polarization cap after 1000 seconds of simulation starting from polarized initial conditions at the tip ($\theta = 90°$ and $\phi = 180°$). Each point represents the result of one stochastic realization. We can see that for the three irregular tip shapes the polarization cap has drifted away from the tip, whereas for the sphere the cap is stable. The dashed red lines delineate a region of $\pm 10°$ from the tip, with the red square in the center representing the tip of the projection. The four plots correspond to the four domains shown in Figure 4.2B.

this particular model of Cdc42 polarization. Again, this is critical in that it implies that simply changing the geometry of the domain can drastically affect the dynamics of polarization. There is clearly an interplay between the geometry, diffusion in the bulk and on the membrane, and the reactions that is leading to this effect on the location of the polarization cap, which we will discuss more later.

In addition to the more detailed mechanistic models of Cdc42 polarization studied above, there are many simplified models of Cdc42 polarization that are simpler mathematically and preserve some of the key features of polarization. We have also looked at the effect of tip geometries on these simplified models of polarization. In particular, we studied the effect of geometry on the simplified model presented in [1, 2]. This model contains only the membrane bound and cytoplasmic versions of Cdc42 with three reactions: attachment and detachment from the membrane and recruitment of cytoplasmic species by membrane bound species (see Figure 4.4A and the S2 Model in Section 4.5 for details). Interestingly, this model has been shown to exhibit clustering behavior only when modeled stochastically, as opposed to deterministically. Again, the advantage to this model is that it is much simpler in the number of species and reactions, while the disadvantage is that it does not fully capture the polarization dynamics seen in cells. Specifically, this model will lead to sporadic clusters that are not stable in time but rather form and break up dynamically and indefinitely. Thus, a different metric is needed to quantify the effect of geometry than was used for previous models. For this reason, we have run the S2 Model in the same four geometries presented in Figure 4.2B for $10,000$ seconds and simply averaged the amount of membrane bound Cdc42 in each voxel over time. The results can be seen in Figure 4.4 below. Again, there is a clear qualitative effect of these geometries on the dynamics of this simplified model. Namely, the clusters are seen in Figure 4.4C-E to systematically stay out of the projection. The overall effect of some negative interaction between the tip geometry and polarization is preserved. Both of these models show that there is a clear effect of geometry on the dynamics of polarization, and more specifically that there is a tendency for polarization to avoid the projection in these geometries. This further raises the question of how cells overcome this effect *in vivo*, which we will explore below.

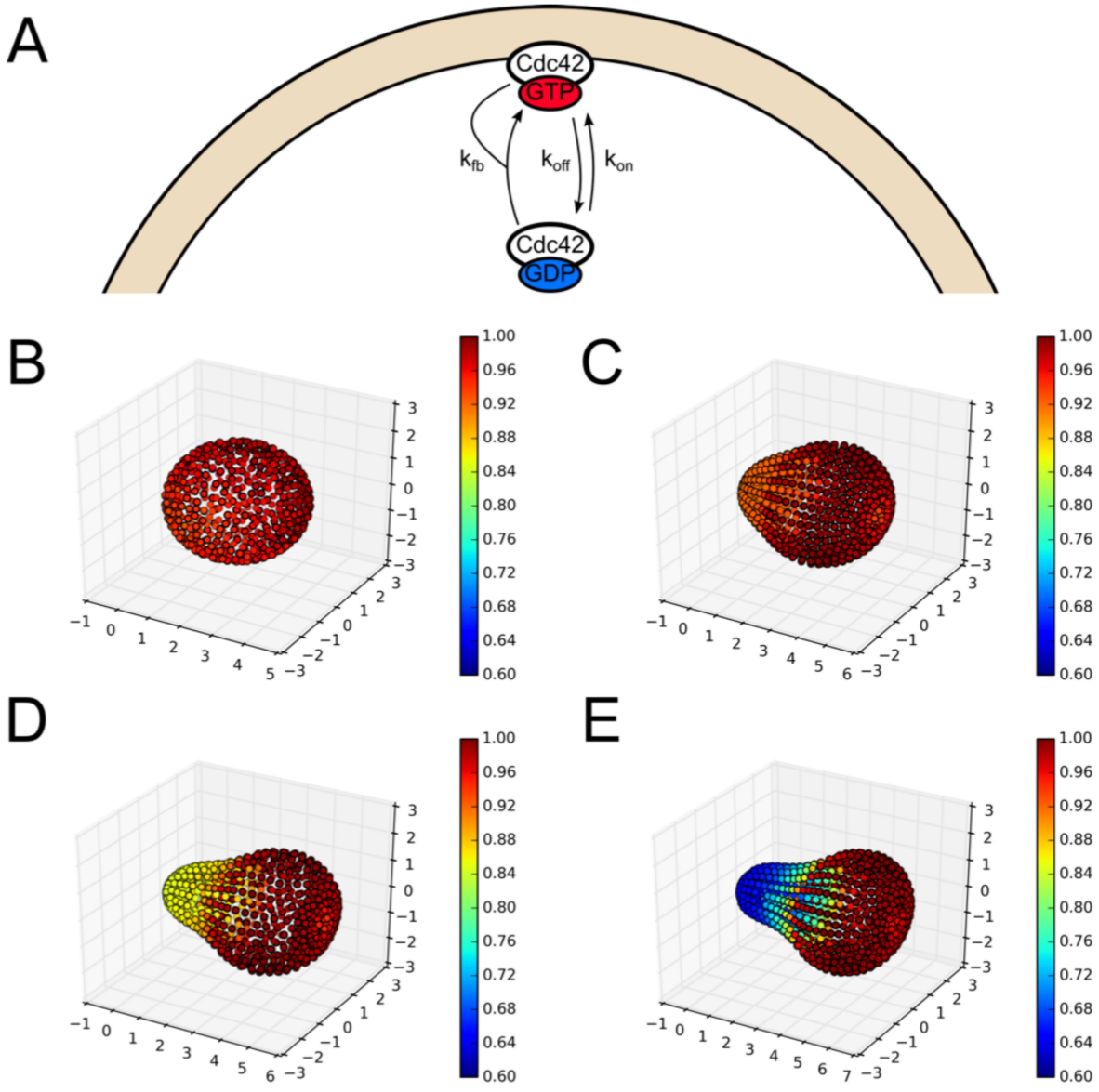

Figure 4.4: **Effect of geometry on a simplified model of Cdc42 polarization.** A: Schematic of the simplified model of Cdc42 polarization. Adapted from [1, 2]. B-E: The normalized time average of the concentration of membrane bound species for each voxel is shown for four different geometries. The model presented in [2] and the S2 Model was run for 100,000 seconds for each geometry in Figure 4.2B with a total of 200 realizations for each. As mentioned above, this model exhibits stochastic clustering that is dynamic in time, with clusters forming and breaking up. A clear bias can be seen, with stochastic clusters systematically staying out of the tip of the projection, which is qualitatively similar to the results presented in Figure 4.3.

4.2.2 Effect of large deformations and changes in density on models of Cdc42 polarization

In addition to the geometries studied in the previous section, we investigated the effect of geometry on the same reaction-diffusion models, for more pathological geometries. Specifically, we simulated the Cdc42 polarization model on geometries with projections much longer than those seen in WT cells. We will discuss the physical relevance of these shapes when comparing to experimental results in the next section. We first ran a computational experiment similar to that presented in Figure 4.3, but on the long projection geometry. The results of this simulation can be seen below in Figure 4.5. Surprisingly, when starting with the model polarized in the tip of the projection, the polarization cap was in fact more stable in the tip of the projection. This is in contrast to the results presented above with much shorter projections. Presumably, this is due to the fact that there are multiple meta-stable points for the polarization cap throughout the geometry. In the case of the short projection, the size of the polarization cap (set by the specific reactions and diffusion rates of the model) is on the same order as the spatial distance between the tip and the more stable position (the neck of the projection in this particular case). While for the longer projection, the size of the polarization cap is much smaller than the length of the projection. We will discuss these results further below.

A related, yet quite distinct, issue to changes in geometry is changes in volume of the cell and density of the species. It is well known that these models, in general, can have very different dynamics with varying density of some or all of the species. In fact, the model presented originally in [2] and above in Figure 4.4A was shown specifically to be a density dependent switch. That is, stochastic clustering fails to occur below some critical density due to all of the molecules being in the cytoplasm at steady state, yet there exists a range of critical densities that exhibit clustering. Eventually, if the density

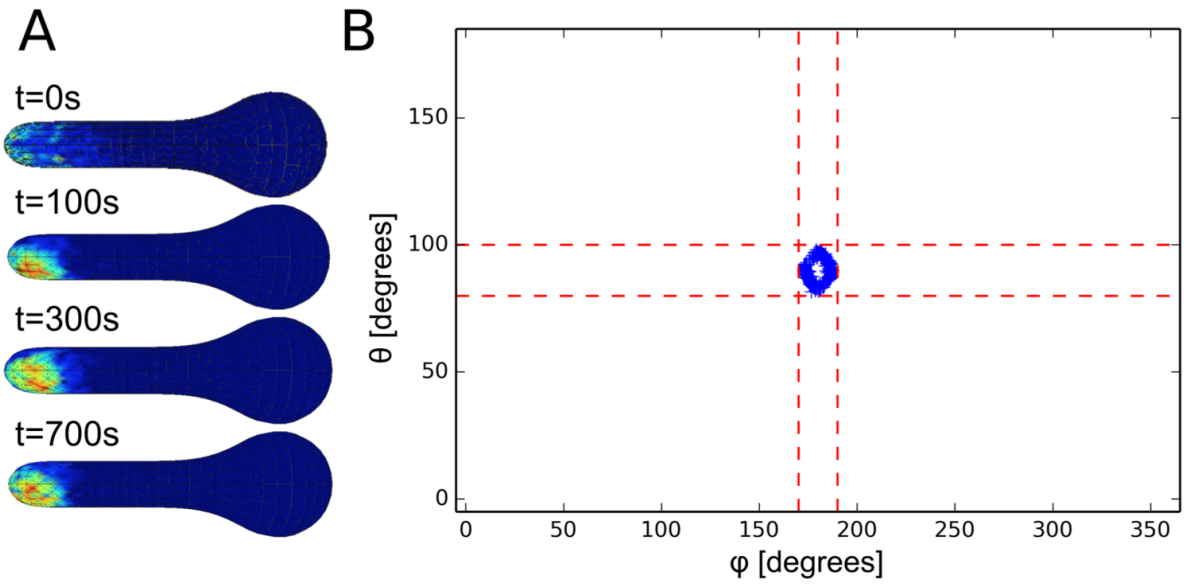

Figure 4.5: **Effect of long projection on Cdc42 polarization.** Visualization of effect of a long projection geometry on Cdc42 polarization. A: Time series for one realization of Cdc42 polarization starting from polarized initial conditions. The polarization cap can be seen to drift slightly away from the tip but still stay in the projection. B: Summary of where the polarization cap ends up starting with polarized initial conditions for 400 realizations after 1000 seconds, similar to previous results. The cap can be seen here to be much more stable in the projection compared to the shorter projection geometry results presented above.

is increased enough, clustering is lost because so many molecules will be on the membrane at steady state that it effectively creates a uniform distribution. The key challenge here is to isolate the effect of geometry from the effects of changes in density. To investigate the role of density in the polarization of Cdc42 for the S1 Model, we ran a series of simulations on spheres of different radii keeping either the number of molecules, or the density, constant. The results of these simulations can be seen below in Figure 4.6. For the constant molecule simulations there seems to be a consistent result. Namely, there appears to be one (and only one) polarization cap with an associated length scale or size. For the small sphere, the size of the polarization cap is larger than the sphere itself thus it appears uniform. For the constant density simulations, there is a variety of behaviors.

Notably, the larger sphere has two distinct polarization sites. This is surprising in that the original model in [16], from which the S1 Model is adapted, explicitly noted that, at the base values, it is important that only one broad polarization site formed and then narrowed, as opposed to some other models that show competition between clusters (for example in [15]). This shows that in addition to cell geometry, whether the cell fixes density or number of molecules also affects polarization. As for the results presented above in Figures 4.3 and 4.4, these geometries deviated only $10 - 15\%$ in volume from the sphere, as opposed to the large scale changes seen in Figure 4.6 and were run with a constant number of molecules as opposed to a constant density. For completeness, these simulations were also run with a constant density and the overall results were similar (see Figure S4 for details). As mentioned above, the density of molecules throughout the spatial domain can have an important effect on these models. To look at the effects of changes in density independently from changes in overall shape we have run a series of simulations on spheres of different radii. The results in Figure 4.3 and Figure S4, which deal specifically with the effect of changes in overall shape, and the results in Figure 4.6, which deal with the effects of changes in density without changes in overall shape, combine to try and disentangle these two related issues. We will discuss these issues further below. These results also raise some interesting questions about how the cell regulates polarization processes to achieve certain functions. For example, a previous work has looked into the possibility of the cell using changes in density to sense cell size or trigger cell cycle transitions [96]. It might be reasonable to ask if the cell uses geometry effects to its advantage in any way.

Our results show that there is an important and noticeable interaction between cell geometry and the models we have considered here. This is important because typically, more realistic geometries have not been considered when models of polarization have been proposed. One interesting prediction here is the difference in stability of an already

formed polarization cap for different geometries. Namely, the polarization cap is stable in the sphere, unstable in a short projection and stable in a long projection (long as compared to the length scale of the polarization cap itself). This is a result that we attempted to observe experimentally. Prompted by these simulation results, we wanted to see to what extent this phenomenon could be observed *in vivo*. We describe our experimental set up and comparison to our results in the next section.

4.2.3 Comparing to experiments

While the main thrust of this work is to elucidate the effect of different geometries on various mathematical models of polarization, we wanted to test some of the overall predictions experimentally. To this end, we devised an experiment that attempts to replicate the conditions in the modeling results presented in Figure 4.3. The main prediction we are testing is that, in the absence of vesicle transport, the Cdc42 polarization cap will be stable in a sphere, unstable in a short projection and stable in a long projection. To achieve long projections, we constructed a *cla4*Δ strain. Cla4 is present in some models of Cdc42 polarization and is thought to negatively regulate Cdc24 via phosphorylation [97, 98]. As a result, some *cla4*Δ cells possess elongated projections, whereas others adopt a more typical morphology. To observe the three different shapes of interest, we allowed *cla4*Δ cells marked with Ste20-GFP (a reporter for active Cdc42) to grow in α-factor for varying amounts of time and form different length projections (Materials and Methods). Once the mating projection was formed, the cells were treated with latrunculin A (LAT-A) to depolymerize actin cables. This, presumably, leaves the cells with only the Cdc42 polarization pathway for polarization in a tip-shaped geometry, analogous to the models. The GFP-tagged polarization site was then tracked over 30 minutes. We observed cells of each shape: spherical, short projection and long projection. For each group, we cate-

gorized the polarization site as either stable (i.e. it stayed in the same spatial location after the addition of LAT-A) or unstable (i.e. it polarized in a different location after the addition of LAT-A). The results of this experiment can be seen in Figure 4.7.

As predicted, the polarization site was more stable in spherical and long projection geometries when compared to shorter projections. While overall this is a qualitative result, it does suggest an interesting interaction between the dynamics of Cdc42 polarization and the shape of the cell in both simulations and experiment. It is difficult to completely isolate the effect of geometry on polarization, as many processes are disrupted in the absence of actin cables, but we think that looking at three different shapes of cells under similar circumstances provides evidence for an effect of geometry on the dynamics of polarization. It should be noted that the experimental results for the spherical cells are not as stable as the simulation and there are multiple possibilities for why this is the case. It could be simply due to the fact that even cells that were categorized as spherical in the experiment were not perfectly spherical as in the model, but in fact ellipsoid which, based on our previous results, could have some effect on the stability of polarization. Despite these potential issues, the experimental results observed for the three classes of cells are consistent with the model simulations. Overall, there is a complex interaction between the nonlinear reaction-diffusion process and the geometry. It is plausible that there is some bias away from the tip for shorter projections due to the length scale of the polarization cap being on the same order as the projection length. This is an interesting result because it raises the question of how the cell overcomes this effect *in vivo*. We explore some possibilities in the next section.

4.2.4 Possible mechanisms to overcome the effect of cell geometry

The results above raise one seemingly important biological question for the interaction of geometry and a variety of reaction-diffusion models of Cdc42 polarization: how does the cell overcome the bias of the Cdc42 cap away from the tip during projection growth? This effect was observed simply by simulating various models of Cdc42 polarization in realistic geometries. A clear first hypothesis is that it is somehow the actin network and vesicle transport that is overcoming this effect. This is relatively difficult to test in a meaningful way simply because the methodology for modeling actin cable formation and vesicle transport in the literature is so diverse. The conclusions about the interaction of the two parallel pathways of reaction-diffusion Cdc42 polarization and actin-mediated vesicle transport are disputed. For example, one major question is whether vesicle delivery provides positive [33] or negative [31] regulation of polarization. The main issue pertains to the role of each pathway in the establishment and maintenance of the polarization site. It is likely that the diversity of opinion arises because of the vastly different ways in which vesicle transport is modeled mathematically. Nonetheless, to try to test this hypothesis, at least initially, we have coupled the previously discussed model of Cdc42 polarization to a model of actin dynamics presented in [3] (see the S3 Model in Section 4.5 for details). The key to this model of polarization is that it is mechanistic and relies on stochasticity to faithfully replicate biological data from mating yeast cells. This combination of a fully dynamic model of Cdc42 polarization and a model of the polarisome is novel.

To investigate the hypothesis that actin-mediated vesicle transport could possibly overcome the negative effect of tip-shaped geometries, we have run similar simulations to those presented in Figure 4.3. Namely, we ran the fully coupled Cdc42 and polarisome model with polarized initial conditions and tracked the polarization cap of both active

Cdc42 and Spa2 in the four shapes shown in Figure 4.2B. The results can be seen in Figure S2 and Figure S3. Again, as with the Cdc42 polarization above, the polarization cap tends to end away from the tip in these geometries, while it is relatively stable in the sphere. To test this conclusion in an even stronger setting, we fixed the active Cdc42 profile as polarized in each geometry and simulated the polarisome model with this fixed input. Even in this case, with the Cdc42 input fixed and polarized throughout the simulation, the polarisome can be seen localizing away from the tip (see Figure S5 for details). We were able to stabilize Spa2 polarization in the tip by increasing the rate of recruitment of Bni1 by active Cdc42 in this fixed Cdc42 distribution setting (see Figure S7 for details). Taken together, these results would seem to indicate, at least for this particular model, that actin dynamics are largely insufficient to overcome the effect of the tip-shaped geometry. In this case, there is again a critical interaction between cell shape and the dynamics of a model of polarization, this time with the addition of actin dynamics.

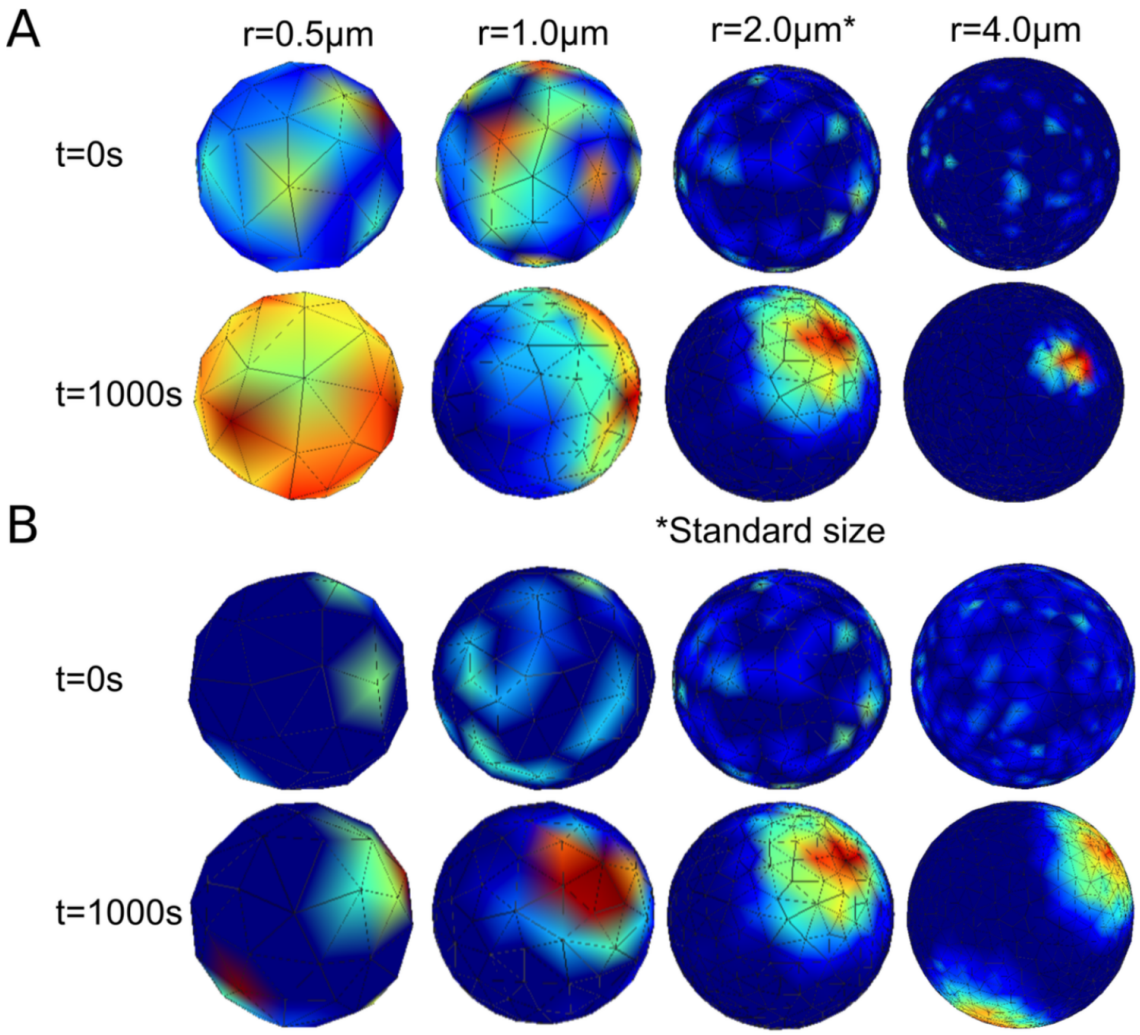

Figure 4.6: **Effect of constant density versus constant molecule count for various spheres.** Visualization of effect (for one stochastic realization) of having either a constant density or a constant number of molecules for spheres of varying radii. A: Simulations on spheres with radii $r = 0.5, 1.0, 2.0, 4.0\mu m$ are run for 1000 seconds (starting with randomly scattered initial conditions) each with a constant number of molecules, set to be the same number of molecules as the base simulation (for a sphere of $r = 2.0\mu m$ with molecule counts given in the S1 Model in section 4.5). For each sphere there is consistently one polarization cap with a certain associated length scale. For the small sphere this length scale is bigger than the sphere itself, thus it appears uniform. For the other spheres there is one polarization cap. B: Here the density is held constant (equal to that of the base simulation) rather than the molecule count. Interestingly, different dynamics can be seen. For example, the large sphere has two fully formed polarization sites as opposed to one. Presumably, the increase in the size of the domain and the number of molecules leads to the possibility of two (or more) polarization sites that will possibly compete and merge given enough time.

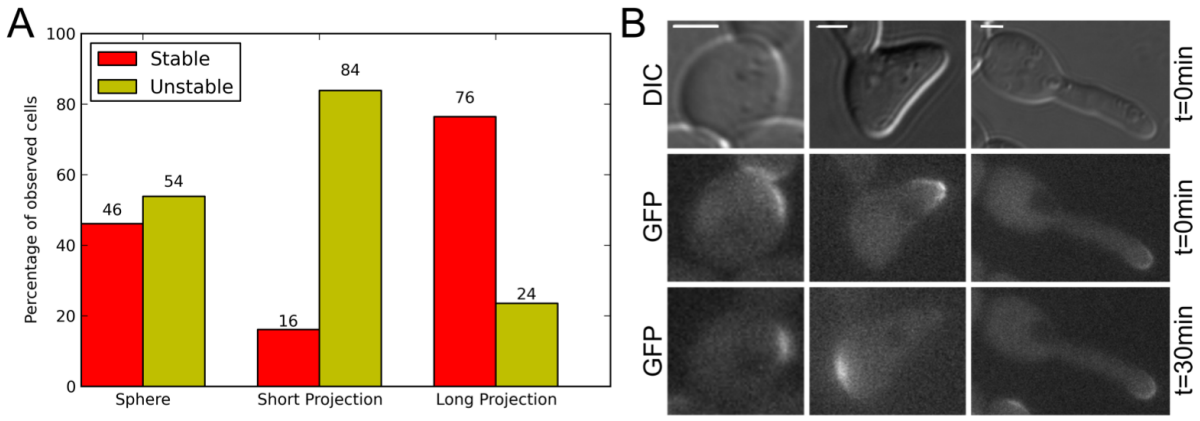

Figure 4.7: **Experimental observations of stability of polarization for different geometries.** A: *cla4*Δ cells were exposed to α-factor for varying amounts of time to observe a series of shapes of projections: spherical (n=26 cells), short projection (n=31 cells) and long projection (n=34 cells). Cells were then characterized as either stable or unstable by comparing the spatial location of the polarization cap immediately after the application of LAT-A and 30 minutes after. If the polarization cap was in the same location after 30 minutes with no actin cables (due to the LAT-A) then the cell was characterized as stable, otherwise it was unstable. The trend of spherical cells and long projection cells being more stable than shorter projection cells is in line with our theoretical prediction. The differences in the percentage of stable polarizations in the short projection cells versus the spherical ($p < 0.05$) and long projection ($p < 0.001$) cells were statistically significant by the chi-square test. B: DIC and Fluorescent images of GFP tagged Ste20 right after the application of LAT-A (t=0min) and 30 min after for a representative cell of each shape. The spherical and long projection cells here show that the polarization cap stays in the same spatial location throughout the experiment while the short projection cell re-polarizes in a different location. We predict that this instability of the shorter projection cells is due to an interaction between the geometry and the dynamics of the Cdc42 polarization network. All scale bars here represent 2 μm.

4.3 Discussion

In this chapter we have shown that there can be a noticeable effect of geometry on the dynamics of certain reaction-diffusion models of polarization in yeast. Specifically, there seems to be a clear bias away from the tip of projection shaped geometries for a number of models tested. This is important when considered in the context of mating projection growth in yeast. When growing a mating projection, the cell establishes a spatial localization of proteins on the membrane, ultimately leading to actin cable formation and vesicle transport. The vesicles carry, among other proteins, cell wall modifying enzymes that change the material properties of the cell wall, leading to projection growth. During the growth of the projection *in vivo*, it is critical that the polarization cap stays at the tip of the projection to direct growth. However, our simulations suggest that current models of polarization could fail to capture this behavior due to a previously underappreciated or unacknowledged effect of geometry on the dynamics of these polarization models. The main goal of this chapter has been to quantify this effect for a variety of different polarization models and geometries.

We first demonstrated the effect complex geometries can have by simulating two different polarization models on realistic, tip-shaped geometries. For a mechanistic and detailed biochemical model of Cdc42 polarization, we showed that even when starting with polarized initial conditions in the tip of the projection, there is a tendency for the polarization cap to drift away from the tip (see Figure 4.3). This effect was further shown by running a simpler model of polarization on these same geometries and noticing again a bias away from the projection (see Figure 4.4). Typically, these models of polarization have been formulated as PDEs in simple geometries such as a line or sphere, thus the effect of complex geometry on the dynamics of the model has not appeared.

To understand this phenomenon further, we ran these models on a variety of tubular

geometries in addition to the canonical projection geometries mentioned above. Interestingly, when simulated in a projection that was much longer than typically seen in WT yeast cells, the polarization cap would in fact stay close to the tip of the projection. This suggests there may be an interaction of length scales present in the problem. Namely, the polarization cap has a certain size in any given geometry. While currently it is not possible to a priori know the size of the polarization cap for an arbitrary geometry, the size of the polarization cap for a variety of shapes can be seen in Figures 4.1, 4.5 and 4.6. The size of the polarization cap will certainly be affected by the rates of reactions and diffusion in the model and the geometry itself. What is clear for the shorter projection geometries, seen in Figure 4.1, is that the polarization cap is of comparable size to the length of the projection. Whereas with longer projections, seen in Figure 4.5, the polarization cap is much smaller than the length of the projection. This is one possible explanation for the difference in stability between the two shapes. Specifically, it appears as though there are multiple metastable spatial locations for polarization in any geometry and the size of the polarization cap (which is related to the rates of reactions and diffusion) relative to these points may determine stability for a given initial site of polarization. Our simulations suggest that there is a complex interaction between the size of the polarization cap and the size of local features present in the geometry of the domain, for example the local radius of curvature or the length of the projection. Another related, yet distinct, phenomenon we considered here is the effect of changes in volume and density. We ran a model of Cdc42 polarization on a series of spheres of varying size, keeping either the number of molecules in the simulation or the density constant (see Figure 4.6). These results show that for large changes in volume and density, there can be significantly different dynamics for these models. The purpose of simulating polarization in spheres of varying radii was to understand the effects of changes in density independently from changes in overall shape. While a general theory for the stability of

a given polarization model in an arbitrary domain is beyond the scope of this work, the results we have presented already raise interesting biological questions.

While the main thrust of this work is to elucidate the effects that complex geometries can have on mathematical models of polarization in yeast, we were curious to see whether similar effects could be observed experimentally. The main prediction we set out to test was that of the polarization of Cdc42 being spatially stable in a sphere, unstable in a short projection and stable in a long projection. To do this, we focused on a mutant cell line *cla4*Δ. These mutant cells can grow abnormally long projections, as Cla4 plays a vital role in septin formation. In an attempt to isolate the effect of geometry on Cdc42 polarization in the absence of actin cables and vesicle transport, the cells were grown in α-factor for varying times to achieve different lengths of projection growth and then LAT-A was added to disrupt actin cable formation, leaving the cells solely with Cdc42 reaction-diffusion dynamics for polarization. Next, cells were categorized as either spherical, short projection or long projection and fluorescent Ste20 (a reporter for active Cdc42) was monitored in time. As predicted by our simulations, the polarization cap was seen to be much more spatially stable in the spherical and long projection cells than in the shorter projection cells. While overall this is a qualitative result, it does suggest that current models of polarization could be lacking elements when more complex geometries are considered.

Based on our simulation and experimental results, one of the first questions that comes to mind is: how does the cell overcome this effect *in vivo*? The first natural thought might be that it is the actin cable network and vesicle transport that is providing the necessary reinforcement. As mentioned above, this is actually quite a difficult hypothesis to test computationally simply due to the wide range of approaches in the literature for mathematically modeling this process. We merged one model of actin polarization with a model of Cdc42 polarization to test if this could provide the necessary feedback

to overcome the effect of geometry (see Figure S2 and Figure S3). Our results suggest that, at least for these particular models, actin dynamics are unlikely to overcome this effect of geometry. Again, as there are a wide variety of methods for modeling vesicle transport, it is still very possible that *in vivo* actin is contributing to overcoming the effect of geometry. One key feature that is typically neglected in models of actin cable formation is that the cables are in fact 1D structures embedded in a 3D space. Because the actin cables have a physical extent, they can be constrained by the geometry of the cell, providing a possible mechanism to overcome geometry effects. While there are methods to model such systems rigorously (see [43]), it is not common. In addition to actin though, there are other possibilities, which we will discuss in the next chapter.

This discussion raises a broader issue. Polarization is an essential part of many biological processes in a wide variety of cell types. Often, when modeling polarization, the effects that complex geometry can have on polarization dynamics are not taken into account. Our results suggest not only that there is a qualitative and important effect on certain models of polarization, but also that these interactions can lead to valuable insights into the relevant biology that might have been overlooked otherwise. Moving forward, it may be necessary to consider the effect of geometry on reaction-diffusion dynamics when models of a given polarization process are being built.

4.4 Materials and methods

4.4.1 Computational setup

All models and simulation results presented in this work were built and performed using PyURDME and MOLNs [13]. Computational meshes for each geometry consisted of a discretization of both the cytoplasm and the membrane (the surface of the shape),

allowing for diffusion both in the cytoplasm and on the membrane as required by the models used in this study. All reactions take place in voxels on the membrane for each geometry. These meshes were generated using Gmsh [99]. Sets of stochastic realizations for each model were run in parallel on a cluster of 64 machines. For simulations with polarized initial conditions (such as those in Figure 4.3), 20 realizations were run for a variety of different initial conditions. This is due to the fact that the specific configuration of the initial conditions could bias the dynamics of the model. To eliminate this bias and explore the full behavior of the model, initial conditions were rotated about the axis of symmetry (resulting in the apparent 4-fold symmetry in Figure 4.3 for example). What is important is that for any given polarized initial condition, there was a clear bias away from the tip of the projection, as discussed in the main text. One major difference in the simulation details and data analysis mentioned above is between the more detailed, mechanistic models of polarization (the S1 Model and the S3 Model) and the simplified Altschuler model (the S2 Model). This is due to a fundamental difference in dynamics between the two classes of models. While the mechanistic models reliably create one stable polarization cap (in the standard spherical geometry they were built for) the Altschuler model is more dynamic in time with clusters forming and breaking up. This is the main reason for the difference in simulation time for the two classes of models. All of the mechanistic model simulation results (found in Figures 4.3, 4.5 and 4.6 and all figures in Section 4.5) were run for the same amount of time (1000s) as this is significantly longer than these models take to come to steady state while the Altschuler model simulation results (found in Figure 4) were run for much longer (100,000s) as, again, it is more dynamic in time and does not come to a steady state with one stable, fixed polarization cap. As far as the number of realizations is concerned, we ran enough realizations to clearly show the trend for each model. For example, the results in Figure 4.3 were run for 800 realizations to clearly show the manifold where the polarization

caps were ending up while the results in Figure 4.5 were run for 400 realizations as the manifold was much easier see with fewer realizations.

Lastly, it is important to note we have no reason to believe that the effect of geometry on these models of polarization is an inherently stochastic phenomenon. That said, it is critical to note that two of the models used here (namely the simplified model of Cdc42 polarization, the S2 model, and the model of actin polarization, the S3 model) have been previously shown to rely on stochastic effects [1, 3]. Specifically, the simplified model from [1] was shown to only exhibit clustering (or polarization) when modeled stochastically as opposed to deterministically (at least for the parameters studied). Also, the model of actin polarization used, adapted from [3] was shown to replicate the experimental data of actin polarization better than the deterministic analog of the model through an effect that was dubbed "spatial stochastic amplification" in [3]. Thus, for these two models specifically it was necessary to model them stochastically for both the spherical and projection shaped geometries to faithfully replicate the dynamics of the model. As mentioned previously, though we don't have any reason to believe that this effect of geometry on the dynamics of these models is itself a stochastic effect, we are showing an effect of geometry on models that rely on stochasticity. The other model used is the paper (the mechanistic model of Cdc42 polarization, the S1 model, adapted from [16]) was the one model used that was originally formulated as a deterministic model. In theory, using a stochastic method to model the same set of reactions as a deterministic model will not be "missing" any important dynamics. Namely, the stochastic model will either replicate directly the deterministic results or there will be differences due to some stochastic effect (in which case the stochastic model will be more accurate if formulated correctly). For this particular case, our stochastic results for the spherical geometry do match the deterministic results from [16] well (although our models are not exactly equivalent as mentioned previously). One major concern with using stochastic methods

is computational efficiency. Namely, the need to run several realizations can often increase the computational requirements of the simulation. We are uniquely positioned to deal with these issues as we have developed software to efficiently simulate stochastic models and leverage cloud computing infrastructure in the process [13]. With all of this in consideration, we found it more straightforward to simulate all of our models using stochastic methods for consistency. It would be interesting to replicate our experiments in a deterministic setting to see if there are any differences in behavior but it is non-trivial to solve these reaction-diffusion models as three-dimensional partial differential equations on irregular domains and we do not currently have a framework for doing this efficiently. In summary, while we have no reason to believe at this moment that the effect of geometry is a stochastic effect in itself, two of the models we have considered rely directly on stochastic effects and in theory modeling any of these reaction-diffusion systems stochastically will not miss any important dynamics. It will be interesting going forward to replicate our simulations in a deterministic setting and compare the results.

4.4.2 Experimental setup

All yeast strains were derivatives of W303-1A and contained the *bar1*Δ mutation that prevents α-factor degradation by deletion of the Bar1 protease. Genetic techniques were performed per standard methods. All strains were cultured in YPD (yeast extract-peptone-dextrose) media supplemented with adenine. GFP-tagging was constructed by genomic integration using vectors amplified and targeted by PCR primers.

To experimentally test the computational predictions, we treated the *STE20-GFP cla4*Δ yeast strain CGY-021 with LAT-A (Invitrogen). LAT-A at a concentration of 50 μM was added to cells exposed to α-factor (1 μM) for 30 minutes (for spherical cells) or 90 minutes (for tip projected cells). These cells were imaged on slides for 30 minutes

every 2 minutes after the addition of LAT-A. Images were acquired with a Nikon TE-300 inverted microscope using a 60x objective (NA = 1.4). Image analysis was manually performed using ImageJ.

The genotype of the strain CGY-021 is *MATa, can1-100, ade2-1, leu2-3,-112, his3-11,-15, trp1-1, ura3-1, bar1::hisG, ste20*Δ*::STE20-GFP-HIS5, cla4*Δ*::KAN*^{R}

4.5 Model details and supporting figures

Figure S1 Spherical coordinates of the center of active Cdc42 polarization for multiple realizations with random initial conditions. Here, the center of the polarization cap is tracked for four different shapes. Plotted is the theta and phi coordinates (explained in Figure 4.2) of the center of the polarization cap after 1000 seconds of simulation starting from randomly scattered initial conditions. Each point represents the result of one stochastic realization. The points of polarization for the sphere are completely random, as expected from these polarization models. In contrast, the cap is forming in a similar pattern to where the caps in Figure 4.1B drifted to for the three irregular shapes, hinting at a globally stable position for the polarization cap in these geometries. Interestingly, the last shape of a longer projection actually seems to be in between randomly polarized in the cell body and preferentially polarized at the neck of the projection. The dashed red lines here are a region of $\pm 10^{\circ}$ from the tip with the red square in the center representing the tip of the projection.

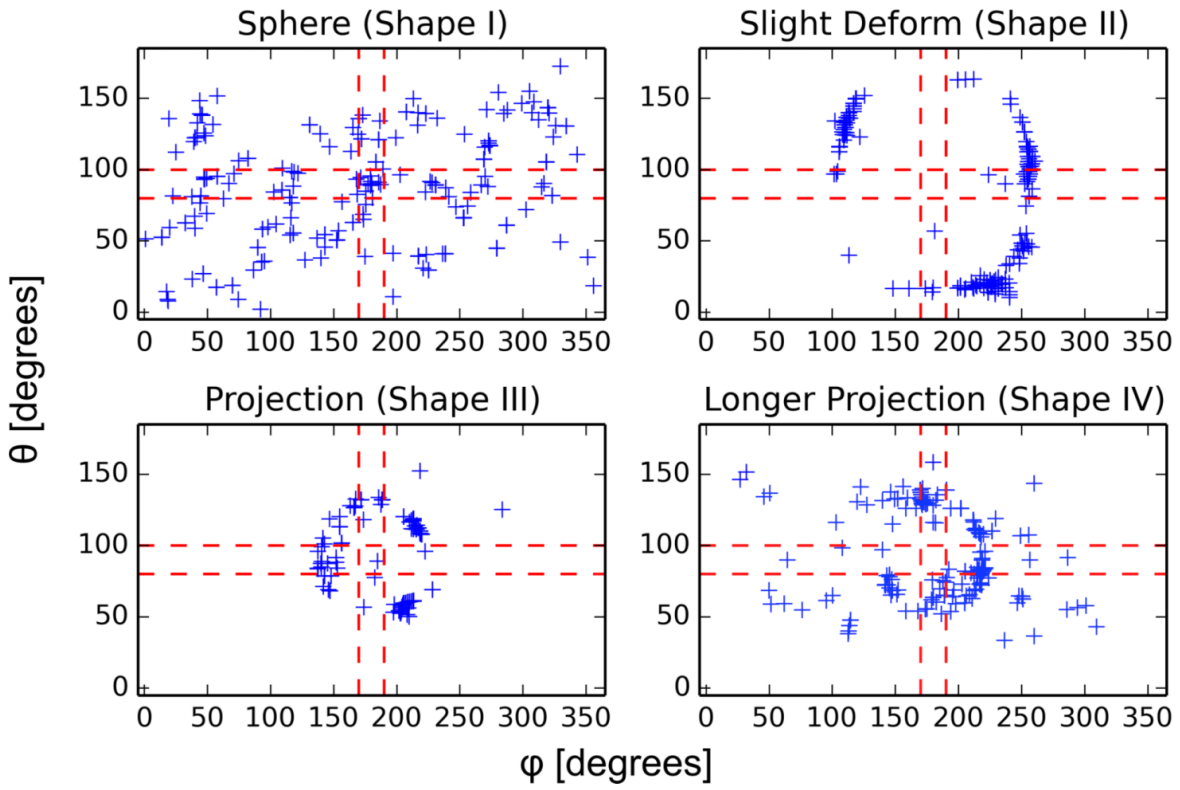

Figure S2 Spherical coordinates of the center of active Cdc42 polarization for multiple realizations with polarized initial conditions, for the combined Cdc42 and polarisome model. To initially test the hypothesis that the actin network and vesicle traffic could overcome the negative effect of the tip shaped geometry, we simulated a combined model of Cdc42 and actin polarization. As with previous simulations, starting from a polarized initial condition in the tip of the projection, the Cdc42 cap is seen to drift away from the tip. This is even with the added positive feedback from the polarisome to Cdc42. It should also be noted that the length scale of actin and Spa2 polarization is smaller than for Cdc42. While this isn't definitive proof that actin isn't helping to keep the polarization cap in the tip of the projection, it does show that for these reaction-diffusion models of Cdc42 and actin polarization, there is a persistent bias away from the tip.

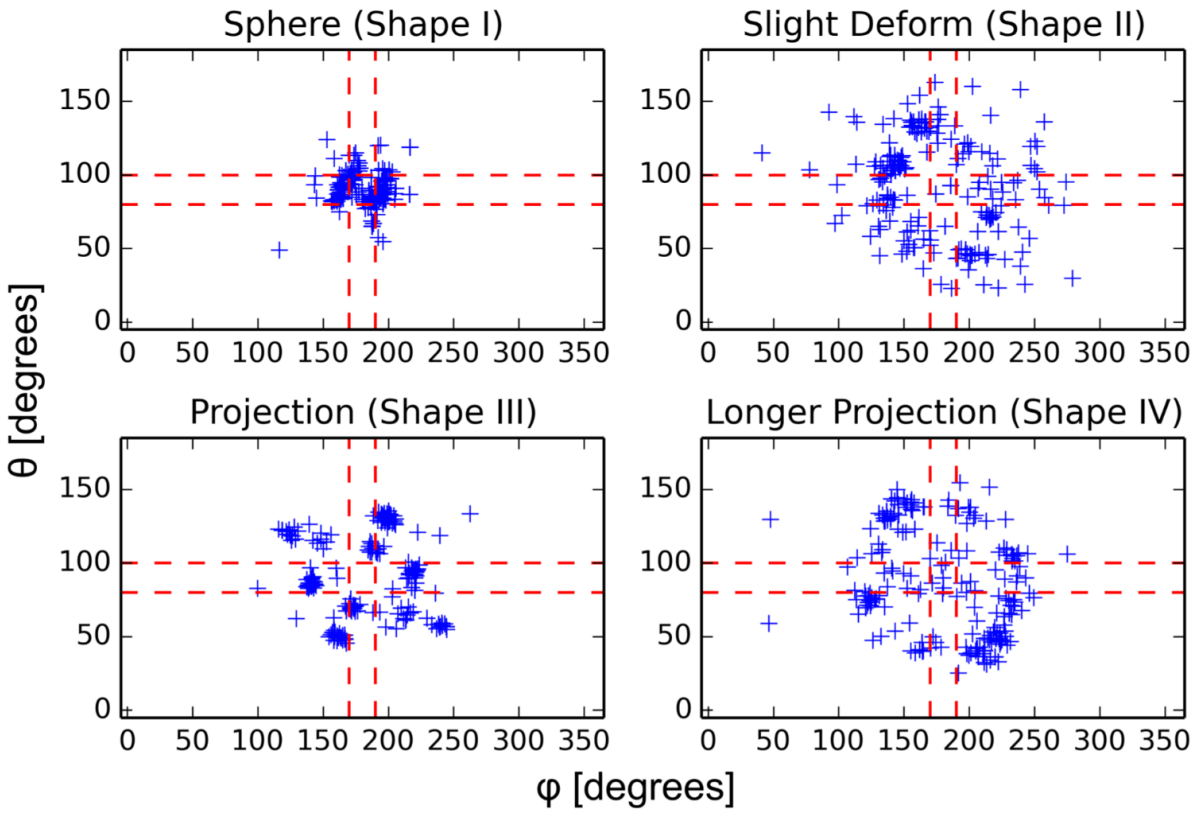

Figure S3 Spherical coordinates of the center of Spa2 polarization for multiple realizations with polarized initial conditions, for the combined Cdc42 and polarisome model. These are the corresponding centers of Spa2 polarization for the results shown in Figure S2.

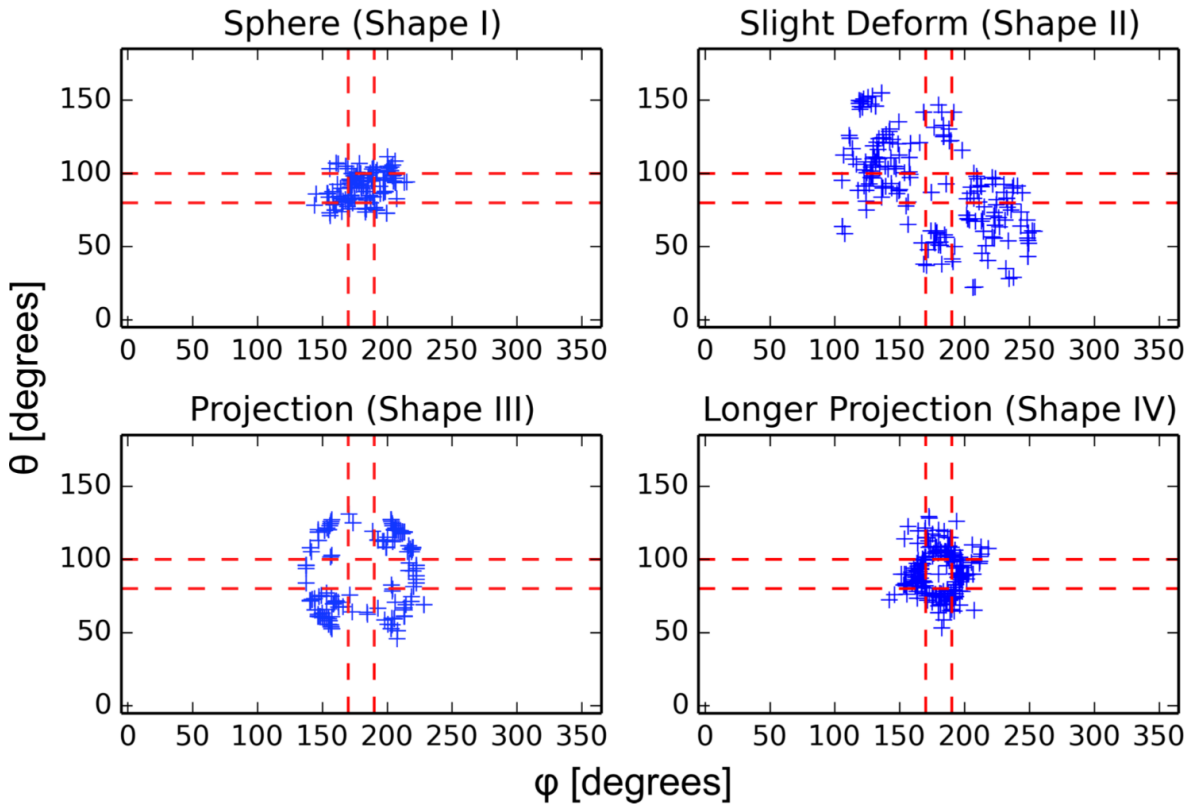

Figure S4 Spherical coordinates of the center of active Cdc42 polarization for multiple realizations with random initial conditions, with constant density rather than constant molecule count. Here, we tested our results presented in Figure S1 by adjusting the molecule count to keep a constant density for each geometry (opposed to a constant molecule count). For these relatively small changes in total volume, the overall behavior of a bias away from the tip is preserved for both constant molecule and constant density.

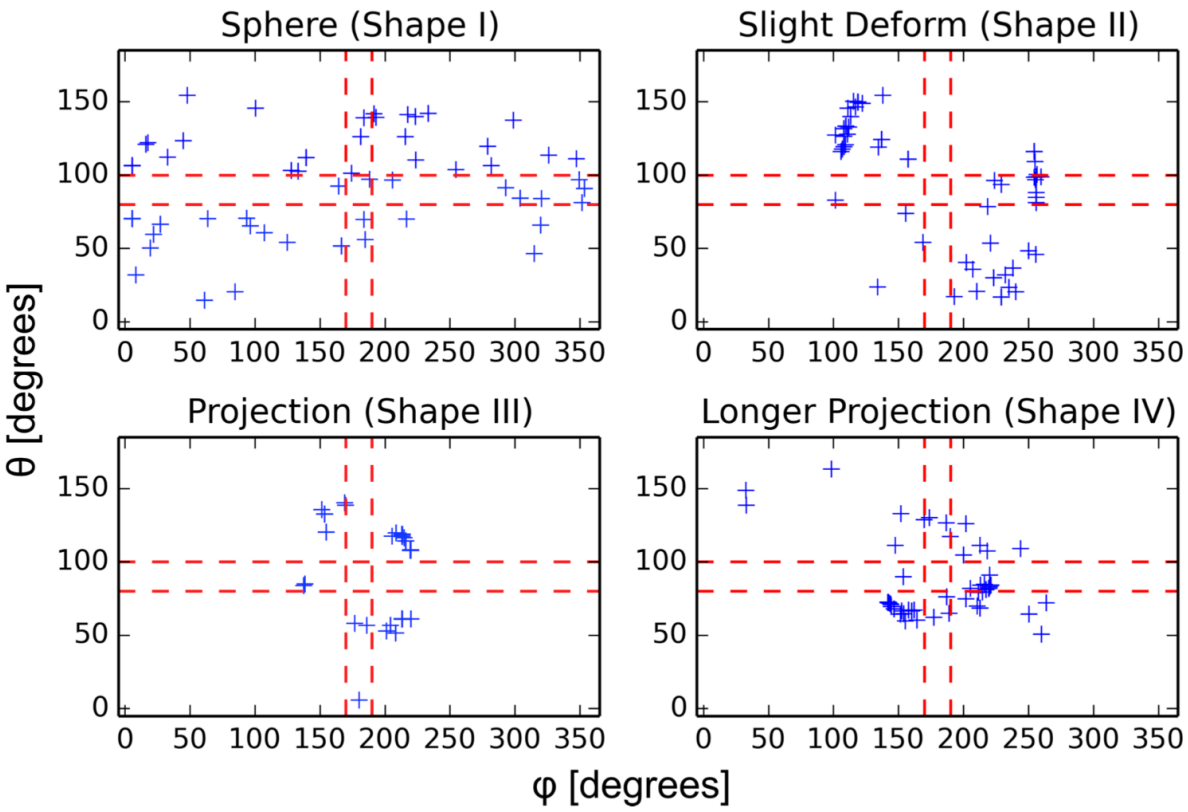

Figure S5 Spherical coordinates of the center of Spa2 polarization for multiple realizations with polarized initial conditions, for the polarisome model with a fixed Cdc42 distribution as input. These results are to be compared to the results presented in Figure S2 and Figure S3. Here the Cdc42 profile is fixed and polarized in the tip of the geometry, rather than fully dynamic as above. This, presumably, would make it more likely for Spa2 to polarize in the tip as geometry is no longer having an effect on the Cdc42 dynamics yet the geometry still appears to have an effect on the polarisome. This further supports our general result of geometry having a significant impact on the dynamics of polarization.

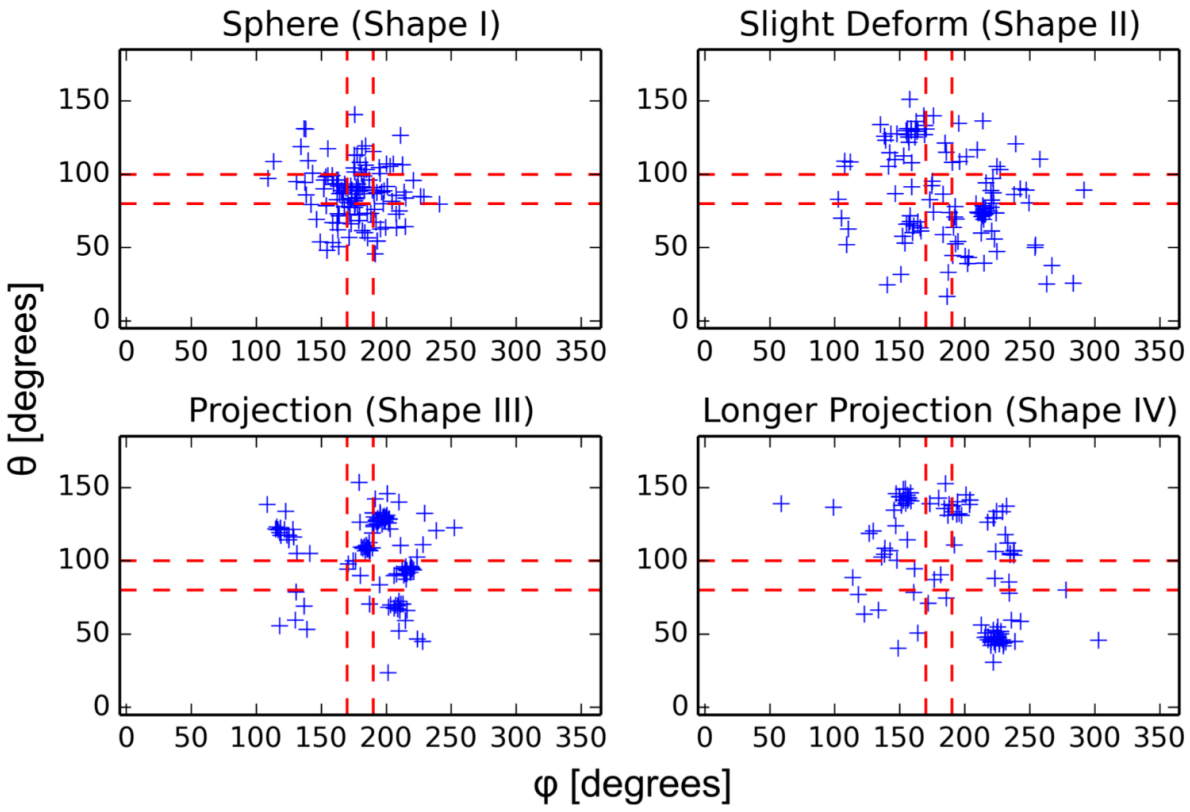

Figure S6 Spherical coordinates of the center of active Cdc42 polarization for multiple realizations with polarized initial conditions and one visualization of drifting with diffusion in the cytoplasm $D_c = 10\ \mu m^2 s^{-1}$. Here, we investigate the role of cytoplasmic diffusion on polarization in different geometries. Specifically, in addition to the cytoplasmic diffusion coefficient of $D_c = 50\ \mu m^2 s^{-1}$ we have tested a variety of other diffusion coefficients and in particular here show results for $D_c = 10\ \mu m^2 s^{-1}$ [100]. While there is a difference in the stability for the slightly deformed geometry, the bias away from the tip for projection shaped geometries is still clear.

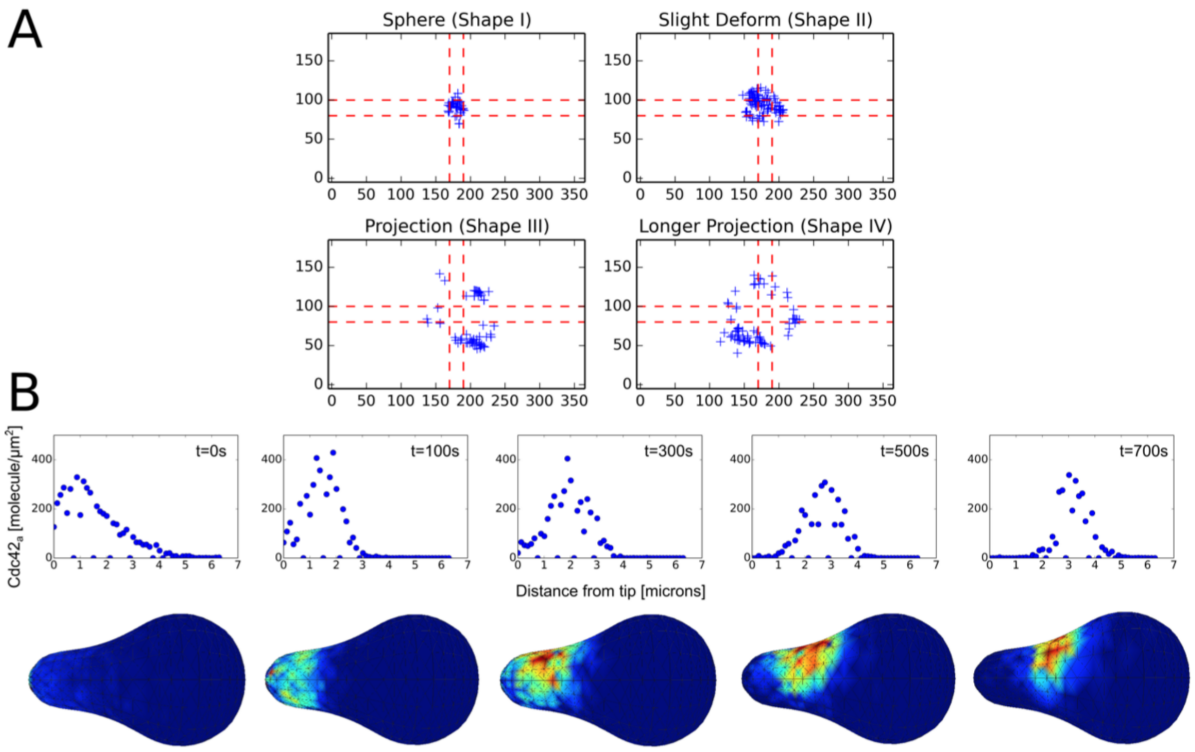

Figure S7 Spherical coordinates of the center of Spa2 polarization for multiple realizations with scattered initial conditions and a fixed active Cdc42 distribution as input and one visualization of the stabilization of polarization in a tip shaped geometry. These results are to be compared to the results presented in Figure S2, Figure S3 and Figure S5. Here the active Cdc42 profile is fixed and polarized in the tip of the geometry, rather than fully dynamic as above. To investigate the possibility of stabilizing Spa2 polarization, we have increased the parameter B_{on} (which is the recruitment of Bni1 by active Cdc42) by a factor of 100. We see that this is in fact enough to stabilize Spa2 polarization in the tip of projection shaped geometries.

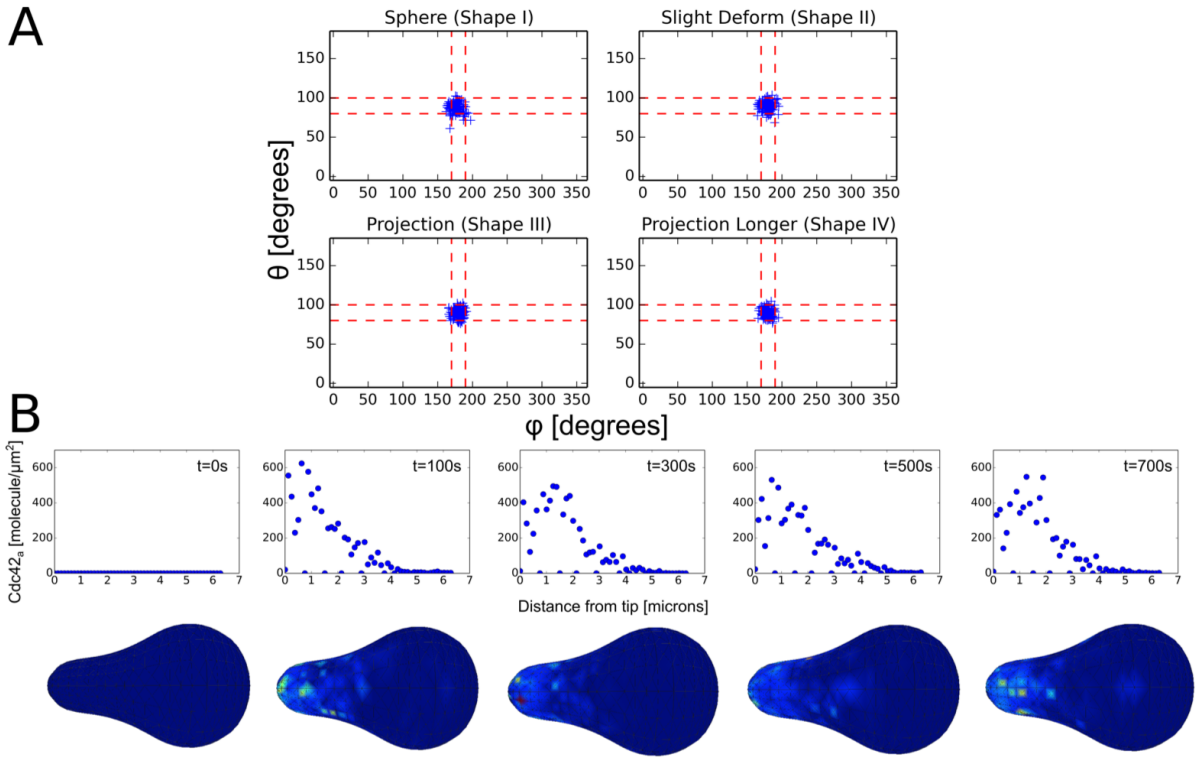
A
Sphere (Shape I)
Slight Deform (Shape II)
Projection (Shape III)
Projection Longer (Shape IV)
θ [degrees]
φ [degrees]
B
t=0s
t=100s
t=300s
t=500s
t=700s
Cdc42a [molecule/μm2]
Distance from tip [microns]

S1 Model Mechanistic model of Cdc42 polarization. Below are the reactions and parameters for one model of Cdc42 polarization used in the main text. This set of reactions is adapted from a model of polarization during budding presented in [16] to account for the mating pheromone present during mating (through the presence of a uniform Gbg field) and a small negative feedback from Cla4.

$$Cdc24_c + Gbg \xrightarrow{\delta_1} Cdc24_m + Gbg$$

$$Bem1_m + Cdc24_c \xrightarrow{\delta_1} Bem1_m + Cdc24_m$$

$$Cdc24_m \xrightarrow{\delta_2} Cdc24_c$$

$$Cdc24_m + Cdc42GDP_m \xrightarrow{\alpha_1} Cdc24_m + Cdc42GTP_m$$

$$Cdc42GTP_m \xrightarrow{\alpha_3} Cdc42GDP_m$$

$$Bem1_c + Cdc42GTP_m \xrightarrow{\gamma_1} Bem1_m + Cdc42GTP_m$$

$$Bem1_m \xrightarrow{\gamma_2} Bem1_c$$

$$Cdc42GDP_c \xrightarrow{\beta_2} Cdc42GDP_m$$

$$Cdc42GDP_m \xrightarrow{\beta_3} Cdc42GDP_c$$

$$Cdc24_m + Cdc42GDP_c \xrightarrow{\beta_1} Cdc24_m + Cdc42GTP_m$$

$$Cdc24_m + Cla4_a \xrightarrow{k_{24d}} Cdc24_c + Cla4_a$$

$$Cla4_m + Cdc42GTP_m \xrightarrow{k_{Cla4a}} Cla4_a + Cdc42GTP_m$$

$$Cla4_a \xrightarrow{k_{Cla4d}} Cla4_m$$

Parameter	Value	Description	Source
D_m	0.0053 $\mu m^2 s^{-1}$	Diffusion constant on membrane	[3]
D_c	50 $\mu m^2 s^{-1}$	Diffusion constant in cytoplasm	Fig S6
R	2 μm	Radius of cell	[3]
N_{42}	3000	Total number of Cdc42 molecules	[16]
N_B	3000	Total number of Bem1 molecules	[98]
N_{24}	1000	Total number of Cdc24 molecules	[16]
α_1	0.2 $\mu m^2 s^{-1}$	Activation of Cdc42 by Cdc24 (membrane)	[16]
α_3	1 s^{-1}	Deactivation of Cdc42	[16]
β_1	0.266 $\mu m^3 s^{-1}$	Activation of Cdc42 by Cdc24 (cytoplasm)	[16]
β_2	0.28 $\mu m s^{-1}$	Attachment of Cdc42 to membrane	[16]
β_3	1 s^{-1}	Detachment of Cdc42 from membrane	[16]
γ_1	0.2667 $\mu m^3 s^{-1}$	Bem1 recruitment by Cdc42	[16]
γ_2	0.35 s^{-1}	Detachment of Bem1 from membrane	[16]
δ_1	0.00297 $\mu m^3 s^{-1}$	Recruitment of Cdc24 by Gbg	[16]
δ_2	0.35 s^{-1}	Detachment of Cdc24 from membrane	[16]
k_{24d}	0.000033 $\mu m^3 s^{-1}$	Detachment of Cdc24 via Cla4	[98]
k_{Cla4a}	0.006 s^{-1}	Activation of Cla4 by Cdc42	[98]
k_{Cla4d}	0.01 s^{-1}	Deactivation of Cla4	[98]

S2 Model. Simplified model of Cdc42 polarization. Below are the reactions and parameters for a simplified model of Cdc42 polarization presented in [2].

$$Cdc42_c \xrightarrow{k_{on}} Cdc42_m$$

$$Cdc42_m \xrightarrow{k_{off}} Cdc42_c$$

$$Cdc42_c + Cdc42_m \xrightarrow{k_{fb}} 2Cdc42_m$$

Parameter	Value	Description	Source
k_{on}	$0.0001/60\ s^{-1}$	Spontaneous on rate	[2]
k_{off}	$9.0/60\ s^{-1}$	Spontaneous off rate	[2]
k_{fb}	$10.0/60\ \mu m^3 s^{-1}$	Feedback rate	[2]

S3 Model Mechanistic model of polarisome formation. Below are the reactions and parameters for the model of actin dynamics adapted from [3] that was combined with the S1 Model in the main text to investigate the possibility of actin dynamics overcoming the effect of geometry on polarization. The model originally presented in [3] was formulated on a 1D domain. We have adapted these parameters and fit them in a similar way as was presented in [3] for a sphere.

$$Bni1_c + Cdc42GTP_m \xrightarrow{B_{on}} Bni1_m + Cdc42GTP_m$$

$$Bni1_m \xrightarrow{B_{off}} Bni1_c$$

$$Actin_c + Bni1_m \xrightarrow{A_{on}} Actin_m + Bni1_m$$

$$Actin_m \xrightarrow{A_{off}} Actin_c$$

$$Spa2_c + Actin_m \xrightarrow{S_{on}} Spa2_m + Actin_m$$

$$Spa2_m \xrightarrow{S_{off}} Spa2_c$$

$$Bni1_c + Spa2_m \xrightarrow{B_{fb}} Bni1_m + Spa2_m$$

Added feedback between Cdc42 polarization and polarisome:

$$Cdc42GDP_c + Actin_m \xrightarrow{\beta_1} Cdc42GTP_m + Actin_m$$

$$Cdc42GDP_m + Actin_m \xrightarrow{\beta_1} Cdc42GTP_m + Actin_m$$

Parameter	Value	Description
D_m	0.0053 $\mu m^2 s^{-1}$	Diffusion constant on membrane
D_c	50 $\mu m^2 s^{-1}$	Diffusion constant in cytoplasm
R	2 μm	Radius of cell
N_B	1000	Total number of Bni1 molecules
N_S	5000	Total number of Spa2 molecules
N_A	40	Total number of Actin cables
B_{on}	0.000256 $\mu m^3 s^{-1}$	Recruitment of Bni1 by Cdc42
B_{off}	22.5 s^{-1}	Detachment of Bni1 from membrane
S_{on}	4.55 $\mu m^3 s^{-1}$	Recruitment of Spa2 by Actin
S_{off}	0.35 s^{-1}	Detachment of Spa2 from membrane
A_{on}	0.197 $\mu m^3 s^{-1}$	Recruitment of Actin by Bni1
A_{off}	$1.57 * 500/(500 + Spa2_m)$	Detachment of Actin from membrane
B_{fb}	0.0304 $\mu m^3 s^{-1}$	Recruitment of Bni1 by Spa2
β_1	0.266 $\mu m^3 s^{-1}$	Recruitment of Cdc42 by Actin

Chapter 5

Combined Model of Polarization and Mechanics

As discussed in the previous chapters, we are interested in understanding how polarization and the mechanics of the cell wall interact to yield mating projection growth in yeast. Up to this point, we have introduced a novel algorithm for simulating spatial stochastic dynamics on moving domains, and we have presented new insights into how the shape of the cell during projection growth can influence polarization dynamics. We now look to combine these contributions and couple models of polarization with mechanics to simulate mating projection growth in a more holistic fashion. To address the issues of polarization mislocalization at the tip of projections discussed in the last chapter, we introduce a novel mechanical feedback mechanism to stabilize growth. This coupling of signaling and mechanics was both a technical and modeling challenge. This work was done in collaboration with Samhita P. Banavar, Brian Drawert, Tau-Mu Yi and Otger Campàs and is currently in preparation for publication [19].

5.1 Simplified model of polarization and mechanical feedback

Our work in Chapter 4 has shown that there is a significant impact of cell shape on the dynamics of several current models of polarization. In particular, there is consistently a bias of the polarization cap away from the tip of projection shaped geometries for all models tested. As discussed in Chapter 4, this is contrary to polarization dynamics *in vivo* as it is critical for the polarization to remain at the tip of the projection to direct growth. To combine polarization and mechanics in such a way that yields stable growth, this issue had to be addressed. To this end, in this chapter we propose a direct mechanical feedback on the dynamics of polarization. In Section 2.3 we discussed the details of the cell wall and the role it plays in growth. Here we focus on a direct connection between the cell wall stress sensors and proteins involved in polarization. In particular, it is known that actin organization is controlled by Rho1 via the actin nucleating protein Bni1 and also that Rho1 is activated by the so called stress sensors Mid2 and Wsc1 [53]. This provides a direct connection between the mechanical state of the cell wall and polarization. Similar connections between polarity and mechanics have been observed in yeast spores [101] but have not been considered fully in other models of yeast polarization. As the biological details of how Rho1 interacts with Bni1 are not fully known, we propose a generic mechanism by which the polymerization of actin has a direct dependence on the strain rate present in the cell wall. Also, as it is computationally intensive to couple a detailed model of polarization and mechanics we will start by focusing on a coarse grained model of polarization that preserves many of the characteristics of more detailed models. A schematic for the reactions we will consider can be seen below in Figure 5.1, and the reactions themselves with relevant parameter values are given in Section 5.5. This is a novel combination of reactions found in [16] and [3] along with our proposed

mechanical feedback reaction.

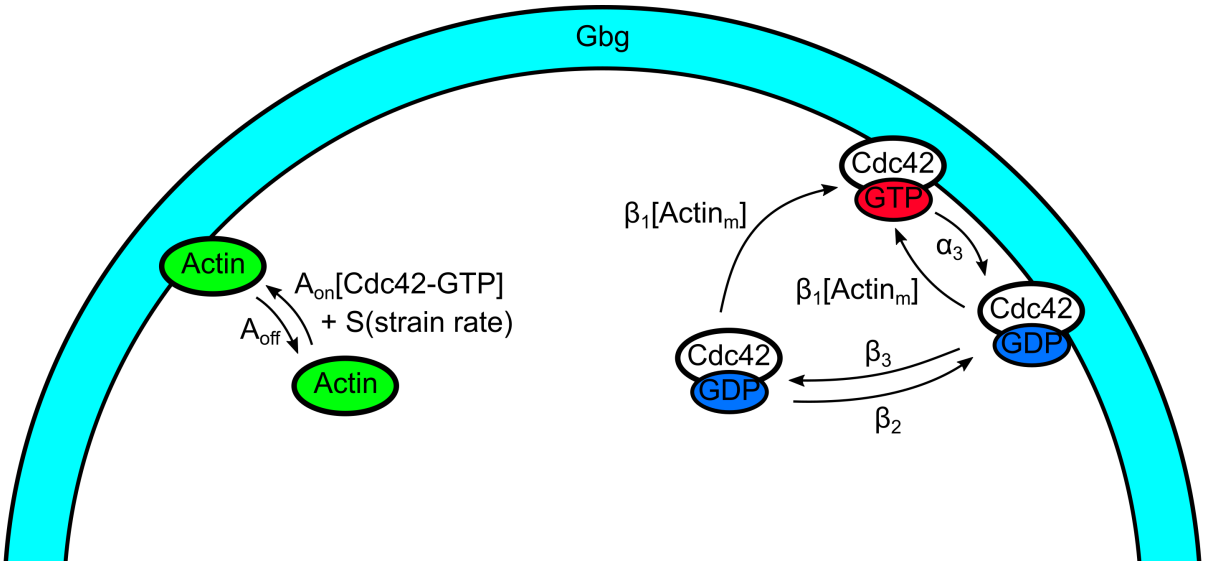

Figure 5.1: A: Schematic of coarse grained model of Cdc42 and Actin polarization.

As a first attempt to couple the model of polarization presented above in Figure 5.1 with a description of the mechanics of the cell wall, we formulate both the reaction-diffusion dynamics and the mechanics of the wall as a coupled system of partial differential equations (PDEs). Following the formulation presented in [18] for the cell wall, we describe the growth of the mating projection as the expansion of an axisymmetric thin shell, parametrized by the arclength s from the projection apex and azimuthal angle ϕ (see Figure 5.2). This growth is powered by the cell's internal turgor pressure, P. The shape of the projection is characterized by its local radius, $r(s,t)$, and the principal curvatures $\kappa_s = \frac{\partial \theta}{\partial s}$ and $\kappa_\phi = \frac{\sin\theta}{r}$, respectively, where $\theta(s,t)$ is the angle between the local outward normal and the axis of growth (Figure 5.2). The coordinates (r, ϕ, z) are standard cylindrical coordinates, and the angle θ and arclength s parameterize changes in normal and tangential directions of the surface, $\hat{n}$ and $\hat{s}$ respectively [62, 61]. The time evolution of the mating projection shape is governed by the mechanics and assembly of

the cell wall, as described below.

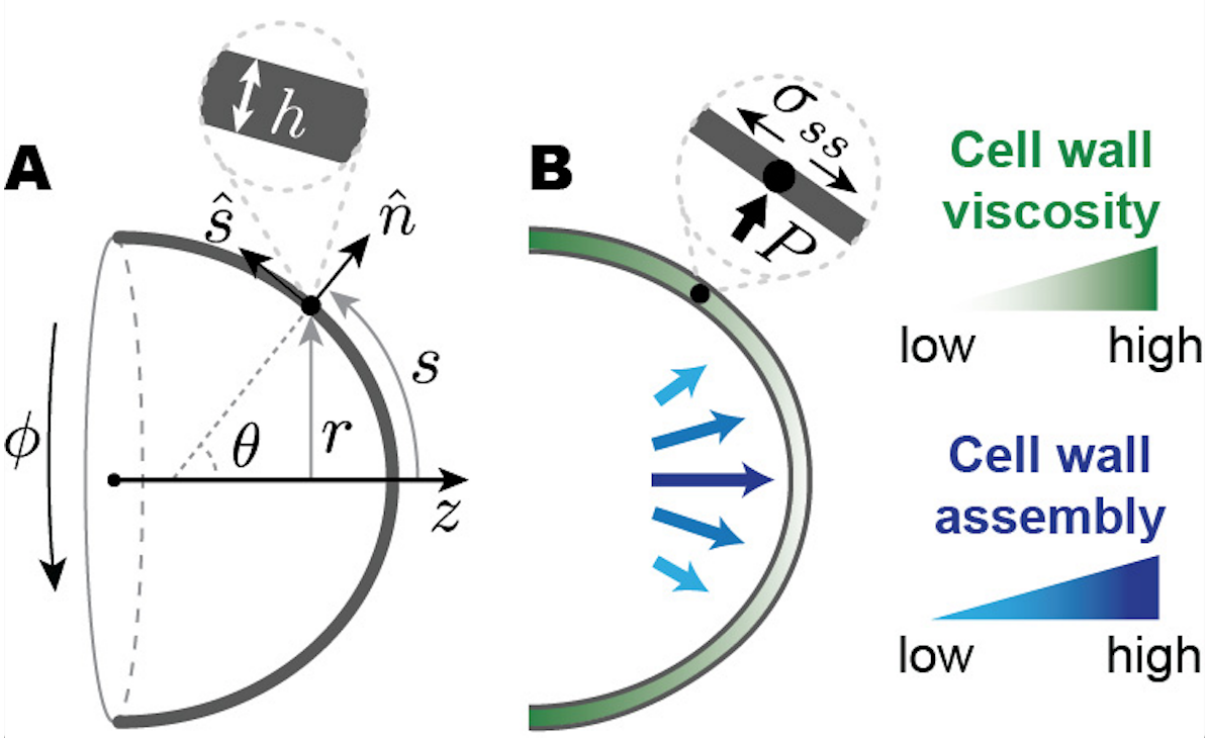

Figure 5.2: A: Geometry of the system and definition of relevant variables. B: Sketch depicting the increasing cell wall viscosity and decreasing cell wall assembly away from the apex. The inset depicts local normal force balance at the cell wall. All variables are defined in the main text.

Building on previous work combining cell wall mechanics and growth in tip-growing cells [61], as well as on the expansion of thin viscous shells [62], we write the equations governing the dynamics of the growing cell wall. Local normal force balance at the cell wall is given by the following equations

$$\sigma_{ss}\kappa_s + \sigma_{\phi\phi}\kappa_\phi = P \tag{5.1}$$

$$\sigma_{ss}\kappa_\phi = P/2 \tag{5.2}$$

where $\sigma_{ss}(s,t)$ and $\sigma_{\phi\phi}(s,t)$ are the tensions along s and ϕ in the wall (Figure 5.2). The

expansion of the cell wall during growth is caused by the tensions and depends on the mechanical properties (rheology) of the cell wall, which govern the response of the cell wall to applied stresses. As discussed in Section 2.3, we assume the cell wall of the growing mating projection to behave as an inhomogeneous viscous fluid, with spatially varying viscosity $\mu(s)$, minimal at the apex and increasing away from it (Figure 5.2). The local tangential velocity $u(s,t)$ of a cell wall with constant density ρ_w, or its strain (expansion) rates $\dot{\epsilon_s} = \frac{\partial u}{\partial s}$ and $\dot{\epsilon_\phi} = \frac{1}{r}\frac{dr}{dt}$ equivalently, can be minimally related to the tensions in the wall by [62, 61]

$$\sigma_{ss} = 4\mu h[\dot{\epsilon_s} + \dot{\epsilon_\phi}/2] \tag{5.3}$$

$$\sigma_{\phi\phi} = 4\mu h[\dot{\epsilon_s}/2 + \dot{\epsilon_\phi}] \tag{5.4}$$

As mentioned in Section 2.3 and [18], cell wall assembly occurs through the synthesis of the primary wall component β1,3-glucan by the synthase Fks1. Accounting for these events, mass conservation of the cell wall gives the following equation

$$\partial_t(rh) + \partial_s(rhu) = \frac{rm_m k_p}{\rho_w} A_m(s,t) \tag{5.5}$$

where $h(s,t)$ is the cell wall thickness, and m_m and k_p are the mass of a β1,3-glucan monomer and the β1,3-glucan assembly rate by Fks1/2 synthases, respectively. For simplicity, we assume that the assembly rate of new cell wall material is proportional to the local surface density of actin A_m, the dynamics of which are given by the reactions in Figure 5.1. The dynamics of actin and Cdc42 can be written in the curved geometry of the cell as follows

$$\partial_t(rC_c) - D_c\partial_s(r\partial_s C_c) = r(-\beta_2 C_c + \beta_3 C_m - \beta_1 C_c A_m) \tag{5.6}$$

$$\partial_t(rC_m) - D_m\partial_s(r\partial_s C_m) = r(\beta_2 C_c - \beta_3 C_m + \alpha_3 C_a - \beta_1 C_m A_m) \tag{5.7}$$

$$\partial_t(rC_a) - D_m\partial_s(r\partial_s C_a) = r(\beta_1 C_c A_m + \beta_1 C_m A_m - \alpha_3 C_a) \tag{5.8}$$

$$\partial_t(rA_c) - D_c\partial_s(r\partial_s A_c) = r(-A_{on} A_c C_a - SA_c[\dot{\epsilon_s} + \dot{\epsilon_\phi}] + A_{off} A_m) \tag{5.9}$$

$$\partial_t(rA_m) = r(A_{on} A_c C_a + SA_c[\dot{\epsilon_s} + \dot{\epsilon_\phi}] - A_{off} A_m) \tag{5.10}$$

where C_c, C_m and C_a represent the concentrations of cytoplasmic, inactive membrane bound, and active membrane bound Cdc42, and A_c and A_m represent the concentrations of cytoplasmic and membrane bound actin, respectively. Equations 5.1-5.10 define a system of coupled PDEs describing the mechanics of the cell wall and polarization. To initially test whether the coarse grained model of polarization given in Figure 5.1 with the proposed mechanical feedback was able to polarize active Cdc42 and membrane bound actin in a tip-shaped geometry, we fixed a geometry and strain rate profile from equations 5.1-5.5 and solved equations 5.6-5.10. The results of this simulation can be seen below in Figure 5.3. As seen below, these coarse grained dynamics with a mechanical feedback, starting with randomly distributed initial conditions for all species yield a polarized steady state for active Cdc42 and membrane bound actin. This preliminary result shows that these dynamics are in fact capable of localizing at the tip of projection shaped geometries. Now that we have seen that this mechanical feedback mechanism can in fact stabilize polarization at the tip of a curved geometry in the deterministic setting we look to couple a three-dimensional spatial stochastic implementation of the model in Figure 5.1 with mechanics and grow a mating projection using the general method presented in Chapter 3.

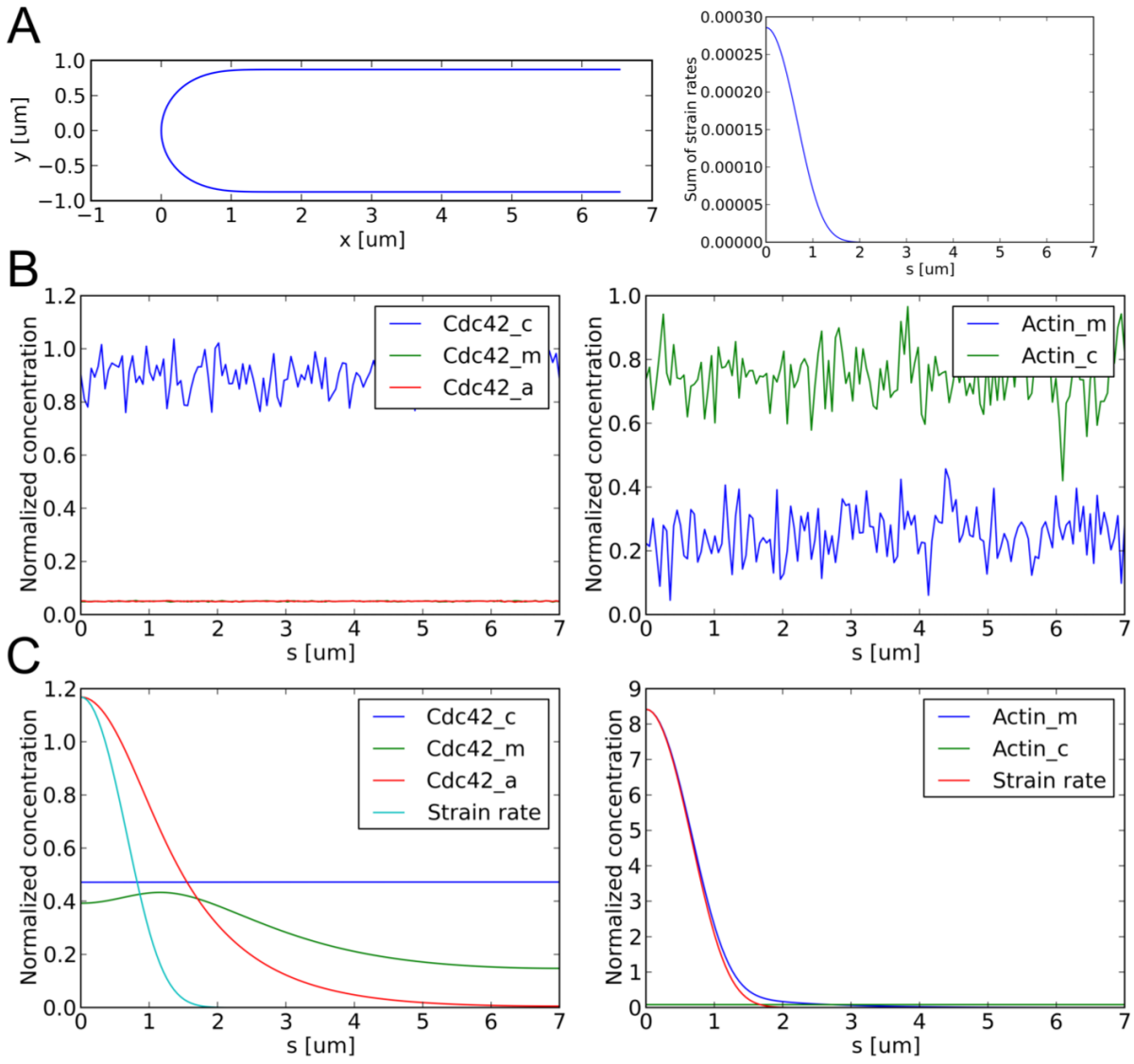

Figure 5.3: A: Tip-shaped geometry and strain rate profile that are used as input to the coarse grained polarization model. B: Randomly distributed initial conditions for Cdc42 and actin in a curved geometry with a specified strain profile. C: Polarized steady state for Cdc42 and actin in a curved geometry with a specified strain profile. In both cases here the concentration of each species was normalized by the total amount of Cdc42 or actin respectively. Also here the strain rate profile is scaled to share a maximum with either Cdc42 or actin for plotting so that the profiles can be more easily compared. The cooperatively of the mechanical feedback for these simulations was $S = 10^6$.

5.2 Effect of mechanical feedback on a three dimensional spatial stochastic model of polarization

In addition to the PDE model presented above, we extended our analysis and investigated the possibility of a mechanical feedback on polarization utilizing three-dimensional spatial stochastic models of polarization. One reason this extension is particularly interesting is that, as discussed in Chapter 4 and [17], we have shown that there can be a significant impact of cell shape on the dynamics of polarization. Specifically, for several three-dimensional reaction-diffusion models of polarization tested, there was a consistent bias of the polarization cap away from the tip of projection shaped geometries. The mechanical feedback on the polymerization of actin cables via Rho1 presented above could potentially provide a remedy for this bias away from the tip while the cell is growing a mating projection. Namely, if the activation of Bni1 (and ultimately actin) via Rho1 is dependent on the strain rate present in the cell wall, then during mating projection growth this preferential activation could in fact stabilize the polarization cap in the tip of the projection. To first investigate this possibility we have fixed a tip-shaped geometry and simulated the dynamics of the coarse grained model of polarization presented in Figure 5.1 both with and without mechanical feedback, similar to the results presented in Figure 4.1. These results can be seen below in Figure 5.4. As with the models presented in 4 and [17], with no mechanical feedback the polarization cap is unstable in the projection geometry (see Figure 5.4A). In contrast, when an exponential strain rate profile is imposed via the mechanical feedback on the attachment of actin, the polarization cap is stabilized in the tip of the projection (see Figure 5.4B). This is another demonstration of the concept that a preferential activation of actin dependent on a strain rate profile can in fact stabilize polarization in these projection geometries.

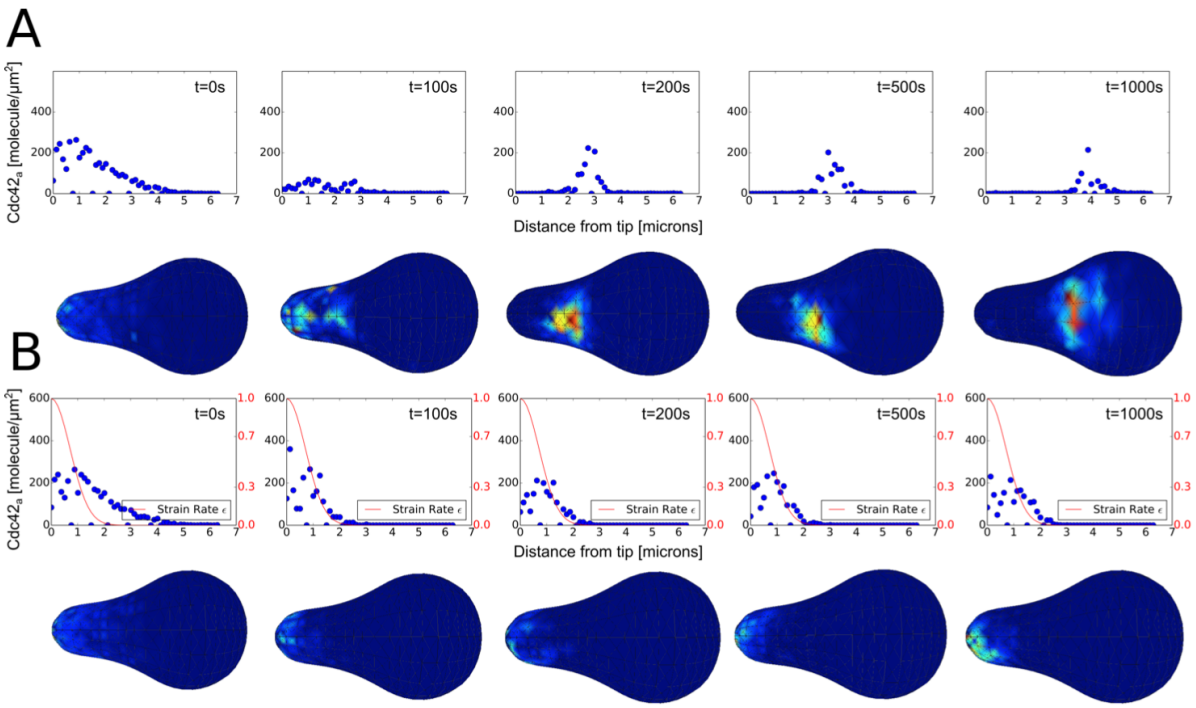

Figure 5.4: A: Visualization of the active Cdc42 polarization cap drifting away from the tip during one realization. The top panel is a plot of the surface density of active Cdc42 versus the distance away from the tip along the perimeter of the shape for various time points (to get a 1D plot, the 3D profile was averaged along the surface of the shape). The bottom panel shows the corresponding 3D visualization of the active Cdc42 distribution. The drifting shown here took place in a matter of 1000 seconds. This simulation was performed with no mechanical feedback (i.e. setting $S = 0$.) B: Visualization of the stabilization of the active Cdc42 polarization cap with the addition of mechanical feedback ($S = 5000$). The imposed strain rate profile is shown in red.

5.3 Coupling polarization and mechanics to simulate projection growth

In the previous sections we have presented a coarse grained model of polarization that contains a novel mechanical feedback on the polymerization of actin. This mechanism of preferential attachment is general and meant to stand in for the interaction between the cell wall stress sensors, Rho1 and the formin Bni1. We have demonstrated that

this model is capable of polarizing at the tip of projection shaped geometries for both the deterministic 2D and stochastic 3D case. Now it is our goal to couple this spatial stochastic model of polarization with equations 5.1-5.5 which describe the mechanics of the cell wall. We will be using a similar operator splitting methodology to that which we presented in Chapter 3 where instead of a domain that is changing in a predetermined manner or governed by an ad-hoc model of growth, we utilize equations 5.1-5.5 to govern the shape of the domain. A schematic for this approach can be seen below in Figure 5.5.

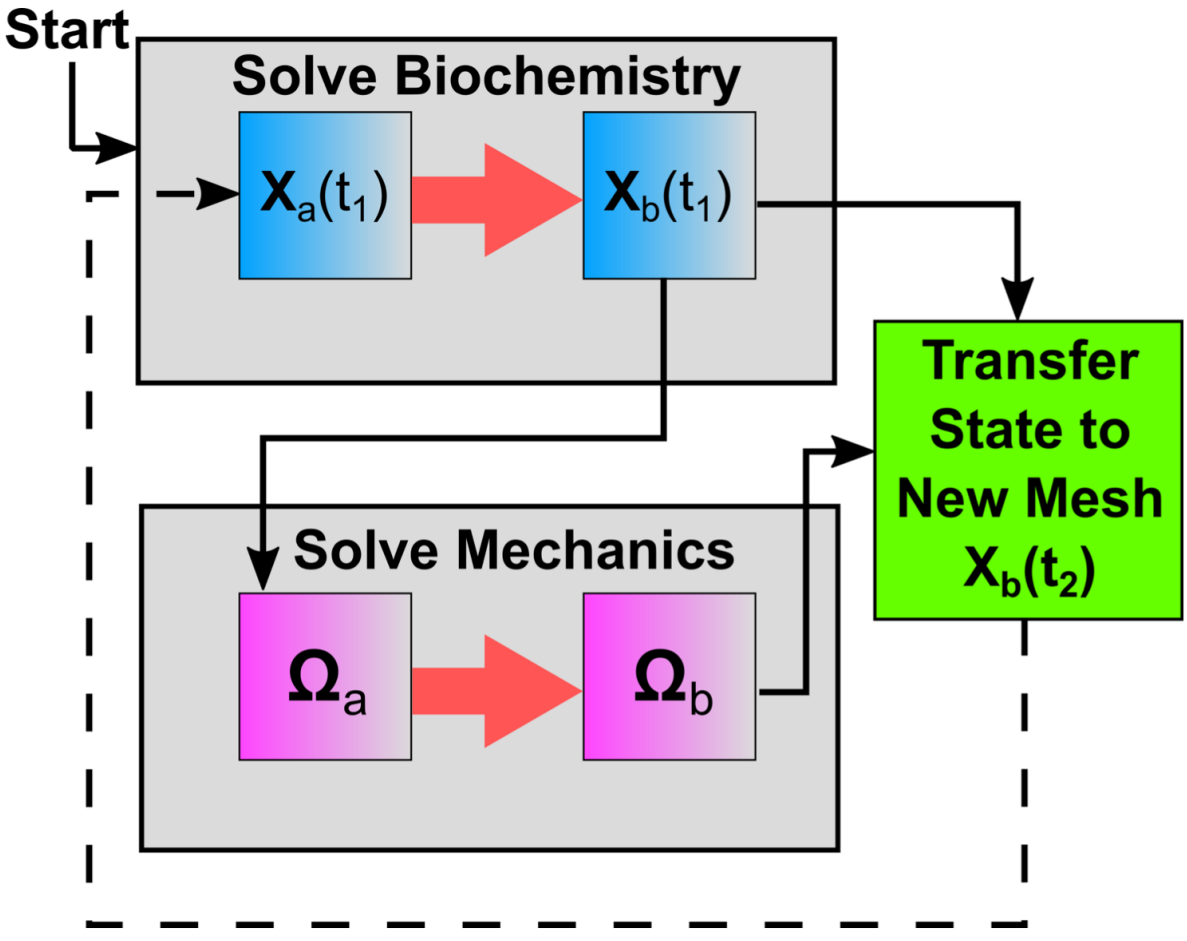

Figure 5.5: Schematic for operator split methodology utilized in the coupling of polarization and mechanics.

The first step of the coupled simulation was to solve the polarization dynamics on

an initial geometry of a sphere with a radius $r = 2\mu m$ for one time step, starting with randomly scattered initial conditions for each species. In theory, throughout the simulation the time step can be chosen such that the shape of the cell does not change dramatically over one time step. The inherent separation of time scales of this problem, with polarization dynamics on the order of minutes and the growth of a mating projection on the order of hours, naturally lends itself to our operator splitting technique. For the results presented in this section, our time step was chosen to be 10 minutes (or 600 seconds) unless otherwise noted. An example of the three dimensional actin distribution after one time step can be seen below in Figure 5.6A. It should be noted that on the initial step there is no strain profile so the mechanical feedback is effectively nonexistent. All of the three dimensional, spatial stochastic simulation in this section was done using PyURDME [13]. Next, the three dimensional actin distribution was fit with a Gaussian along the arc length s and used as input to equation 5.5 describing the dynamics of cell wall assembly in the mechanics equations. To do this, the arc length for each voxel in the three dimensional mesh was calculated and each voxel was assigned to a histogram bin along the arc length. This histogram of molecule counts versus s was then averaged over the time step and divided by the appropriate surface area to yield a surface concentration. An example of a fit actin concentration profile after one time step can be seen below in Figure 5.6B.

The next step in the coupled simulation was to solve the mechanics equations 5.1-5.5 over the same time step with the initial geometry and actin profile as specified above. As mentioned previously, these equations were solved by discretizing the arc length s which yields a system of differential algebraic equations (DAEs) via the method of lines (MOL). This system of DAEs was solved using the SUNDIALS package [70]. The result of solving the mechanics equations is a change in shape. An example of the change in shape over one time step can be seen below in Figure 5.7A. The new two dimensional shape was

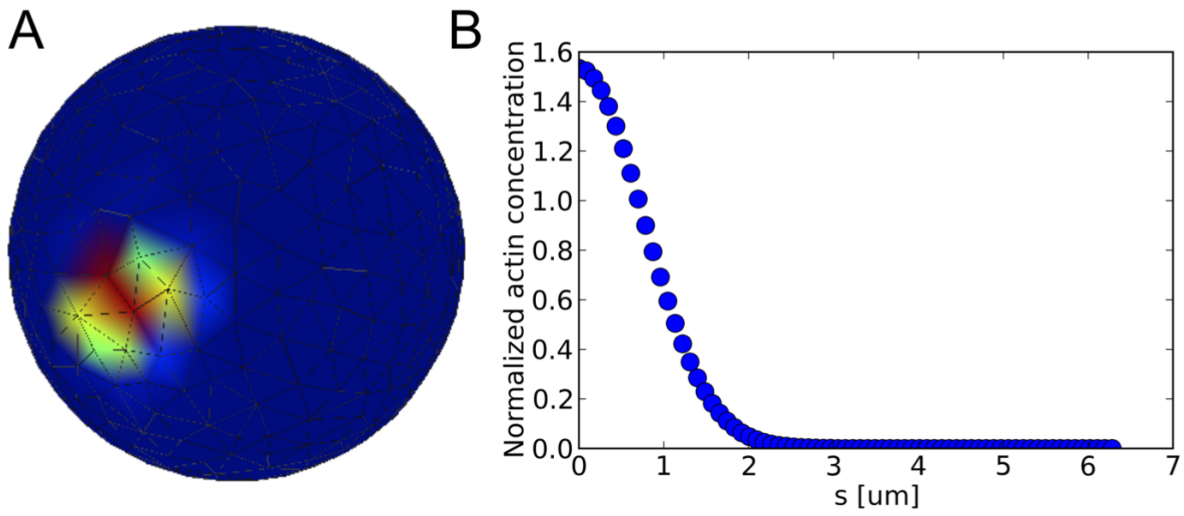

Figure 5.6: A: The three dimensional distribution and polarization of actin after one time step. B: Corresponding two dimensional Gaussian fit for the actin profile versus arc length.

then used to create the three dimensional, tetrahedral mesh for the stochastic simulation of polarization over the next time step. To do this, the discretized two dimensional shape was converted into a downsampled, three dimensional point cloud of the cell surface by rotation using the software Meshlab [102] (an assumption of the mechanics formulation is an axisymmetric cell shape). This point cloud was then converted into a tetrahedral mesh using Gmsh [99]. Next, the biochemical state was transferred from the last mesh to the new one using the technique from Figure 3.3 (see Figure 5.7C). The biochemical state was then simulated over the next time step on the new geometry. Importantly, another output of the mechanics equations is the current strain profile of the cell wall (see Figure 5.7B). This profile was rotated and converted into a three dimensional field and used to assign each voxel in the computational mesh a strain rate. The strain rate in each voxel then encodes the mechanical feedback on the attachment rate of actin presented in Figure 5.1. This iterative process then repeats for several time steps to yield the growth of a mating projection. The input to the equations describing the mechanics of the cell wall is

the distribution of actin from the polarization simulation which is used in 5.5 as a proxy for the distribution of cell wall synthases. The mechanics then yield a new cell shape and a resultant strain rate profile to be used in the coarse grained model of polarization. It is in this way that a detailed model of polarization and a physically based model of mechanics are coupled to yield stable projection growth. One example of the resultant three dimensional growth of a projection (along with the actin distribution) can be be seen below in Figure 5.7D.

5.4 Discussion

Understanding how walled cells are able to achieve stable morphogenesis and shape change is an important question in biology. The cell wall is critical for maintaining the shape and mechanical integrity of plant, bacterial and fungal cells. Any change in material properties of the cell wall must be heavily regulated to avoid cell lysis. In yeast cells, the growth of a mating projection presents a useful model problem for understanding this type of morphogenesis. In Section 2.3 of this dissertation and [18] we presented a theoretical model that showed that a mechanical feedback between cell wall expansion and assembly is necessary for stable projection growth. Our goal in this chapter was to further explore the connections between the biochemical signaling responsible for actin cable formation and cell wall morphogenesis by presenting a fully coupled model of polarization and mechanics.

During yeast mating, the cell responds to a extracellular gradient of mating pheromone via an intracellular cascade of protein reactions. This cascade leads to polarization of key proteins on the membrane and actin cable formation. In Chapter 4 we demonstrated that cell shape can have a significant impact on the dynamics of polarization for a variety of current reaction-diffusion models. Specifically, there seems to be a consistent

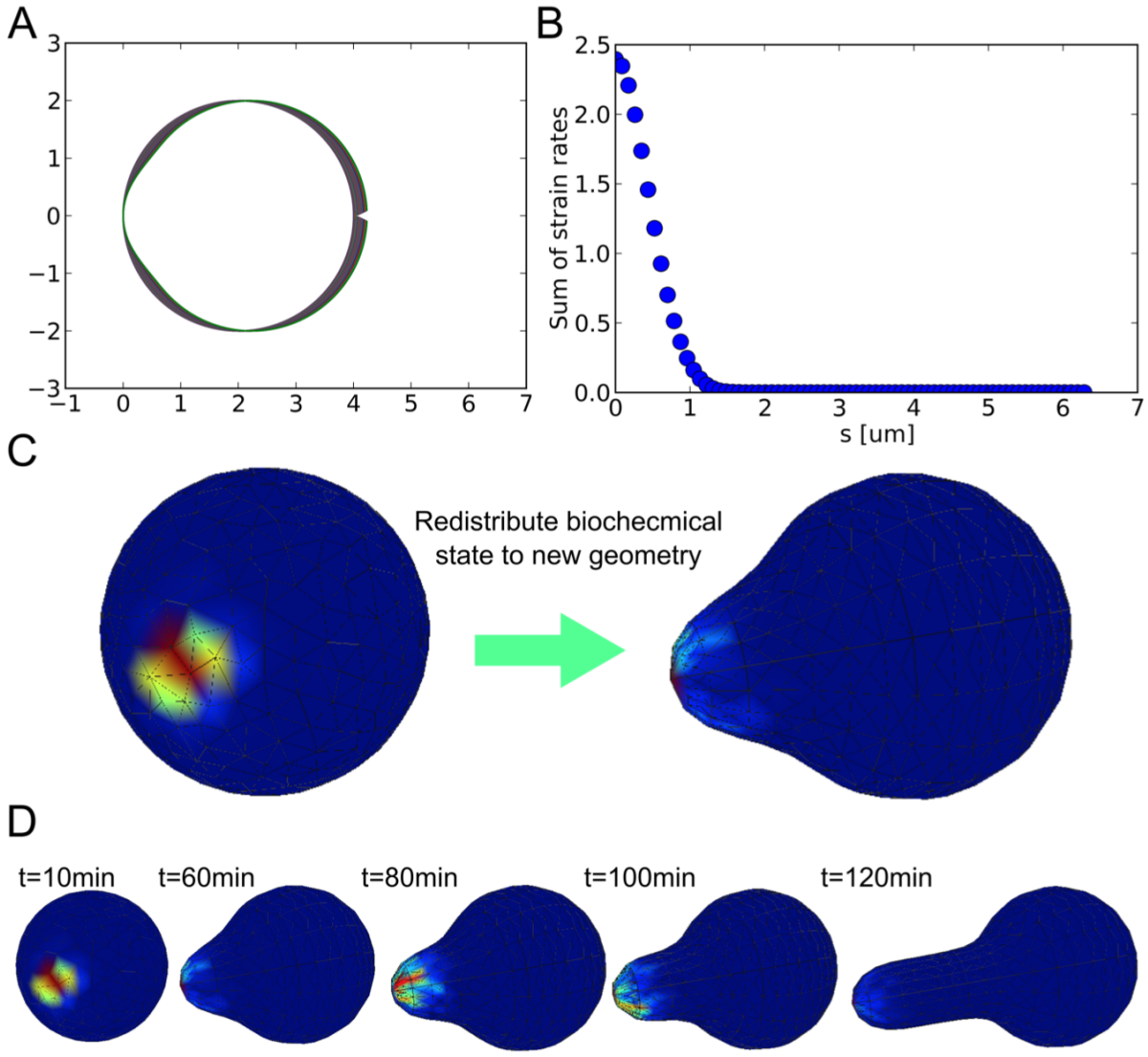

Figure 5.7: A: Time evolution of the cell shape for one time step resulting from the solution of equations 5.1-5.5. B: The resultant strain profile that is used to determine the reaction rate for mechanical feedback on actin attachment as seen in Figure 5.1. C. After each time step of the mechanics equations a new computational mesh is generated. The biochemical state is redistributed from the old mesh to the new one using the method shown in Figure 3.3. D: One example of stable mating projection growth from the coupled simulation described above. The cooperatively of the mechanical feedback for these simulations was $S = 5000$.

bias of the polarization cap away from the tip of projection shaped geometries. This is in contrast to what is seen *in vivo* where it is critical for polarization to remain at

the tip of growing projections to direct growth. To address this issue in the context of a coupled model of polarization and mechanics, we have proposed a direct mechanical feedback on the dynamics of polarization (see Figure 5.1). In particular, we have implemented this feedback as a strain rate dependent attachment of actin in our coarse grained polarization model. This mechanism is representative of the known link between the cell wall stress sensors (Mid2 and Wsc1) and the actin nucleator Bni1 via the protein Rho1 [53]. While there is still experimental work to be done to establish the details and validity of such a mechanism, we believe that this type of preferential activation by strain rate is a general way to stabilize current reaction-diffusion models of polarization during mating projection growth. In general, the details of the mechanisms responsible for the establishment and maintenance of polarization are disputed and currently being studied. Our proposed mechanical feedback is an elegant possible mechanism to aid in the maintenance of polarization during mating projection growth.

To investigate the properties of our proposed coupled model of polarization and mechanics, we first numerically solved the PDEs governing coarse grained polarization (equations 5.6-5.10) in a curved geometry with a corresponding strain profile set by the mechanics equations (equations 5.1-5.2). These results showed that, at least preliminarily, this model was able to polarize in tip-shaped geometries (see Figure 5.3). Next we tested this same model in a three dimensional spatial stochastic simulation. Specifically we showed that in the absence of our proposed mechanical feedback, the polarization cap was unstable in projection shaped geometries (see Figure 5.4A). The addition of an imposed strain rate profile stabilized the polarization cap in the tip of the projection shaped geometry (see Figure 5.4B). This polarization model was then used in a fully coupled model of polarization and mechanics.

Simulating a fully coupled model of polarization and mechanics posed a technical challenge. Part of this challenge was due to the different mathematical formulations of

each component of the model. Specifically, the polarization dynamics are described by a three dimensional, spatial stochastic reaction-diffusion system while the mechanics of the cell wall are described by an axisymmetric PDE. This coupling was achieved using an operator splitting methodology originally presented in Chapter 3. In each time step the polarization dynamics are solved on a static geometry. This yields an actin profile which is used as input to equation 5.5 which governs cell wall assembly. Next the mechanics equations were solved over the time step to yield the new shape and strain rate profile of the cell. This shape was converted into a computational mesh for the next stochastic simulation and the strain rate profile was used in our proposed mechanical feedback reaction. In this way the coupled dynamics were iterated for several time steps to yield stable projection growth (see Figure 5.7D).

Overall the results presented in this chapter raise some intriguing possibilities about the connections between cell wall mechanics and polarization during mating projection growth. Our approach for coupling these different dynamics is general and could yield insight into other systems where directed growth is essential. The traditional paradigm of treating biochemical signaling and cell mechanics as separate might fail to capture key biological mechanisms. In the future we hope to investigate experimentally the possible influence of Rho1 on polarization during projection growth. We also hope to implement our coupled model for more detailed models of polarization and more thoroughly characterize the characteristics of projection growth for different parameter regimes. This could lead to new insight about which mechanisms are important during projection growth and lead to comparisons between experimental and modeled protein dynamics. Mechanical feedback may very well be yet another mechanism involved in the maintenance of polarization in yeast.

5.5 Model details and parameter values

Model 1: Reactions for the coarse grained model of Cdc42 and actin polarization presented in Figure 5.1.

$$Cdc42GDP_c \xrightarrow{\beta_2} Cdc42GDP_m$$

$$Cdc42GDP_m \xrightarrow{\beta_3} Cdc42GDP_c$$

$$Cdc42GDP_c + Actin_m \xrightarrow{\beta_1} Cdc42GTP_m + Actin_m$$

$$Cdc42GDP_m + Actin_m \xrightarrow{\beta_1} Cdc42GTP_m + Actin_m$$

$$Cdc42GTP_m \xrightarrow{\alpha_3} Cdc42GDP_m$$

$$Actin_c + Cdc42GTP_m \xrightarrow{A_{on}} Actin_m + Cdc42GTP_m$$

$$Actin_c \xrightarrow{S\dot{\epsilon}} Actin_m$$

$$Actin_m \xrightarrow{A_{off}} Actin_c$$

Parameter	Value	Description	Source
D_m	0.0053 $\mu m^2 s^{-1}$	Diffusion constant on membrane	[3]
D_a	0.0 $\mu m^2 s^{-1}$	No actin diffusion on membrane	[3]
D_c	10 $\mu m^2 s^{-1}$	Diffusion constant in cytoplasm	[100]
R	2 μm	Radius of cell	[3]
N_{42}	3000	Total number of Cdc42 molecules	[16]
N_A	40	Total number of Actin cables	[3]
α_3	1 s^{-1}	Deactivation of Cdc42	[16]
β_1	0.266 $\mu m^3 s^{-1}$	Activation of Cdc42 by Cdc24	[16]
β_2	0.28 $\mu m s^{-1}$	Attachment of Cdc42 to membrane	[16]
β_3	1 s^{-1}	Detachment of Cdc42 from membrane	[16]
A_{on}	0.197 $\mu m^3 s^{-1}$	Recruitment of Actin by Bni1	[3]
A_{off}	$785/(500 + Spa2_m)$	Detachment of Actin from membrane	[3]
S	varied	Cooperativity of mechanical feedback	

Chapter 6

Conclusions and Future Directions

The wide variety of structures and patterns found in the natural world is one of the hallmarks of life. Understanding how these structures form and maintain themselves over time is a classic problem in physics and biology. In this dissertation we have concerned ourselves with the particular model system of morphogenesis during yeast mating. Specifically, we have presented results related to the mathematical modeling of the biochemical processes governing protein pattern formation during mating and how these dynamics can yield cell shape change. In this problem, intercellular biochemical signaling and cell mechanics are closely coupled.

Computational methods and mathematical modeling have become essential tools in systems biology research over the last half century. One issue that has become increasingly important to understanding intracellular signaling is the inherent stochasticity of biochemical reactions. In Section 2.2 we discussed the current approaches for spatial stochastic simulation. We also mentioned our work on PyURDME, a software framework for the simulation of spatial stochastic reaction-diffusion systems. This framework was designed to efficiently and reproducibly create, simulate and analyze these often complex models. We also mentioned MOLNs, a computational platform that can leverage

high-performance computing and cloud services to scale up simulations. These software developments then served as the basis for our later biological inquires into yeast mating projection growth.

The first step in the process of mating projection growth is the localization (or polarization) of proteins on the membrane of the cell. This is a well-studied, yet not fully understood, example of pattern formation in biology. There are several models of polarization at varying levels of mathematical complexity. In Section 2.1 we reviewed several of these models and discussed some of the current issues in the field. As mentioned above, our concern here was the growth of the mating projection, which inherently involves geometries that are changing in time. In Chapter 3 we presented a novel method for spatial stochastic simulation on moving domains. We first described the mathematical details of the method and then validated it against other existing techniques. Next we demonstrated the utility of the method with a variety of biologically relevant example problems. The development of our method was motivated by our problem of interest in yeast mating but is general for spatial stochastic dynamics on time-dependent domains.

Using the technical advances introduced above we went on to explore the biology of the problem. One insight in particular that we gained was the effect that complex cell geometries can have on the dynamics of polarization. In Chapter 4 we presented our work elucidating the effects that tip-shaped geometries can have on current models of polarization. Specifically, there seems to be a consistent bias of the polarization cap away from the tip of projection shaped geometries. This is in contrast to what is seen *in vivo* where it is critical for polarization to remain at the tip of growing projections to direct growth. Our work raised questions about which mechanisms could possibly be missing from current models of polarization to overcome such effects.

While polarization is certainly necessary for mating projection growth, it is not the whole story. The cell wall is a critical structure in plant, bacterial and fungal cells

responsible for defining cell shape and providing mechanical integrity. In Section 2.3 we discussed the structure of the cell wall and how it is maintained. We also discussed work that showed that a mechanical feedback between cell wall expansion and assembly is necessary for stable projection growth. In Chapter 5 we finished by presenting a model coupling the dynamics of polarization and cell wall mechanics. To stabilize polarization in the tip of growing projections we proposed a novel mechanical feedback for polarization. This coupled model was a technical challenge that ultimately led to a simulation of stable mating projection growth from the initial polarization to the final projection.

There are still several questions that remain unanswered about the interaction of polarization and cell mechanics. One interesting direction, building on the work we presented in Chapter 5, is the experimental exploration of the effects of Rho1 on the stability of polarization during mating projection growth. These are difficult experiments because Rho1 is a signaling hub that effects many proteins downstream. Another interesting direction, as mentioned in Chapter 5, is to incorporate more detailed models of polarization into our coupled simulation framework and to more thoroughly explore the characteristics of these coupled models for different parameter regimes. These advances could potentially lead to more quantitative comparisons between experiment and simulation such as the spatial distribution of specific proteins during growth. This feedback between simulation and experiment has been a mainstay of our approach throughout this dissertation and has been shown to lead to useful biological insights. Our general methodology for coupling polarization and mechanics could also be used to study other model problems where cells are changing shape in time or growing projections such as chemotaxis.

To conclude, understanding how biological structures form, maintain themselves over time and change in response to stimuli is a formidable task. In this dissertation we focused on the model problem of mating projection growth in yeast. Even in this seemingly

simple example there are several issues that are not well understood. We have developed software and computational techniques that have enabled us to gain new insight into this problem. Moving forward we hope our work can help advance the understanding of the interactions between biochemical pattern formation and the physical structure of the cell.

Bibliography

[1] S. J. Altschuler, S. B. Angenent, Y. Wang, and L. F. Wu, *On the spontaneous emergence of cell polarity*, *Nature* **454** (Aug, 2008) 886–889.

[2] A. Jilkine, S. B. Angenent, L. F. Wu, and S. J. Altschuler, *A density-dependent switch drives stochastic clustering and polarization of signaling molecules*, *PLOS Computational Biology* **7** (11, 2011) 1–11.

[3] M. J. Lawson, B. Drawert, M. Khammash, L. Petzold, and T.-M. Yi, *Spatial stochastic dynamics enable robust cell polarization*, *PLOS Computational Biology* **9** (07, 2013) 1–12.

[4] N. Barkai and S. Leibler, *Biological rhythms: Circadian clocks limited by noise*, *Nature* **403** (2000), no. 6767 267–268.

[5] J. Paulsson, O. G. Berg, and M. Ehrenberg, *Stochastic focusing: fluctuation-enhanced sensitivity of intracellular regulation*, *Proceedings of the National Academy of Sciences* **97** (2000), no. 13 7148–7153.

[6] M. Thattai and A. Van Oudenaarden, *Intrinsic noise in gene regulatory networks*, *Proceedings of the National Academy of Sciences* **98** (2001), no. 15 8614–8619.

[7] D. T. Gillespie, *A general method for numerically simulating the stochastic time evolution of coupled chemical reactions*, *Journal of Computational Physics* **22** (1976), no. 4 403 – 434.

[8] D. T. Gillespie, *Exact stochastic simulation of coupled chemical reactions*, *J. Phys. Chem.* **81** (Dec., 1977) 2340–2361.

[9] D. Fange and J. Elf, *Noise-induced min phenotypes in e. coli*, *PLOS Computational Biology* **2** (06, 2006) 1–12.

[10] D. Bernstein, *Simulating mesoscopic reaction-diffusion systems using the Gillespie algorithm*, *Phys. Rev. E* **71** (Apr, 2005) 041103.

[11] J. Elf and M. Ehrenberg, *Spontaneous separation of bi-stable biochemical systems into spatial domains of opposite phases*, in *Systems Biology, IEE Proceedings*, vol. 1, pp. 230–236, IET, 2004.

[12] A. B. Stundzia and C. J. Lumsden, *Stochastic simulation of coupled reaction–diffusion processes*, *Journal of computational physics* **127** (1996), no. 1 196–207.

[13] B. Drawert, M. Trogdon, S. Toor, L. Petzold, and A. Hellander, *MOLNs: A cloud platform for interactive, reproducible and scalable spatial stochastic computational experiments in systems biology using PyURDME*, *SIAM Journal on Scientific Computing* (2016).

[14] B. Drawert, S. Hellander, M. Trogdon, T.-M. Yi, and L. Petzold, *A framework for discrete stochastic simulation on 3d moving boundary domains*, *The Journal of Chemical Physics* **145** (2016), no. 18 184113, [http://dx.doi.org/10.1063/1.4967338].

[15] A. B. Goryachev and A. V. Pokhilko, *Dynamics of Cdc42 network embodies a Turing-type mechanism of yeast cell polarity*, *FEBS Letters* **582** (2008), no. 10 1437–1443.

[16] B. Klnder, T. Freisinger, R. Wedlich-Sldner, and E. Frey, *Gdi-mediated cell polarization in yeast provides precise spatial and temporal control of cdc42 signaling*, *PLOS Computational Biology* **9** (12, 2013) 1–12.

[17] M. Trogdon, B. Drawert, C. Gomez, S. P. Banavar, T.-M. Yi, O. Camps, and L. R. Petzold, *The effect of cell geometry on polarization in budding yeast*, *PLOS Computational Biology* **14** (06, 2018) 1–22.

[18] S. P. Banavar, C. Gomez, M. Trogdon, L. R. Petzold, T.-M. Yi, and O. Camps, *Mechanical feedback coordinates cell wall expansion and assembly in yeast mating morphogenesis*, *PLOS Computational Biology* **14** (01, 2018) 1–19.

[19] M. Trogdon, S. P. Banavar, B. Drawert, T.-M. Yi, O. Camps, and L. R. Petzold, *Combining polarization and mechanics to understand yeast mating morphogenesis*, *In Preparation* (2018).

[20] A. M. Turing, *The chemical basis of morphogenesis*, *Philosophical Transactions of the Royal Society of London B: Biological Sciences* **237** (1952), no. 641 37–72.

[21] A. Gierer and H. Meinhardt, *A theory of biological pattern formation*, *Kybernetik* **12** (1972), no. 1 30–39.

[22] T. Biancalani, D. Fanelli, and F. Di Patti, *Stochastic turing patterns in the brusselator model*, *Phys. Rev. E* **81** (Apr, 2010) 046215.

[23] N. V. Kampen, *Stochastic processes in physics and chemistry*. North Holland, 2007.

[24] L. J. Schumacher, T. E. Woolley, and R. E. Baker, *Noise-induced temporal dynamics in turing systems*, *Phys. Rev. E* **87** (Apr, 2013) 042719.

[25] J. Schnakenberg, *Simple chemical reaction systems with limit cycle behaviour*, *Journal of Theoretical Biology* **81** (1979), no. 3 389 – 400.

[26] P. K. Maini, T. E. Woolley, R. E. Baker, E. A. Gaffney, and S. S. Lee, *Turing's model for biological pattern formation and the robustness problem*, *Interface Focus* **2** (2012), no. 4 487–496, [http://rsfs.royalsocietypublishing.org/content/2/4/487.full.pdf].

[27] Y. Cao and R. Erban, *Stochastic turing patterns: Analysis of compartment-based approaches*, *Bulletin of Mathematical Biology* **76** (Dec, 2014) 3051–3069.

[28] J. Halatek and E. Frey, *Highly canalized mind transfer and mine sequestration explain the origin of robust mincde-protein dynamics*, *Cell Reports* **1** (2012), no. 6 741 – 752.

[29] M. Loose, E. Fischer-Friedrich, J. Ries, K. Kruse, and P. Schwille, *Spatial regulators for bacterial cell division self-organize into surface waves in vitro*, *Science* **320** (2008), no. 5877 789–792, [http://science.sciencemag.org/content/320/5877/789.full.pdf].

[30] D. Pruyne and A. Bretscher, *Polarization of cell growth in yeast. I. Establishment and maintenance of polarity states*, *Journal of Cell Science* **113** (2000), no. 3 365–375, [http://jcs.biologists.org/content/113/3/365.full.pdf].

[31] J. M. Dyer, N. S. Savage, M. Jin, T. R. Zyla, T. C. Elston, and D. J. Lew, *Tracking shallow chemical gradients by actin-driven wandering of the polarization site*, *Current Biology* **23** (2015/07/31, 2013) 32–41.

[32] M. Jose, S. Tollis, D. Nair, J.-B. Sibarita, and D. McCusker, *Robust polarity establishment occurs via an endocytosis-based cortical corralling mechanism*, *The Journal of Cell Biology* **200** (2013), no. 4 407–418, [http://jcb.rupress.org/content/200/4/407.full.pdf+html].

[33] T. Freisinger, B. Klünder, J. Johnson, N. Müller, G. Pichler, G. Beck, M. Costanzo, C. Boone, R. A. Cerione, E. Frey, and R. Wedlich-Söldner, *Establishment of a robust single axis of cell polarity by coupling multiple positive feedback loops*, *Nat Commun* **4** (May, 2013) 1807. Article.

[34] A. McClure, M. Minakova, J. Dyer, T. Zyla, T. Elston, and D. Lew, *Role of polarized g protein signaling in tracking pheromone gradients*, *Developmental Cell* **35** (2015), no. 4 471 – 482.

[35] A. Jilkine and L. Edelstein-Keshet, *A comparison of mathematical models for polarization of single eukaryotic cells in response to guided cues*, *PLOS Computational Biology* **7** (04, 2011) 1–15.

[36] N. S. Savage, A. T. Layton, and D. J. Lew, *Mechanistic mathematical model of polarity in yeast*, *Molecular Biology of the Cell* **23** (2012), no. 10 1998–2013, [http://www.molbiolcell.org/content/23/10/1998.full.pdf+html].

[37] A. B. Goryachev and M. Leda, *Many roads to symmetry breaking: molecular mechanisms and theoretical models of yeast cell polarity*, *Molecular Biology of the Cell* **28** (2017), no. 3 370–380, [http://www.molbiolcell.org/content/28/3/370.full.pdf+html].

[38] A. Mogilner, J. Allard, and R. Wollman, *Cell polarity: Quantitative modeling as a tool in cell biology*, *Science* **336** (2012), no. 6078 175–179, [http://science.sciencemag.org/content/336/6078/175.full.pdf].

[39] F. O. Bendez, V. Vincenzetti, D. Vavylonis, R. Wyss, H. Vogel, and S. G. Martin, *Spontaneous cdc42 polarization independent of gdi-mediated extraction and actin-based trafficking*, *PLoS Biol* **13** (04, 2015) e1002097.

[40] Y. Mori, A. Jilkine, and L. Edelstein-Keshet, *Wave-pinning and cell polarity from a bistable reaction-diffusion system*, *Biophysical Journal* **94** (2008), no. 9 3684 – 3697.

[41] J. Halatek and E. Frey, *Rethinking pattern formation in reaction-diffusion systems*, *Nature Physics* (2018).

[42] M. Pablo, S. A. Ramirez, and T. C. Elston, *Particle-based simulations of polarity establishment reveal stochastic promotion of turing pattern formation*, *PLOS Computational Biology* **14** (03, 2018) 1–25.

[43] S. Hellander, *Single molecule simulations in complex geometries with embedded dynamic one-dimensional structures*, *The Journal of Chemical Physics* **139** (2013), no. 1 014103, [https://doi.org/10.1063/1.4811395].

[44] C. W. Gardiner, *Handbook of stochastic methods for physics, chemistry and the natural sciences*, vol. 13 of *Springer Series in Synergetics*. Springer-Verlag, Berlin, third ed., 2004.

[45] D. T. Gillespie, *A general method for numerically simulating the stochastic time evolution of coupled chemical reacting systems*, *J. Comput. Phys.* **22** (1976) 403–434.

[46] M. A. Gibson and J. Bruck, *Efficient exact stochastic simulation of chemical systems with many species and many channels*, *The Journal of Physical Chemistry A* **104** (2000), no. 9 1876–1889, [http://dx.doi.org/10.1021/jp993732q].

[47] S. Engblom, L. Ferm, A. Hellander, and P. Lötstedt, *Simulation of stochastic reaction-diffusion processes on unstructured meshes*, *SIAM Journal on Scientific Computing* **31** (2009), no. 3 1774–1797.

[48] A. Logg and G. N. Wells, *Dolfin: Automated finite element computing*, *ACM Trans. Math. Softw.* **37** (Apr., 2010) 20:1–20:28.

[49] F. M. Klis, A. Boorsma, and P. W. J. D. Groot, *Cell wall construction in saccharomyces cerevisiae*, *Yeast* **23** (2006), no. 3 185–202, [https://onlinelibrary.wiley.com/doi/pdf/10.1002/yea.1349].

[50] R. Teparić and V. Mrša, *Proteins involved in building, maintaining and remodeling of yeast cell walls*, *Current Genetics* **59** (Aug., 2013) 171–185.

[51] D. E. Levin, *Cell wall integrity signaling in Saccharomyces cerevisiae*, *Microbiology and Molecular Biology Reviews* **69** (2005), no. 2 262–291.

[52] R. Rodicio and J. Heinisch, *Together we are strong—cell wall integrity sensors in yeasts*, *Yeast* **27** (2010), no. 8 531–540.

[53] D. Levin, *Regulation of Cell Wall Biogenesis in Saccharomyces cerevisiae: The Cell Wall Integrity Signaling Pathway*, *Genetics* **189** (2011), no. 4 1145–1175.

[54] S. Bartnicki-Garcia, F. Hergert, and G. Gierz, *Computer simulation of fungal morphogenesis and the mathematical basis for hyphal (tip) growth*, *Protoplasma* **153** (1989).

[55] S. Tindemans, N. Kern, and B. Mulder, *The diffusive vesicle supply center model for tip growth in fungal hyphae*, *Journal of Theoretical Biology* **238** (2006), no. 4 937–948.

[56] R. Bernal, E. Rojas, and J. Dumais, *The mechanics of tip growth morphogenesis: what we have learned from rubber balloons*, *JOMMS* **2** (2007), no. 6 1157–1168.

[57] A. Goriely and M. Tabor, *Self-Similar Tip Growth in Filamentary Organisms*, *Phys. Rev. Lett.* **90** (2003), no. 10 108101–4.

[58] B. Goldenbogen, W. Giese, M. Hemmen, J. Uhlendorf, A. Herrmann, and E. Klipp, *Dynamics of cell wall elasticity pattern shapes the cell during yeast mating morphogenesis*, *Open Biology* **6** (2016), no. 9 160136–14.

[59] J. Abenza, E. Couturier, J. Dodgson, J. Dickmann, A. Chessel, J. Dumais, and R. Salas, *Wall mechanics and exocytosis define the shape of growth domains in fission yeast*, *Nature Communications* **6** (2015) 1–13.

[60] T. Drake and D. Vavylonis, *Model of Fission Yeast Cell Shape Driven by Membrane-Bound Growth Factors and the Cytoskeleton*, *PLoS computational biology* **9** (Oct., 2013) e1003287.

[61] O. Campas and L. Mahadevan, *Shape and Dynamics of Tip-Growing Cells*, *Current Biology* **19** (2009), no. 24 2102–2107.

[62] B. Van De Fliert, P. Howell, and J. Ockenden, *Pressure-driven flow of a thin viscous sheet*, *J. Fluid Mech.* **292** (1995), no. -1 359–376.

[63] D. J. Adams, *Fungal cell wall chitinases and glucanases*, *Microbiology* **150** (July, 2004) 2029–2035.

[64] C. Douglas, F. Foor, J. Marrinan, N. Morin, J. NielsenI, A. Dahl, P. Mazur, W. Baginsky, W. Li, M. Elsherbeini, J. Clemas, S. Mandala, B. Frommer, and M. Kurtz, *The Saccharomyces-Cerevisiae Fks1 (Etg1) Gene Encodes an Integral Membrane-Protein Which Is a Subunit of 1,3-Beta-D-Glucan Synthase*, *Proceedings of the National Academy of Sciences* **91** (1994), no. 26 12907–12911.

[65] T. Utsugi, M. Minemura, A. Hirata, M. Abe, D. Watanabe, and Y. Ohya, *Movement of yeast 1,3-beta-glucan synthase is essential for uniform cell wall synthesis*, *Genes to Cells* **7** (2002), no. 1 1–9.

[66] P. Delley and M. Hall, *Cell Wall Stress Depolarizes Cell Growth Via Hyperactivation of RHO1*, *The Journal of Cell Biology* **147** (1999), no. 1 163–174.

[67] E. Cabib and J. Arroyo, *How carbohydrates sculpt cells: chemical control of morphogenesis in the yeast cell wall*, *Nature Reviews Microbiology* **11** (2013), no. 9 648–655.

[68] E. Bi and H. Park, *Cell Polarization and Cytokinesis in Budding Yeast*, *Genetics* **191** (2012), no. 2 347–387.

[69] B. Philip and D. Levin, *Wsc1 and Mid2 Are Cell Surface Sensors for Cell Wall Integrity Signaling That Act through Rom2, a Guanine Nucleotide Exchange Factor for Rho1*, *Mol. Cell. Biol.* **21** (2001), no. 1 271–280.

[70] A. C. Hindmarsh, P. N. Brown, K. E. Grant, S. L. Lee, R. Serban, D. E. Shumaker, and C. S. Woodward, *SUNDIALS: Suite of nonlinear and differential/algebraic equation solvers*, *ACM Transactions on Mathematical Software (TOMS)* **31** (2005), no. 3 363–396.

[71] G. Servant, O. D. Weiner, P. Herzmark, T. Balla, J. W. Sedat, and H. R. Bourne, *Polarization of chemoattractant receptor signaling during neutrophil chemotaxis*, *Science* **287** (2000), no. 5455 1037–1040, [http://science.sciencemag.org/content/287/5455/1037.full.pdf].

[72] K. C. Huang, Y. Meir, and N. S. Wingreen, *Dynamic structures in Escherichia coli: spontaneous formation of MinE rings and MinD polar zones*, *Proceedings of the National Academy of Sciences* **100** (2003), no. 22 12724–12728.

[73] S. S. Andrews and D. Bray, *Stochastic simulation of chemical reactions with spatial resolution and single molecule detail*, *Physical biology* **1** (2004), no. 3 137.

[74] S. S. Andrews, N. J. Addy, R. Brent, and A. P. Arkin, *Detailed simulations of cell biology with smoldyn 2.1*, *PLOS Computational Biology* **6** (03, 2010) 1–10.

[75] R. A. Kerr, T. M. Bartol, B. Kaminsky, M. Dittrich, J.-C. J. Chang, S. B. Baden, T. J. Sejnowski, and J. R. Stiles, *Fast Monte Carlo simulation methods for biological reaction-diffusion systems in solution and on surfaces*, *SIAM Journal on Scientific Computing* **30** (2008), no. 6 3126–3149.

[76] J. S. van Zon and P. R. ten Wolde, *Simulating biochemical networks at the particle level and in time and space: Green's function reaction dynamics*, *Phys. Rev. Lett.* **94** (Apr, 2005) 128103.

[77] J. E. Segall, *Polarization of yeast cells in spatial gradients of alpha mating factor*, *Proceedings of the National Academy of Sciences* **90** (1993), no. 18 8332–8336.

[78] A. Trinci and P. Saunders, *Tip growth of fungal hyphae*, *Microbiology* **103** (1977), no. 2 243–248.

[79] T. Newman, *Modeling multicellular systems using subcellular elements.*, *Mathematical biosciences and engineering: MBE* **2** (2005), no. 3 613–624.

[80] D. Thalmeier, J. Halatek, and E. Frey, *Geometry-induced protein pattern formation*, *Proceedings of the National Academy of Sciences* **113** (2016), no. 3 548–553.

[81] A. Ghosh and T. T. Marquez-Lago, *Simulating stochastic reaction-diffusion systems on and within moving boundaries*, *PLoS ONE* **10** (07, 2015) e0133401.

[82] R. E. Baker, C. A. Yates, and R. Erban, *From microscopic to macroscopic descriptions of cell migration on growing domains*, *Bulletin of Mathematical Biology* **72** (2009), no. 3 719–762.

[83] C. A. Yates, *Discrete and continuous models for tissue growth and shrinkage*, *Journal of Theoretical Biology* **350** (2014) 37 – 48.

[84] C. A. Yates, R. E. Baker, R. Erban, and P. K. Maini, *Going from microscopic to macroscopic on nonuniform growing domains*, *Phys. Rev. E* **86** (Aug, 2012) 021921.

[85] T. I. Moore, C.-S. Chou, Q. Nie, N. L. Jeon, and T.-M. Yi, *Robust spatial sensing of mating pheromone gradients by yeast cells*, *PLoS ONE* **3** (12, 2008) 1–11.

[86] T.-M. Yi, H. Kitano, and M. I. Simon, *A quantitative characterization of the yeast heterotrimeric g protein cycle*, *Proceedings of the National Academy of Sciences* **100** (2003), no. 19 10764–10769.

[87] B. Drawert, M. J. Lawson, L. Petzold, and M. Khammash, *The diffusive finite state projection algorithm for efficient simulation of the stochastic reaction-diffusion master equation*, *The Journal of chemical physics* **132** (2010), no. 7 074101.

[88] W. Giese, M. Eigel, S. Westerheide, C. Engwer, and E. Klipp, *Influence of cell shape, inhomogeneities and diffusion barriers in cell polarization models*, *Physical Biology* **12** (2015), no. 6 066014.

[89] F. Spill, V. Andasari, M. Mak, R. D. Kamm, and M. H. Zaman, *Effects of 3d geometries on cellular gradient sensing and polarization*, *Physical Biology* **13** (2016), no. 3 036008.

[90] A. F. M. Mare, V. A. Grieneisen, and L. Edelstein-Keshet, *How cells integrate complex stimuli: The effect of feedback from phosphoinositides and cell shape on cell polarization and motility*, *PLOS Computational Biology* **8** (03, 2012) 1–20.

[91] J. Meyers, J. Craig, and D. Odde, *Potential for control of signaling pathways via cell size and shape*, *Current Biology* **16** (2006), no. 17 1685 – 1693.

[92] D. Odde, *Getting cells and tissues into shape*, *Cell* **144** (2011), no. 3 325 – 326.

[93] M. Howard, *Cell signalling: Changing shape changes the signal*, *Current Biology* **16** (2006), no. 17 R673 – R675.

[94] S. R. Neves, P. Tsokas, A. Sarkar, E. A. Grace, P. Rangamani, S. M. Taubenfeld, C. M. Alberini, J. C. Schaff, R. D. Blitzer, I. I. Moraru, and R. Iyengar, *Cell shape and negative links in regulatory motifs together control spatial information flow in signaling networks*, *Cell* **133** (2008), no. 4 666 – 680.

[95] M. D. Onsum, K. Wong, P. Herzmark, H. R. Bourne, and A. P. Arkin, *Morphology matters in immune cell chemotaxis: membrane asymmetry affects amplification*, *Physical Biology* **3** (2006), no. 3 190.

[96] K. M. Schmoller, J. J. Turner, M. Kõivomägi, and J. M. Skotheim, *Dilution of the cell cycle inhibitor whi5 controls budding yeast cell size*, *Nature* **526** (Oct, 2015) 268–272. 26390151[pmid].

[97] M.-P. Gulli, M. Jaquenoud, Y. Shimada, G. Niederhuser, P. Wiget, and M. Peter, *Phosphorylation of the cdc42 exchange factor cdc24 by the pak-like kinase cla4 may regulate polarized growth in yeast*, *Molecular Cell* **6** (2000), no. 5 1155 – 1167.

[98] C.-S. Chou, Q. Nie, and T.-M. Yi, *Modeling robustness tradeoffs in yeast cell polarization induced by spatial gradients*, *PLOS ONE* **3** (09, 2008) 1–16.

[99] C. Geuzaine and J. Remacle, *Gmsh: a three-dimensional finite element mesh generator with built-in pre- and post-processing facilities*, *International Journal for NUmerical Methods in Engineering* **79** (2009), no. 11 1309–1331.

[100] B. D. Slaughter, J. W. Schwartz, and R. Li, *Mapping dynamic protein interactions in map kinase signaling using live-cell fluorescence fluctuation spectroscopy and imaging*, *Proceedings of the National Academy of Sciences* **104** (2007), no. 51 20320–20325, [http://www.pnas.org/content/104/51/20320.full.pdf].

[101] D. Bonazzi, J.-D. Julien, M. Romao, R. Seddiki, M. Piel, A. Boudaoud, and N. Minc, *Symmetry breaking in spore germination relies on an interplay between polar cap stability and spore wall mechanics*, *Developmental Cell* **28** (2017/10/11, 2014) 534–546.

[102] P. Cignoni, M. Callieri, M. Corsini, M. Dellepiane, F. Ganovelli, and G. Ranzuglia, *MeshLab: an Open-Source Mesh Processing Tool*, in *Eurographics Italian Chapter Conference* (V. Scarano, R. D. Chiara, and U. Erra, eds.), The Eurographics Association, 2008.